UNIVERSITY OF ZAGREB
FACULTY OF SCIENCE
DEPARTMENT OF GEOPHYSICS

Martina Tudor

FACTORS AFFECTING OPERATIONAL FORECAST OF DETRIMENTAL WEATHER CONDITIONS USING ALADIN LIMITED AREA NUMERICAL WEATHER PREDICTION MODEL

DOCTORAL THESIS

Zagreb, 2017.

UNIVERSITY OF ZAGREB
FACULTY OF SCIENCE
DEPARTMENT OF GEOPHYSICS

Martina Tudor

FACTORS AFFECTING OPERATIONAL FORECAST OF DETRIMENTAL WEATHER CONDITIONS USING ALADIN LIMITED AREA NUMERICAL WEATHER PREDICTION MODEL

DOCTORAL THESIS

Supervisor: Prof. Dr. Piet Termonia
Doc. Dr. Sc. Nataša Strelec Mahović

Zagreb, 2017.

SVEUČILIŠTE U ZAGREBU
PRIRODOSLOVNO-MATEMATIČKI FAKULTET
GEOFIZIČKI ODSJEK

Martina Tudor

ČIMBENICI KOJI UTJEČU NA OPERATIVNU PROGNOZU OPASNIH VREMENSKIH PRILIKA ALADIN NUMERIČKIM MODELOM NA OGRANIČENOM PODRUČJU

DOKTORSKI RAD

Mentor: prof.dr.sc. Piet Termonia
doc. dr. sc. Nataša Strelec Mahović

Zagreb, 2017.

Factors affecting operational forecast of detrimental weather conditions using ALADIN limited area numerical weather prediction model

Doctoral Thesis

in Meteorology

Submitted to the
Faculty of Science, Department of Geophysics
of the
University of Zagreb

in Partial Fulfillment of the Requirements for the Degree of
Doctor of Natural Science

by
Martina Tudor

Advisor
Prof. Dr. Piet Termonia

Doc. Dr. Sc. Nataša Strelec Mahović

Zagreb, September 2017

List of Abbreviations

ALADIN	Aire Limitée Adaptation dynamique Développement InterNational
MCUF	Monitoring coupling update frequency
DHMZ	Meteorological and hydrological service of Croatia
RMPD	rapidly moving pressure disturbances
DFI	digital filter initialization
SSDFI	scale selective DFI
LBC	lateral boundary conditions
LAM	limited area models
LACE	Limited Area for Central Europe
NWP	Numerical weather prediction
ARPEGE	Action de Recherche Petite Echelle Grande Echelle
IFS	Integrated forecast system
ECMWF	European centre for the medium-range weather forecast
RHS	right hand side
PV	potential vorticity

[type=,title=Abbreviations]

Abstract

Severe weather represents storms, cyclones, fronts, severe wind or thick fog and other phenomena. Limited area models (LAM) can simulate or forecast such phenomena in higher resolution and using dedicated model set-up. This thesis explores ALADIN model capabilities to forecast threatening weather conditions for wider area of the Republic of Croatia. The research focuses on the consequences of a fast cyclone entering LAM domain through lateral boundary too quickly to be detected, frequency of such events, mechanism for automatic detection of such events and methods to treat the problem in the operational forecast. The solution will be applied to events with severe weather such as windstorms and/or intensive precipitation.

This thesis deals with problems of temporal interpolation of the lateral boundary conditions for a limited area model. The lateral boundary conditions are taken from a large scale model and usually available with an interval of several hours. However, these data are used at the lateral boundaries every model timestep, which is usually se veral minutes. Therefore, the lateral boundary conditions are interpolated in time.

Three hourly temporal resolution of lateral boundary data for limited area models (LAMs) can be too infrequent to resolve rapidly moving storms. This problem is expected to be worse with increasing horizontal resolution. In order to detect intensive disturbances in surface pressure moving rapidly through the model domain, a filtered surface pressure field (MCUF) is computed operationally in the ARPEGE global model of Météo France. The field is distributed in the coupling files along with conventional meteorological fields used for lateral boundary conditions (LBCs) for the operational forecast using limited area model ALADIN (Aire Limitée Adaptation dynamique Développement InterNational) in the Meteorological and hydrological service of Croatia (DHMZ). Here an analysis is performed of the MCUF field for the LACE coupling domain for the period since 23rd January 2006, when it became available, until 15th November 2014. The MCUF field is a good indicator of rapidly moving pressure disturbances (RMPDs). Its spatial and temporal distribution can be associated to the usual cyclone tracks and areas known to be supporting cyclogenesis. Alternative set of coupling files from IFS operational run in ECMWF is also available operationally in DHMZ with 3 hourly temporal resolution

but the MCUF field is not available. Here, several methods are tested that detect RMPDs in surface pressure a posteriori from the IFS model fields provided in the coupling files. MCUF is computed by running ALADIN on the coupling files from IFS. The error function is computed using one time step integration of ALADIN on the coupling files without initialization, initialized with digital filter initialization (DFI) or scale selective DFI (SSDFI). Finally, the amplitude of changes in the mean sea level pressure is computed from the fields in the coupling files. The results are compared to the MCUF field of ARPEGE and the results of same methods applied to the coupling files from ARPEGE. Most methods give a signal for the RMPDs, but DFI reduces the storms too much to be detected. The error function without filtering and amplitude have more noise, but the signal of a RMPD is also stronger. The methods are tested for NWP LAM ALADIN, but could be applied to other LAMs and benefit the performance of climate LAMs.

Limited-area models (LAM) use higher resolutions and more advanced parameterizations of physical processes than global numerical weather prediction models, but suffer from one additional source of error - the lateral boundary conditions (LBC). The large scale model passes the information on its fields to LAM only over the narrow coupling zone at discrete times separated by a coupling interval of several hours. The LBC temporal resolution can be lower than the time necessary for a particular meteorological feature to cross the boundary. A LAM user who depends on LBC data acquired from an independent prior analysis or parent model run can find that usual schemes for temporal interpolation of large scale data provide LBC data of inadequate quality. The problem of a quickly moving depression that is not recognized by the operationally used gridpoint coupling scheme is examined using a simple one-dimensional model. A spectral method for nesting a LAM in a larger scale model is implemented and tested. Results for a traditional flow-relaxation scheme combined with temporal interpolation in spectral space are also presented.

Key words: Limited area model; Lateral boundary conditions; Coupling; Storms; Temporal interpolation ; Interpolation error; Fourier transform; Spectral coefficients; Phase; Amplitude

Table of Contents

Chapter 1

Introduction

Global numerical weather prediction (NWP) models cover the whole Earth. On the other hand, limited area models (LAMs) are computed over domains that cover only part of it and therefore require forecast lateral boundary conditions (LBCs). LAMs are used in NWP for a variety of research and specific operational applications. The known and major limitation of these LAMs is related to their LBCs (Warner et al. 1997). The LBCs are a unique and unavoidable aspect of LAMs that represents a significant limitation to their utility and application.

- The spatial and temporal resolution of LBCs is poorer than that of the LAM. The LBCs are interpolated in space and time.
- If LBCs arrive from another forecast model, then any error it has will propagate into the LAM forecast.
- The variations of the model fields on the scale of the size of the LAM domain and larger are prescribed by LBCs and do not interact with the LAM solution on the interior.
- The LBC formulation can produce inertia-gravity waves that propagate through the LAM domain.
- The differences in the formulations of the model that provides the LBCs and the LAM that uses them can result in spurious gradients at lateral boundaries that influence the forecast over the LAM domain.

The LBCs of LAMs have a significant impact on the evolution of the predicted fields through the propagation of boundary errors onto the interior of the domain. They are taken from lower resolution models that are run using with different formulations of dynamics and/or physics parametrizations. The numerical techniques used for interfacing the two grids inevitably generate errors that propagate through the LAM domain (Warner et al. 1997). The solution that is often recommended is to distance

the lateral boundaries from the area of meteorological interest. However, one should instead develop and use LBC formulations that generate minimum error in the LAM solution.

Frequently used terms

Host model is the model that provides the LBCs.

Guest model is the LAM that uses these LBCs.

One-way nesting refers to a situation where the LBC data is specified externally usually with data from an integration performed on a coarser grid and on a larger domain.

Two way nesting refers to a situation where the fine mesh model is dynamically coupled to the coarse mesh model to form a single dynamic system.

Coupling update interval/frequency is the time between two successive data files from the host model.

Coupling files/fields/data large scale data used for coupling.

1.1 The relaxation method

The most popular method for introducing large scale data into LAM is the relaxation method proposed by Davies (1976). The method is a pragmatic solution that allows for the large scale modes to enter and exit the LAM dimain (Figure 1.1) without spurious reflections.

The solutions of the global model and LAM can be different at the lateral boundaries. If the outgoing boundary is forced to zero, an outgoing wave will be reflected and produce small scale noise (Figure 1.2a). If the solution of the global model imposed at the outflow boundary is only slightly different, several modes of the outgoing wave are reflected (Figure 1.2b).

Finally, a relaxation scheme applied on a boundary zone eight grid-points wide using a linear profile of the relaxtion function α substantially reduces the amplitude of the reflected wave, while a *tanh* function profile of α removes the reflected wave (Figure 1.2c). In cases when the signal at the lateral boundary varies rapidly in time, temporal interpolation distorts the signal and reduces extremes (Figure 1.2d). This work wil mostly focus on the errors introduced by temporal interpolation of the LBCs.

The interior flow is relaxed to the external fully prescribed flow in the vicinity of the lateral boundary. The Davies (1976) method consumes gravity vawe energy,

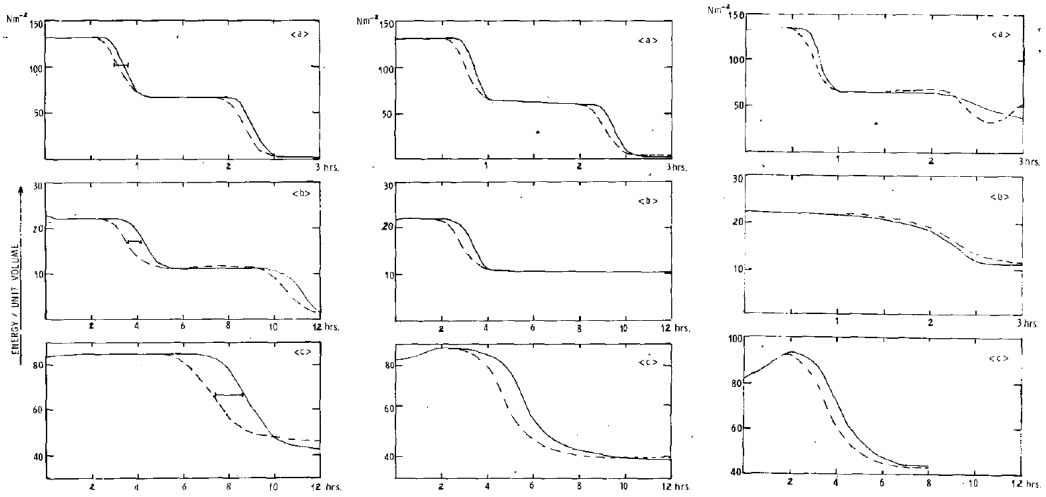

Figure 1.1: Evolution of the total perturbation energy per unit volume for (a) the external mode, (b) the first internal model and (c) the second internal mode in the case of ne shear (left), shear with (centre) and (right). The results are shown for the limited area domain with boundary relaxation (dashed) and the extended domain (solid line). The time needed for a particular mode to cross the boundary region is denoted by horizontal bars. From Davies (1976).

error and fine spatial scale PV near the lateral boundaries. The method gives an adequate representation of outgoing gravity waves and allows for transmission of geostrophically balanced flow out of the interior of the LAM domain.

If every field at every boundary point is supplied by the host model, then the mathematical initial-boundary value problem is ill-posed McDonald (1999). There is no well posed treatment of the primitive equations so pragmatic solutions of various kinds are used:

- over-specify the fields on the boundary and use assorted filters to control the noise are fairly well posed, waves exit LAM domain without false reflection,
- stretched coordinates are only pseudo LAM, the domain is in fact global, but with much higher resolution over the region of interest,
- interactive nested grid actually requires running a global model simultaneously.

For an operational LAM, one-way nesting is used with flow relaxation scheme of Davies (1976) (except for ETA model where Mesinger (1977) is used). Imposing u, v, and ϕ on all boundaries when solving shallow water equations in ill-posed problem (McDonald 1999). Over-specifying the boundary causes unphysical reflections which propagate errors back into the integration area. This can be avoided by discretizing in such a way that outflow boundary points are never used (e.g. upstream differencing scheme). The number of required boundary conditions is equal to the number

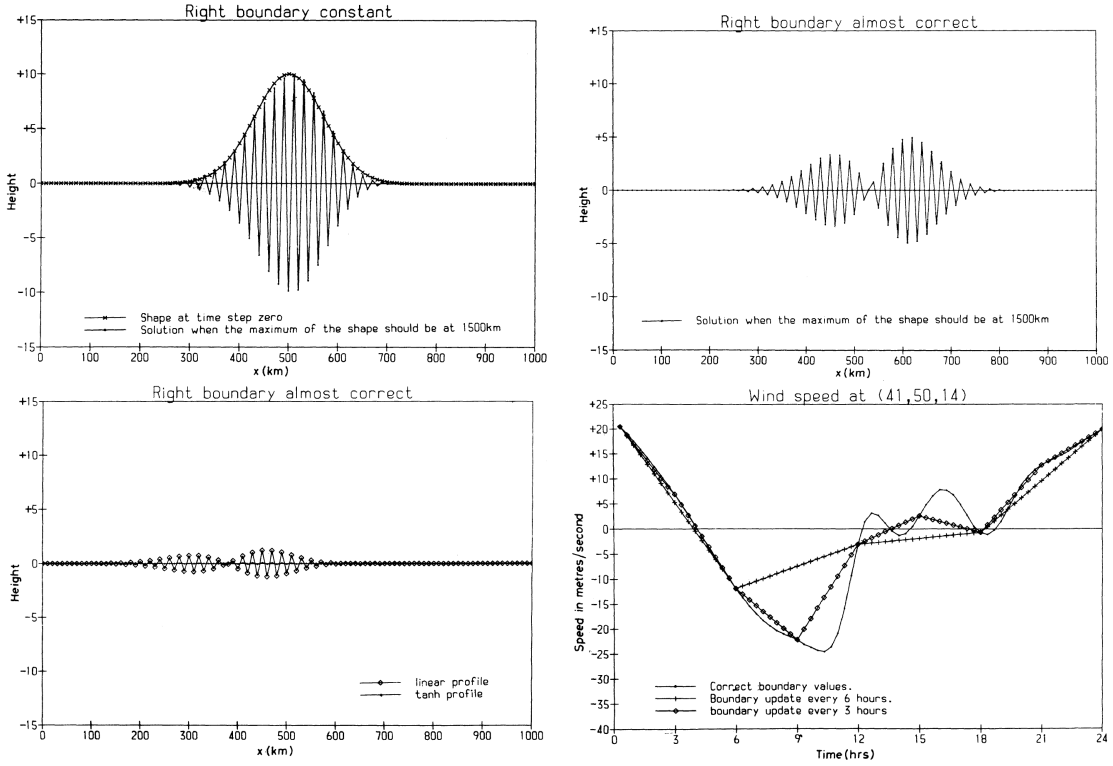

Figure 1.2: (a) The initial shape (line with x) that was advected from lef to right with $u_0 = 20m/s$ and after 13.89 hours (50000 sec) when it sould be outside the domain, at x=1500 km for an experiment when the RHS boundary is held constant and equal to zero. (b) The solution imposed at the right hand side changes in time so that it mimics the shape of a wave moving at speed of $u_1 = 18m/s$. This shows what happens when there is a small discrepancy in the evolution of the host and the guest model. (c) A relaxation scheme is used with a boundary zone of 8 gridpoints, using the linear (diamonds) and the tanh (dots) profile of α. (d) Plot of the grid-point value at level 14 of the westerly wind produced by the semi-Lagrangian integration of a primitive equation model with a 55 km resolution in the horizontal and on 16 levels in the vertical (line with dots). If this is a host model suplying the wind as boundary values to a finer mesh model, the actually used values for 6 hourly update (plus sign) and 3 houly update (diamonds) are shown. From McDonald (1999).

of inwardly directed characteristic velocity components - the negative eigenvalues of the diagonalized matrix of the equation system. Adding viscous terms increases the number of boundary conditions required for well posedness. Spurious reflections at the boundary, the consequences of the flow relaxation scheme, can be minimized by careful choice of the relaxation function and the width of the boundary zone.

$$\psi_i = (1 - \alpha_i)\psi_i^I + \alpha_i\psi_i^E \tag{1.1}$$

where

$$\alpha_i = 1 - tanh\frac{i-1}{2} \tag{1.2}$$

for $i = 1, ..., n$ with $n = 8$ minimizes false reflections of both gravity and Rossby waves and successfully transfers the external forcing to LAM.

The relaxation scheme applied to u and v destroys the geostrophic balance and creates false divergence and vorticity throughout the boundary relaxation zone (McDonald 1999). There are two possible solutions with the following drawbacks:

- relax the divergence toward that of the host model and get false vorticity, or
- relax the vorticity toward that of the host model and get false divergence.

Horizontal diffusion weakens the problem that arises due to over-specification. Another problem arises due to the incopatibility of orography between the host and the guest models. LBC forcing at low levels should be weak to minimize imbalances in the boundary zone fields due to incopatibilities in the model physics. This can yield spurious precipitation in the boundary zone.

Boundary errors eventually corrupt the whole forecast domain and the initial conditions become irrelevant. A sharply varying field (a front for instance) entering the LAM domain will be smoothed over the coupling interval (3 or 6 hours), rather than be a sudden phenomenon. The host model grid may be so coarse that it excessively smooths the information being supplied to the boundary (Caian and Geleyn 1997).

Usual tests of the effectiveness of boundary updating include:

1. run a global forecast with a coarse grid,
2. run a global model with a fine grid,
3. run the same model (!) on a limited area using LBCs from (1) and (2).

The difference between (3) and (2) is a measure of LBC flaws. The acid test (Staniforth 1997) states that a LAM solution should match larger scale model solution integrated over much larger area with similar resolution. One can see in the example

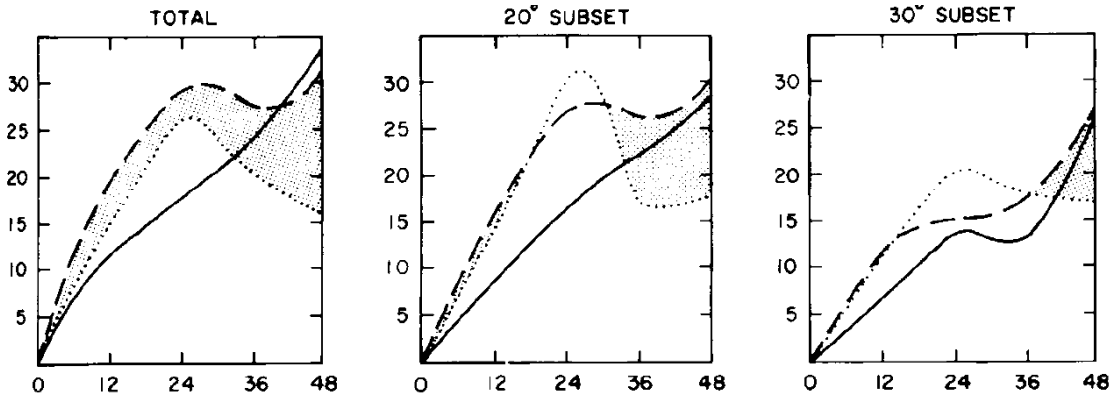

Figure 1.3: RMS 500 hPa differences (m) for the whole LAM domain (left), and subdomains that exclude 20^o (middle) and 30^o (right) of the lateral boundaries, between hemispheric simulation in 5^o and 2.5^o (full line), 2.5^o hemispheric simulation and 2.5^o LAM with 5^o LBCs (dashed) and 2.5^o LAM with 2.5^o LBCs (dotted). From Baumhefner and Perkey (1982).

(Figure 1.3) that the error computed as the difference betweein (3) and (2) depends on the extention of the LAM area that is used in the computation of the errors.

The errors are usually classified as:

Errors due to boundary formulation: LBC update every timestep with data from fine mesh global model. There should be no difference between an experiment with global model in fine mesh and LAM for the flow relaxation scheme.

Temporal boundary error: global model and LAM run on the same mesh, but the boundaries are refreshed (or used from) every Nth step.

The spatial boundry error: LBCs are refreshed every timestep, but LAM is using LBC from coarse mesh global model (and then compared to the results from the experiment using fine global mesh).

It is difficult to find quantitative information on the errors associated with the various nesting strategies. The cyclic environment of operational data assimilation worsens the situation since any LBC error is eventually spread over the whole domain. The iterative nature of 4D-Var helps spreading the LBC error through the domain. On the other hand, the host model information being supplied at LAM boundary could be regarded as observations with an error structure (Gustafsson 2012).

The LBC formulation produces only a small error and it is effectively transparent when there is no difference in temporal and spatial resolution between the LAM and the host model (Davies 2014). The hydrostatic approximation changes the form of partial differential equations. Therefore, for the hydrostatic primitive equations,

well-posed LBCs cannot be formulated (Oliger and Sundström 1978). But matching of LBCs at boundaties is more important than well-posedness (Davies 2014). Well-posedness is not completely out of reach for a hydrostatic LAM. It is also determined by the advection scheme used in the model. ALADIN System (Termonia et al. 2017) uses semi-Lagrangian advection that is up-wind and therefore satisfies the condition that LBCs are in fact prescribed only at inflow boundaries.

1.2 Further issues

1.2.1 Ensemble forecasting

In a LAM ensemble, if small perturbations are introduced to the initial conditions, but not the LBCs, the simulations do not diverge. The forecast that starts from the perturbed state remains close to the forecast that starts from an umperturbed initial conditions. The forecasts might even converge with time. When designing and implementing a regional ensemble data assimilation and prediction system, the LBC errors have to be represented and accounted for. Indivudual LAM members can use output from a global ensemble predictions system as LBCs. Otherwise, all members of a regional ensemble could use the same LBCs yielding an uderdispersive result. Alternatively, LBC perturbations can be constructed (El Ouaraini et al. 2015).

LBC constraints on a small-scale error variance growth are sufficient to cause uderdispersive LAM ensemble simulations. LAM ensembles remain uderdispersive even when using a complete set of LBCs from an external ensemble forecast. The small-scale constraints on error growth are present in any modelling system using coarsely resolved or temporally interpolated one-way LBC forcing. Errors in the buffer zone are the greatest near the midpoint of the LBC update cycle when respective linearly and nonlinearly evolving exernal and internal solutions are most incosistent (Figure 1.4). Once introduced, the LBC pulse errors continue to propagate inward and modify the LAM solution. The LAM solution becomes more infected with each successive error pulse, therefore the LBC inconsistency becomes stronger and generates larger errors that propagate farther inward (see Figure 1.4).

1.2.2 Data assimilation

The data assimilation problem is usually seen as a process to estimate the initial conditions for a NWP model. Model state contains scales that are too large to be resolved by LAM. The errors at these scales cannot be assessed properly by LAM. A LAM 3D-Var system differs from the large scale one due to use of scale-selective

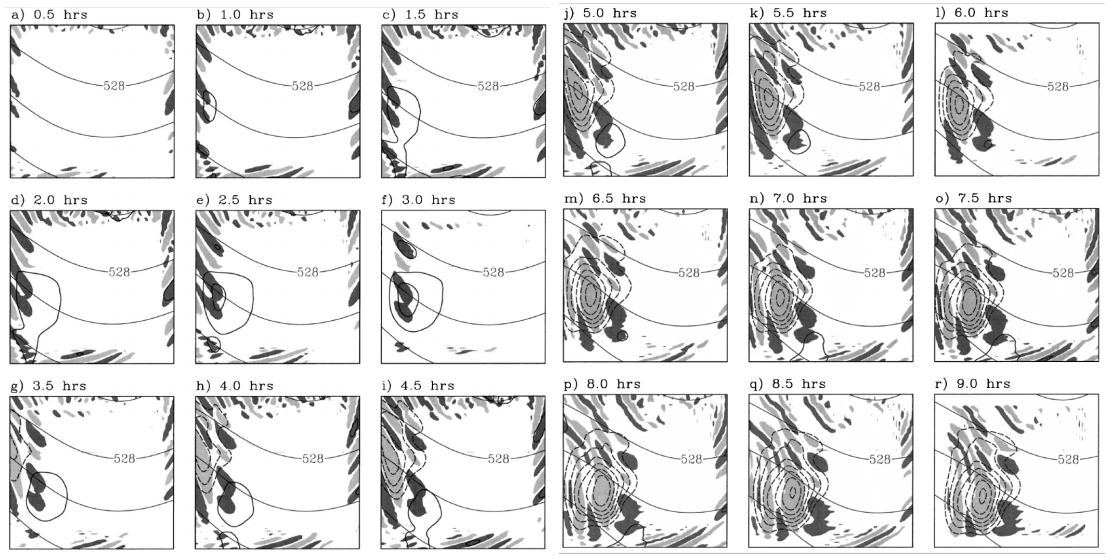

Figure 1.4: Streamlines from the host model run (curves, interval $12 \times 10^6 m^2/s$), vorticity errors exceeding $0.5 \times 10^{-5} s^{-1}$ (positive light, negative dark grey) and stream function errors (continuous for positive, dashed for negative, interval $5 \times 10^4 m^2/s$). From Nutter et al. (2004).

background error covariance models (Široka et al. 2003).

Using 3D-Var data assimilation cycle often means applying it to a global analysis. A minimization problem for a sum of three additive cost functions is obtained (Guidard and Fischer 2008). Resulting augmented information assimilation cycle produces first guess forecasts that are slightly closer to observations. More observations are kept during the quality control and assimilated in the subsequent analysis.

An explicit large-scale error constraint is applied. The large scale forecast errors can be handled by a large scale model providing the LBCs. Then the larger scales are constrained to the output of the large scale models during LAM 3D-Var (Guidard and Fischer 2008).

The LAM data assimilation can be extended to include LBCs during the data assimilation time window (Gustafsson 2012). The results of using the 4D-Var scheme that controls the LBCs show it can be important for cases when disturbance move quickly into or through the domain. A LAM 4D-Var data assimilation requires the tangent linear and adjoint version of the coupling scheme. A new lateral boundary control variable can be introduced and a 4D-Var cost function constraint. Alternatively, the model domain for the tangent linear and adjoint model can be extended.

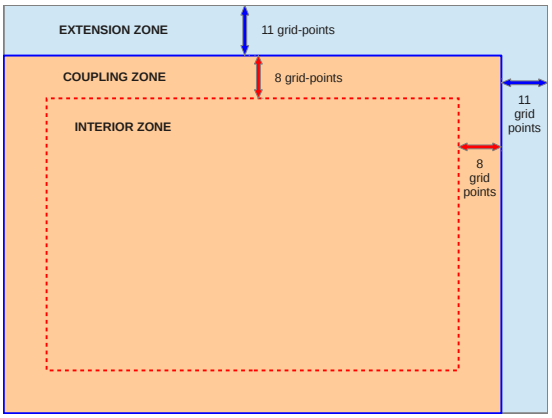

Figure 1.5: The zones of a LAM domain, the extension zone where the model field is modified to make the field periodic over the whole domain, the coupling zone where the fields are relaxed towards the large scale solution and the internal or central zone where we have the true LAM solution.

1.3 Implementation in the ALADIN System

ALADIN System is a bi-periodic LAM. The time dependent boundary fields are extended into a zone outside integration area in such a way that periodic fields are obtained (Haugen and Machenhauer 1993). Fields are made cyclic over an extended domain by relaxation to boundary fields that are smoothly connected in an extension zone outside the integration area (Figure 1.5). The number of gridpoints in the extended integration area is determined so that the nonlinear terms in the model equations will be computed without aliasing by the transform method using quadratic truncation: $J \geq 3M + 1$ and $K \geq 3N + 1$ where M and N are wavenumber truncations for the model variables and LAM uses an elliptic truncation where $\frac{m^2}{M^2} + \frac{n^2}{N^2} \leq 1$. Although energy of the small scale is controlled by the non-aliased spectral truncation of the non-linear terms, some energy might accumulate at the smallest resolved scales due to spectral blocking. Therefore, a weak numerical diffusion is applied at the end of each timestep.

1.3.1 Coupling procedure

A shallow-water spectral LAM that applies double Fourrier spectral representation on the model variables requires usage of time-dependent doubly periodic lateral boundary conditions (Haugen and Machenhauer 1993). The coupling procedure in the ALADIN System uses Davies (1976) scheme at the lateral boundaries. Relaxation is usually applied at the end of each time step and this is how it is done in a purely gridpoint LAM. Solving Helmholtz equation in spectral space is one of the major advantages of spectral models and requires the RHS of the Helmholtz opera-

tior to be prepared at the end of the gridpoint computations by evaluating the RHS of the semi-implicit equation:

$$(I - \Delta t L)\psi^{t+\Delta t} = \psi_{exp}^{t+\Delta t} + \Delta t L(\psi_{exp}^{t-\Delta t} - 2\psi^{t}) \tag{1.3}$$

where ψ is the model state vector, t is the current time-step, Δt is the time step, L is the linear operatior of the SI scheme, I is the identity operator and the subscript exp is for the result of the explicit computations (actually all grid-point computations).

Once the evaluation of the Helmholtz operator has started, the state variables cannout be coupled with LBC. The solution is to do the coupling in spectral space. But, there is no cheap solution for this because Davies (1976) type relaxation scheme is non-linear:

$$\psi^{c} = (1 - \alpha)\psi^{I} + \alpha\psi^{LS} \tag{1.4}$$

where α is the relaxation coefficient that varies in the horizontal, ψ^{I} is the state vector of LAM, ψ^{LS} is the state vector from the host model and ψ^{c} is the new LAM state vector after coupling. The problem has two solutions (Rádnoti 1995):

- do the coupling step at the begining of the grid-point computations
- after the RHS is computed, it is coupled with $(I - \Delta t L)\psi_{LS}^{t+\Delta t}$.

ALADIN System uses the latter solution and the boundary relaxation is performed in the gridpoint space after all the other gridpoint computations have been completed.

The relaxation function α varies from zero in the extension zone to one in the central zone:

$$\alpha = 1 - (p + 1)z^{p} + pz^{p+1}, \tag{1.5}$$

where z represents the distance from the extension zone and varies from 0 (in gridpoints at the edge of the coupling zone towards the extension zone) to 1 (in gridpoints at the edge of the coupling zone towards the central zone). The parameter p is a tuning parameter. The reflections at the boundaries are minimum for $p = 2.16$ (for a coupling zone 8 gridpoints wide).

1.3.2 Extension zone and bi-periodization

The bi-periodization of fields is accomplished by using splines in the experiments using ALADIN System performed in this Thesis. The alternative way of using **?** bi-periodization and coupling is briefly described later in the text. The field f_i with a dimension $i = 1, ..., n$ where n is the dimension of the whole domain (including

the extension zone) has physical values outside the extension zone, up to the point $m < n$. The gridpoints $m+1, ..., n$ are in the extension zone and filled with a continuous function in a way that makes the whole field periodic on the interval $i = 1, ..., n$. This is done using a spline function:

$$f(m+z) = a_0 + a_1 z + a_2 z^2 + a_3 z^3 \tag{1.6}$$

where

$$\begin{aligned} a_0 &= f_m \\ a_1 &= \frac{f_1 - f_m}{k} - \frac{k}{6}(2D_m + D_1) \\ a_2 &= \frac{1}{2} D_m \\ a_3 &= \frac{D_1 - D_m}{6k} \end{aligned} \tag{1.7}$$

where $k = n - m + 1$ is the width of the extension zone expressed in the number of gridpoints and

$$D_1 = \frac{3}{2+\lambda} \frac{2d_1 - \lambda d_m}{2-\lambda} \tag{1.8}$$

$$D_m = \frac{3}{2+\lambda} \frac{2d_m - \lambda d_1}{2-\lambda} \tag{1.9}$$

with $\lambda = k/(k+1)$. These are in fact smoothed versions of the following estimates of the second order derivatives in the points 1 and m:

$$d_m = \frac{2}{k+1} \left(f_{m-1} - f_m + \frac{f_1 - f_m}{k} \right), \tag{1.10}$$

$$d_1 = \frac{2}{k+1} \left(f_2 - f_1 + \frac{f_m - f_1}{k} \right). \tag{1.11}$$

The spline satisfies the condition of continuity in the points $i = 1$ and $i = m$. The second order derivatives satisfy the conditions $f''(m) = D_m$ and $f''(n+1) = D_1$.

The splines are applied in both directions on the horizontal. Finally, the resulting two-dimensional fields are smoothed in the extension zone using a filter:

$$\begin{aligned} f^s_{i,j} = &\frac{1}{4} f_{ij} + \frac{1}{8}(f_{i+1,j} + f_{i-1,j} + f_{i,j+1} + f_{i,j-1}) \\ &+ \frac{1}{16}(f_{i+1,j+1} + f_{i+1,j-1} + f_{i-1,j+1} + f_{i-1,j-1}) \end{aligned} \tag{1.12}$$

1.4 Alternatives to Davies (1976) method

In an overview of different pragmatic treatments of lateral boundaries in LAMs, Davies (1983) finds that:

Flow relaxation the prognostic variables are subjected to a forcing in a marginal zone that constrains them to relax towards the externaly specified field on a time scale that varies with the distance from the lateral boundary.

Diffusive damping scheme A straightforward approach to alleviate the noise problem generated in the vicinity of the lateral boundaries due to overspecification or inappropriate boundary data is to introduce a marginal zone of large diffusion of prognostic variables in the vicinity of the lateral boundaries.

Tendency modification scheme In the marginal zone, the tendencies are assigned a weighted average of the externally specified fields and the internall determined fields so that the externally specified fields become less important inward. Model variables are also subjected to a scale-selective spatial filtering procedure.

The pseudo-radiation boundary scheme There is no direct modification of the prognostic variables in the marginal zones, but only a direct specification of the variables at the lateral boundary itself.

Various pragmatic LBC schemes have underlying problems that should be considered before their implementation and refinement as well as when interpreting model results. ETA model solution is to use all fields at inflow, all at outflow, except velocity tangential to boundary, and use upstream advection scheme close to the boundary that causes significant damping. Therefore this is in fact a boundary damping zone.

Variable resolution (Côté et al. 1993, 1998) solves the LBC problem in such a way that limited region in high resolution is surrounded by region of low resolution with intermediate zone where the resolution changes gradually.

Robert and Yakimiw (1986) study a problem associated with the specification of lateral boundaries in LAMs through usage of linearized non-divergent barotropic vorticity equation in one-dimension. A pillow forms on the inflow boundary, both for one-dimensional vorticity equation and for the shallow water equations.

Juang and Kanamitsu (1994) develop a regional spectral model that predicts deviations from the global model forecast and avoid LBC nesting used in most regional problems. However, they stil have to reduce the perturbation on the lateral boundary. Experiments with longer nesting periods have less noise in the mean sea level pressure field along the lateral boundaries than those with shorter nesting

periods. No noise was found for precipitation field. But, this noise could also be valuable high resolution information. The lateral boundary relaxation is performed over the whole domain for the dynamical part of the total tendency. Additionally, they blend the total tendency over the entire regional model domain to satisfy the assumption that perturbations approach zero along lateral boundaries. But, this was found unneccessary, since it works in the same way as blending.

Juang and Hong (2001) evaluate performance of a regional spectral model on different domain sizes and horizontal resolutions on a case of winter cyclogenesis with propagation of synoptic scale disturbances thorugh lateral boundaries. The results on smaller domains were found much closer to the base field, although they generated higher resolution features than the base fields. Domain nesting is introduced in physical space over the entire domain through injection of the coarse grid information, while spectral nesting is introduced in the spectral space. The treatment of the lateral boundaries becomes the pure lateral boundary noise reduction. Their resutls show that:

- it is not necessary to have a large domain in order to avoid lateral boundary influence and
- multinesting is not neccessary in order to have a very fine resolution forecast over a small domain.

Laprise (2003) identifies scales resolved by LAM and their non-linear interactions less accurate in LAMs than in global models. LAMs do not resolve very large scales that are not periodic on the LAM domain. The assignment of the values on the lateral boundaries is neccessary to represent scales too large to be periodic on the LAM domain. The LBCs contain information at lower temporal and spatial resolution. It takes time and space for a LAM to generate the higher resolution information (Denis et al. 2002, 2003; Laprise 2008).

Transparent boundary conditions

McDonald (2000) explores the problem of LBCs in a semi-Lagrangian model when the origin point of the trajectory lies outside the domain. To thest this, a bell curve of width $L/10$ is advected along the x axis (L is the length of the domain).

Search for well-posed boundary conditions for the initial-boundary value problem using semi-Lagrangian discretization starts in McDonald (2000), where three options are found to be stable:

- trajectory truncation - if departure point is outside the boundary, truncate it to be at the boundary,
- time interpolation - between two timesteps,

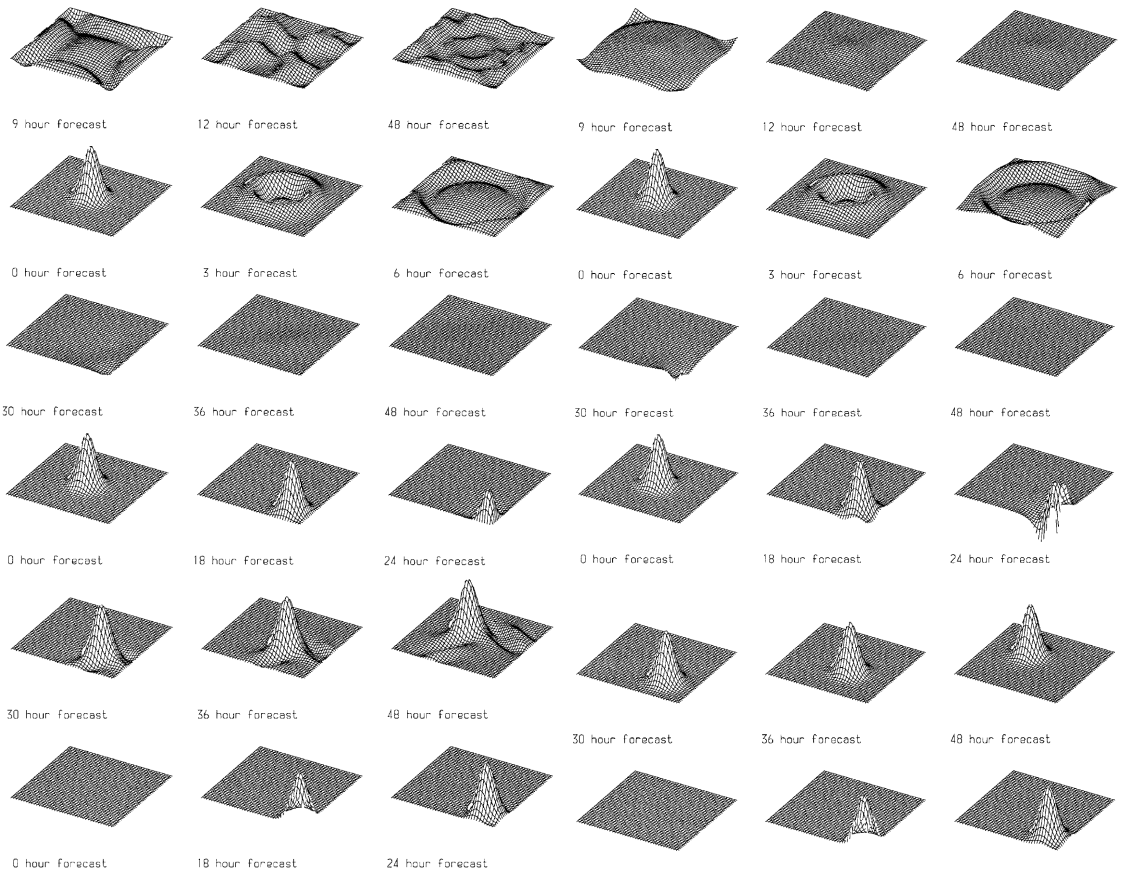

Figure 1.6: The adjustment of a bell shape when imposing (a) ϕi and (b) $\phi - \sqrt{\phi_0} v_N$ on the boundaries. The advection of a bell shape out of the area when imposing (c) ϕ and (d) $\phi - \sqrt{\phi_0} v_N$ on the boundaries. The advection of a bell shape into the area when imposing (e) ϕ and (f) $\phi - \sqrt{\phi_0} v_N$ on the boundaries. From McDonald (2002).

- well posed buffer zone using extrapolation with Taylor series.

Only a subset of all variables should be imposed on the boundaries. The initial-boundary-value problem is well posed if this subset has been chosen correctly. Using Davies (1976) scheme, we overspecify the boundaries and damp the resulting noise with a relaxation scheme.

McDonald (2003) derives an alternative to Davies (1976) scheme that considers transparency and well posedness and tests it for the shallow water equations. A system can be well posed and simultaneously reflect all waves from the boundary.

Transparent boundaries mean that all waves exit LAM comain without reflection and enter without their amplitude and phase being changed as well as without exciting spurious hign-frequency noise.

The boundary conditions are incorporated into equations that describe unidirectional waves yielding transparent boundary conditions (McDonald 2002). The

linearized shallow water equations are dicretized using semi-Lagraingian approach and tested on:

- adjustment waves radiating out of the area (Figures 1.6 and **??**),
- geostrophically balanced disturbance advected in (Figures **??** and **??**), and
- geostrophically balanced disturbance advected out (Figures **??** and **??**).

Three types of boundary conditions were imposed, all are stable, but the first one reflects waves much more than the other two. The semi-Lagrangian discretization increases the time-step and causes deterioration in accuracy.

More accurate mathematical techniques for imposing the LBCs in spectral models are a matter of research (Termonia and Voitus 2008; Voitus et al. 2009).However, so far one has not been able to find a better method than the Davies scheme. Therefore, the present work is based on the Davies relaxation.

Spectral coupling

Radu et al. (2008) studies implementation of a spectral coupling method to a recgional climate model (RCM) with an aim to prove that RCMs are able to maintain the large-scale circulation of the driving GCM and modify only the small scales. Spectral coupling (or spectral nudging) is seen as a solution to overcome LBC limitations:

- Spectral nudging method is able to avoid the deviation of RCM from the GCM in large spatial scales for stationary and transient parts.
- It artificially increases intense precipitation events when humidity is not relaxed.
- Possibly missing large-scale information is provided to the RCM and removes some imbalances that result from the specification at the lateral boundary.
- Large scale features that develop in the RCM differently than in the GCM solution that is imposed at the boundaries is seen as the problem and it is solved by using spectral nudging.

Just as the method of flow relaxation (Davies 1976) does not remove all the false reflections of the wave from the outgoing boundary, it is also plausible that using the spectral coupling the energy reflects back to the waves it came from preventing the usual energy cascade.

1.5 Detecting the temporal interpolation problem

There are numerous weaknesses of a LAM forecast caused by the LBCs, and overview was provided by Warner et al. (1997). The quality of the temporal interpolation of lateral boundary coupling data for LAMs needs improvement. A LAM user who depends on LBC data received from elsewhere or stored on storage of limited capacity can find the usual schemes for temporal interpolation of LBC data of unsatisfactroy quality. The quality of LBC data for operational as well as research purposes is severely restricted in its amount because of limited storage and data transfer capacity. Large scale fields are usually available in temporal resolutions of several hours, but they are needed at each LAM timestep. Consequently, LBCs are computed at every LAM timestep using large scale fields that are interpolated in time. This corrupts the fields, especially those modes that have timescales shorter than the coupling interval. The situation can be made even worse when the most popular of all coupling procedures (Davies 1976) is used, since the fields are taken only from the narrow area close to the edge of the domain. Consequeently, small scale features that are quick enough to enter the domain during one coupling interval are not suitably represented by the interpolated data. The time interval between the two subsequent coupling files containing LBC data is refered to as the coupling interval. Its choice is usually based more on technical limitations of storage and/or data transfer than on scientific facts.

The problem was thorughly analyzed in Termonia (2003) for a case of rapidly moving storm entering the operational forecast domain of ALADIN Belgium. In Termonia (2003), it is investigated how the quality of the temporal interpolation of lateral-boundary coupling data for limited-area models (LAMs) can be improved or kept under control, while increasing the data transfer between the coupling and the coupled model only marginally. This problem is approached from the point of view of a user of a LAM who depends on coupling data that is received from elsewhere. Lateral boundary conditions are usually interpolated linearly in time, but this smoothes the temporal evolution of the field. A large scale model forecasts the storm and the spatial interpolation procedure keeps it. As a consequence of linar temporal interpolation and temporally sparse data, LAM receives wrong (distorted) information at the lateral boundaries and produces a wrong solution. If the input LBC data were available in higher temporal resolution, the particular storm would be forecast.

The temporal interpolation can be corrected using the higher-order time derivatives of the fields. However, these time derivatives have to be computed somehow, and in Termonia (2003) they are estimated by a one-time-step integration well enough to be useful.

This procedure also allows the user of a LAM to formulate a criterion to decide operationally in which situations the quality of the linear interpolation will be unacceptable. A dimensionless estimate of the truncation error of the linear interpolation can be computed:

$$e_T = \frac{1}{4}\left|\frac{]F'(t_2) - F'(t_1)]\,(t_2 - t_1)}{F(t_1) + F(t_2)}\right| \tag{1.1}$$

The linear interpolation is safe to use if $e_T \ll 1$, but the critical value should be determined on physical grounds. The maximum value of e_T over the model domain is E_T.

The idea has been implemented in a numerical weather prediction limited-area model ALADIN, and has led to a substantial reduction of the errors of a forecast of one of the French Christmas storms in December 1999. The fields are usually initialized using digital filter initialization (DFI) after spatial interpolation. But, this procedure is computationally demanding to be used operationally for each file containing forecast LBCs. It is usually done for the initial conditions only. Therefore, the truncation error was computed for experiments when the fields were filtered with DFI and without filtering. The signal of a rapidly moving storm is clear in both sets of experiments.

1.5.1 Monitoring of the coupling-update frequency

The coupling update frequency - the time interval between the two coupling files - from a large scale model that are used for LBCs, are usually available with an interval $\Delta t = 3h$. On the other hand, the large scale model timestep is $\delta t = 5 - 10min$. Termonia (2004) computes the information loss caused by infrequent availability of LBCs. The problem is approached as a problem of undersampling. The coupling-update frequency can be monitored by using a digital recursive filter in the large scale model.

The Nyquist frequency of the original time resolution is $\omega_N = \frac{\pi}{\delta t}$. But small scale LAM will receive data with a new Nyquist frequency $\Omega_N = \frac{\pi}{\Delta t}$. Therefore, all the information contained in modes with frequencies larger than Ω_N is lost. The information loss is computed in the time domain by means of a high-pass filter with a pass band for all the frequencies $|\omega| \geq \pi/\Delta t$, having a frequency response function of 1.

Different modes will be affected by the time interpolation in different ways. The mode $c(\tau)$ moves in time along the unit circle from 1 to $c(\Delta t)$ (Figure **??**). A mode with frequecy $|\omega| \leq \pi/\Delta t$ is dampened by the interpolation, and loses $1 - cos(\omega\Delta t/2)$ of the amplitude (Figure **??**a). A mode with $\pi/\Delta t \leq \omega \leq 2\pi/\Delta t$ is completely corrupted and the interpolation creates the opposite phase (Figure **??**b).

The filter is applied to the field the surface pressure only. In principle, it should be applied to all model variables (in 3D). That would be really computationally expensive. Therefore it is applied only to the logarythm of the surface pressure field $\Pi = \ln P_s$ (that is in 2D). In case of a Christmats storm of 1999, the storm was moving rapidly through the domain of ALADIN France (Figure **??**). It passed through ALADIN Belgium domain (drawn as a square in Figure **??**) in less than 9 hours. The filtered surface pressure field (Figure **??**) clearly shows the position of the cyclone, but with a delay of 90 minutes (half the coupling update interval). The filter is applied to a spectrally truncated field that contains only large scales. This is less computationally demanding and reduces noise (Figure **??**). Finally, the filter shows a signal when there is a storm propagating rapidly through the domain (Figure **??**) and this signal is reduced for increased coupling update frequency.

1.6 Fixing the rapidly moving storm problem

Once a storm enters the LAM domain too rapidly to be properly modelled using the existing LBC procedure, one can apply one of the following cures:

- boundary error restarts,
- gridpoint nudging,
- the windowing method.

These methods are computationally expensive and one wishes to use them only when needed, so a method to detect rapidly moving storms in the LBC data is still needed. This Thesis also presents an alternative temporal interpolation method applied on a simple problem.

1.6.1 Digital-filtering initialization

The initial state of an atmospheric model is usually unbalanced (Lynch and Huang 1992). The same can be said for a large scale field interpolated to a guest LAM grid. First, the large scale fields (Figure **??**a) are interpolated to the new grid. This creates mountain waves (compare Figure **??** a and b). If the unbalanced field is used as initial state for a model run, high intensity inertia-gravity waves will be generated in order to adjust the state to an equilibrium.

Digital-filtering initialization (DFI) of atmospheric models relies on the fact that the gravity-inertia waves have higher frequencies than the meteorologically relevant rotational modes and assumes that a frequency exists that separates them (Lynch 1997).

The filter is applied in the diabatic DFI scheme (Lynch et al. 1997). First an adiabatic backward integration is performed from time zero to $-T_{span}$. The fields are filtered to obtain the model state at time $\frac{1}{2}T_{span}$. Then, a diabatic integration forward up to $\frac{1}{2}T_{span}$ is performed. The fields are filtered again to obtain a new filtered model state at time zero.

Therefore, one uses DFI to clear these waves, artificially created by the interpolation. But the storm looses much of its intensity (Figure **??**) for both Dolph-Chebyshev (Lynch 1997) and Lancozs filter.

Termonia (2008) shows that a Doppler effect of fast-propagating storms may shift the frequencies of the small-scale rotational modes into the frequency categories that are deemed to be the ones of the gravity-inertia waves. The Doppler effect is that an observer that is observing a monochromatic wave of wavenumber κ that oscillates with frequency ω moving at a speed c will observe a frequency $\omega + c\kappa$ that is shifted from the original frequency.

The impact of this effect in DFI manifests itself to a substantial extent in a case of a forecast of a rapidly propagating storm (i.e., a reduction the depth of the eye of the storm by about 6-7 hPa).

As a cure, in Termonia (2008), it is proposed to make the filtering scale selective by filtering the large spatial scales more than the small ones. The scale selective filter leaves the storm almost intact, and leads to a more balanced initial state.

1.6.2 Boundary error restarts

Global models run with timesteps of about 10 minutes, but the LBC data are provided usually with an interval of 3 hours. Te operational LAMs are usually run with timesteps of 1 to 5 minutes. Athough LAM uses data with 1 min interval, this time series does not contain any meaningful meteorological/physical information on time scales shorter than 3 hours.

In the current operational practice, the coupling update frequencies of the LBC data are usually determined by technical constraints, such as data transfer and storage capacity. The required temporal resolution of the lateral boundary conditions is quantified in Termonia et al. (2009) using the time scales of cross-boundary fluxes. In standard forecast cases, coupling updates of about 3 h are sufficient for a mesoscale LAM of 7-9 km horizontal resolution. The same coupling interval can lead to errors in the coupling data of about 10 hPa in rare cases of severe storms. But, one should update the coupling fields with the period equal to the host model time step. This is not feasible in most existing operational applications.

The forecast of the storm can be substantially improved by restarting the model run. Since the coupling files contain spectral coefficients and therefore data over the

whole domain. The forecast can be resumed using data from the coupling files as the initial conditions. The fields are first interpolated to the guest model grid and initialized by the SSDFI. The time when the model forecast run should be stopped and re-started from the LBC data can be determined from the MCUF field.

What is the temporal resolution of LBCs needed to adequately represent the signal in the surface pressure and other atmospheric fields? First, the time series of the host model output is resampled in a low temporal resolution with a time interval T. Then a time series of the higher temporal resolution is recreated using a time step of the LAM. The error for the surface pressure field with 3 hourly coupling update interval can be 11.5 hPa (Termonia et al. 2009).

For this particular case, hourly coupling update interval would produce an error of 4 hPa, and an error lower than 1 hPa could be achieved using coupling update interval of about 15 minutes. This means that a global model should produce LBC files every model timestep.

Other model variables, such as temperature and wind requre similar coupling update intervals in order to keep the errors below 1 K and 5 m/s respectively (Figure **??**). The information lost by the temporal interpolation is $1 - cos(\pi f T)$ while all the information is lost for the modes in the frequency band $|f| \geq \frac{1}{2T}$. Therefore, the information loss due to sampling and interpolation can be quantified as and implemented as a recursive digital filter.

A second-order Butterworth filter is applied to the logarythm of the surface pressure in ARPEGE. A solution to the problem can be to restart the model from the interpolated LBCs once the feature is inside the domain (Termonia et al. 2009). However, then the small scale information gained by LAM is lost. The problem is particularly annoying if the operational suite uses data assimilation, especially if the storm enters the domain during the cycling period (between the two analysis times, in the first 3 or 6 hours).

1.6.3 Gridpoint nudging

An operational high-pass filter of the surface pressure field is used to detect and to localize a propagating storm in the global model ARPEGE. This information is subsequently used to locally reinject the available uncorrupted storm in the coupled model (Termonia et al. 2011). Gridpoint nudging is applied to the surface pressure in a subarea of the domain, limited to a region around the eye of the depression. This restores the strength of the storm, while keeping the model state in the rest of the domain.

1.6.4 The windowing method

Regional spectral models have previously periodized and blended limited-area data through ad hoc low-order schemes justified by intuition and empiricism. Boyd (2005) uses the same functions to make fields periodic and couple them the the large scale solution. These windowing functions are infinitelly differentiable and based on a Fourier extension method of the LAM domain. Periodicity and blending are ensured and the high-order Fourier spectral accuracy is preserved. It was first applied to a simple problem of one-dimensional Burgers' equation discretized using an Eulerian explicit scheme (Boyd 2005).

However, these tests hardy prove the applicability of the method in a full three-dimensional NWP model. Operational NWP models use timesteps substantially larger than those imposed by the Courant-Friedrichs-Lewy (CFL) limit. The windowing based formulation was implemented in the ALADIN System (Termonia et al. 2012).

A windowing function B is defined in such a way that $B = 1$ on the physical doman and $B = 0$ in the extension zone.

$$B = \begin{cases} 0 & \text{for} |x| \geq 2\theta - \chi \\ \frac{1}{2} + \frac{1}{2} erf[\frac{L}{2} \frac{(2\theta - \chi - |x|) - (|x| - \chi)}{(2\theta - \chi - |x|)(|x| - \chi)} & \text{for} |x| \leq 2\theta - \chi \text{and} |x| \geq \chi \\ 1 & \text{for} |x| \leq \chi \end{cases} \tag{1.2}$$

where L is a tunable parameter and erf(x) is the error function. All derivatives of B are zero at the boundaries of the coupling zone. Inside the coupling zone, B changes from zero to one as a continuous function. One can use the erf function as proposed by Boyd (2005) or the α function. The periodization procedure is achieved by multiplying function f with the function B. The coupling zone and the extension zone can, but do not have to, overlap.

ALADIN System uses semi-Lagrangian advection that allows time steps much longer than the CFL limit. The semi-Lagrangian scheme can propagate errors quickly and deeply into the physical domain. This effect is limited if the extension zone and the coupling zone do not overlap.

The bi-periodization of the fields is performed during the preparation of LBCs based on the data from the large scale model. When semi-Lagrangian advection is computed, some origin points are situated outside the LAM domain and therefore truncated. However, this truncation is no longer neccessary, when using the Boyd scheme, since the data near the edges of the extension zone are almost physical. This depends on how deeply semi-Lagrangian trajectories penetrate into the extension zone.

The experiments in Degrauwe et al. (2012) are carried out for an extension zone

of 12 and 48 points. The error measures are computed over the domain with respect to the host model:

- RMSE of geopotential ϕ, and
- the absolute divergence.

The absolute divergence is a measure for the erroneous (gravity) waves generated by the periodization.

Bi-periodization using windowing method gives better results than the spline method in the ALADIN System. However, there was no difference in results using the erf function and the α function. Overlapping the relaxation and the extension zones was detrimental for the forecast using the ALADIN System. The improvements are demonstrated for cases when a storm propagates quickly into the domain interior. However, this is not evident in the scores computed over a longer validation period.

Chapter 2

Methods for automatized detection of rapid changes in lateral boundary condition fields for NWP limited area models

2.1 Introduction

Operational lateral boundary conditions (LBCs) are provided to limited area models (LAMs) at a time interval of several hours, refered to as the coupling update period. These data are used at lateral boundaries of the LAM domain every LAM time-step of several minutes. Consequently, LBC data of the large scale model are (linearly) interpolated in time. The interpolation procedure distorts the model fields and can lead to LAM forecast failures in case of fast propagating storms. The problem of linear interpolation of model fields in time for cases with rapidly moving storms that enter the LAM domain is expected to become worse as both global models and LAMs move to higher resolutions. These storms are associated to rapidly moving pressure disturbances that will be refered as RMPDs in this text. The problem could be even more pronounced in climate LAM's that couple to large scale data that are available with a longer interval.

One needs LBC data to represent scales that are too large to be periodic on LAM domain (Laprise 2003). Various schemes for treating LBC data suffer from different problems (Davies 1983). Model errors propagate from the lateral boundaries through the domain during the forecast time (Nicolis 2007), these errors amplify and spread further with longer time of integration (Nutter et al. 2004). A large LAM domain was recommended (Staniforth 1997) to prevent boundary induced errors from propagating to the area of interest. However, there are problems that can not

be cured by making LAM domain larger (Vánnitsem and Chome 2005). For an overview of issues related to LBCs, see Warner et al. (1997).

Regional climate models are expected to develop small scale features due to high resolution surface forcings, nonlinearities in atmospheric dynamics and hydrodynamic instabilities (Denis et al. 2002). Large coupling update interval can make LBCs act as a filter of small scale features that (should) enter the LAM domain. Climate LAM without small scale information in the initial conditions and LBCs develop small scale variance even in the absence of surface forcing due to nonlinear cascade of variance (Laprise 2008), but it takes several days.

Currently, there are two sets of LBC data that can be used for operational forecast using ALADIN (ALADIN International team 1997) (Aire Limitée Adaptation dynamique Développement InterNational) LAM in Meteorological and Hydrological Service of Croatia (DHMZ). One is from global Integrated Forecast System (IFS) of the European Centre for Medium-Range Weather Forecasts (ECMWF) and another is from the global model Action de Recherche Petite Echelle Grande Echelle (ARPEGE, see eg. Cassou and Terray (2001)) of Meteo France. The LBCs from the global numerical weather prediction (NWP) models ARPEGE and IFS are operationally provided with a 3 hour interval. These are used for running the operational ALADIN forecast in 8 km resolution (Tudor et al. 2013). Coupling is performed along the lateral boundaries in the 8 gridpoints from domain edge by means of Davies (1976) coupling scheme and using linear interpolation in time of the input fields from the global model.

Termonia (2003) has analysed the Lothar storm (Wernli et al. 2002) and found that the three hourly coupling update interval is insufficient for resolving the storm in lateral boundaries. Also, Davies (2014) finds that 3 hourly LBCs lose information for 12 km resolution LAM coupled to 12 km resolution large scale model (see Figure 5c in Davies (2014)). In order to monitor the occurrence of potential LAM forecast failures due to insufficient coupling update frequency, a recursive high-pass filter (Termonia 2004) has been implemented to the ARPEGE model and applied to the surface pressure field. The filtered surface pressure field is refered to as monitoring of the coupling update frequency (MCUF) field. Large values of the MCUF field indicate a RMPD in the surface pressure through that model grid point. A value larger than a threshold value suggests that a fast cyclone has moved through the area.

The MCUF field is provided since 06 UTC run on 23^{rd} January 2006 in the coupling files from global model ARPEGE, run operationally in Meteo France, for the common coupling domain used for LBC data in 6 countries (Austria, Croatia, Czech Republic, Hungary, Slovakia and Slovenia). This common domain will be refered to as the LACE domain (Limited Area for Central Europe). The horizontal

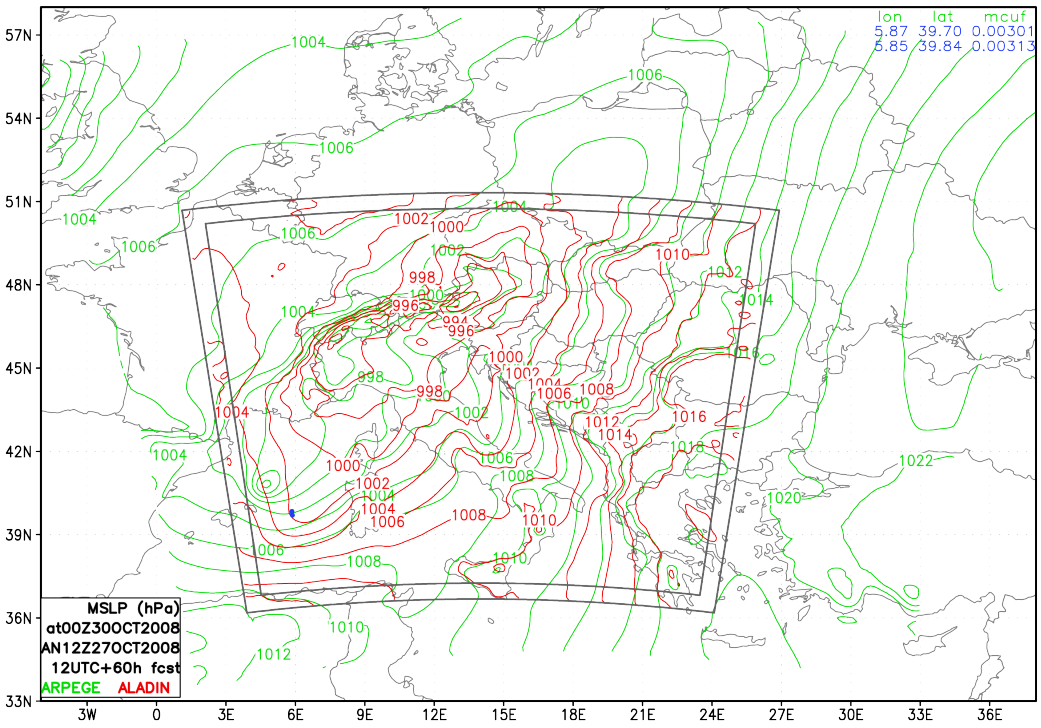

Figure 2.1: Mean sea level pressure (hPa) from ARPEGE (green) and ALADIN (red) operational 60 hour forecast starting from 12 UTC analysis on 27^{th} Oct 2008. The coordinates and values of MCUF field exceeding the 0.003 threshold are listed in the upper right corner and plotted as blue dots on the map.

Table 2.1: Model (ARP-ARPEGE), period (form 06 UTC on first date to 00 UTC on the last date), horizontal resolution and total number of the coupling files for which the rapid changes of surface pressure field were analyzed, the field was used received from Meteo-France and computed by ALADIN for files received from ECMWF. The rapid changes in surface pressure for the first 3 hours were ommited from the analysis due to evidence of model spin-up for some periods.

model	period (from-to)	resolution (km)	total num of files	whole > 0.003	domain > 0.004	MCUF > 0.005	> 0.003 cpl zone
ARP	23Jan2006 – 06Feb2008	20.678	64292	906	270	93	235
ARP	06Feb2008 – 11May2010	15.400	72600	1017	383	141	400
ARP	11May2010 – 16Nov2014	10.610	151756	1122	293	125	243
ARP	23Jan2006 – 16Nov2014	all	288648	3045	946	359	878
ARP	01Nov2010 – 16Nov2014	10.610	129674	995	259	108	186
IFS	01Nov2010 – 16Nov2014	15.400	147350	698	178	67	109

resolution of the LACE coupling domain provided from ARPEGE has changed over the years (see Table B.1) but the aerial coverage of the LACE coupling domain provided from ARPEGE remained te same (see the aerial coverage of the green isolines in Figure 2.1). Local operational domains are smaller than the LACE domain, but have higher horizontal resolution and have coupling zones 8 gridpoints wide along lateral boundaries. If the point with the large MCUF value is inside the coupling zone of the ALADIN domain, it can be expected that the ALADIN model run will miss the cyclone strength due interpolation of boundary data in time. These events are expected to be rare, at least according to the analysis performed on one year of data for the Belgian domain (Termonia et al. 2009). But rapid changes in surface pressure are associated to the most intensive storms moving rapidly, pose a threat to the public and require warning. It is very important that operational NWP models forecast such events. The frequency of such events is analysed for the LACE domain on almost 9 years of data from the operational ARPEGE fields (since 23^{rd} January 2006 until 15^{th} November 2014).

The most obvious solution to this problem is to increase the frequency of the available LBC data and most of the centres that run both global models and LAMs use hourly input fields for the LAMs. However, this solution is not very practical for the meteorological services that run only LAMs and rely on LBC data from somewhere else. On the other hand, if 3 hourly data is insufficient for global model run in roughly 16 km resolution and LAM in 8 km resolution, then hourly data would be less satisfactory when both global model and LAM move to higher resolutions (as was already announced at various meetings in 2014). Also, running old cases from stored archive data requires using LBCs with 3 hours interval.

There are other solutions proposed to solve the problem of errors in LBCs caused by time interpolation of fields. The first one (Termonia et al. 2009) is to restart the model forecast from the coupling file when the storm is inside the domain using the scale selective digital filter initialization (Termonia 2008). The second one is to insert the storm by means of gridpoint nudging (Termonia et al. 2011). Both of these require to stop the model run, insert the storm artifically and continue the model run from there. Using corrected interpolation with time derivatives (Termonia 2003), Boyd's periodization method (Boyd 2005; Termonia et al. 2012) can also improve the forecast (Degrauwe et al. 2012), and alternative methods of interpolating LBC data in time (Tudor and Termonia 2010) do not require restarts, but are computationally expensive, so these would also be used only when needed. However, in order to apply any of these solutions, we should first detect the RMPD in the fields used on lateral boundaries.

Using MCUF implies that the global model computes it operationally and distributes the field in the output files together with the other forecast fields. However,

LAM can be coupled to various global model forecasts or larger scale LAMs for operational forecast, and re-analyses for climate model studies or simulations of specific phenomena. With the exception of ARPEGE, global models do not provide a field that would diagnose rapid changes in pressure that occured in each grid-point during a time interval between two consecutive output files. The centers that provide global model fields could be discouraged to compute MCUF field due to computational cost and potentially complex implementation in the model code, and especially to re-run the re-analysis cycles to provide such data for studies of historical weather. It is therefore usefull to detect RMPDs a posteriori using the standard meteorological fields usually provided in model output. The method should enable automatic detection of a RMPD to be usefull in the operational forecast as well as in the climate simulations using LAM. Fast-moving disturbances in the upper layers of the atmosphere or inertia-gravity waves are more common. These are also a source of error in LAMs while MCUF detects disturbances only in the surface pressure. The focus of this chapter are rapidly moving disturbances in surface pressure, but a method that detects them could be applied to an upper level field.

LAMs used for simulations of climate use input LBCs that are available in coupling update interval of 3 hours or more. Simultaneously, LAMs tend towards higher horizontal resolutions. A number of climate studies has been performed (Hamdi et al. 2012; De Troch et al. 2013; Hamdi et al. 2014) using ALADIN in combination with ERA40 (Uppala et al. 2005) and ERAInterim (Dee et al. 2011) datasets for LBCs. These applications would also benefit from a method that would detect RMPDs a-posteriori from the standard meteorological fields used for LBC.

The NWP suite at DHMZ is focused on forecasting weather on the area of Croatia. Cyclones that affect that area often originate from western Mediterranean and Adriatic. That area is recognized as a particularly active region with respect to cyclones (Campinis at al. 2000; Alpert et al. 1990). Severe precipitation events occur when cyclone produces convergence of the moist air and a large quantity of precipitable water (Lionello et al. 2006). Western Mediterranean experiences flash flood events that arise from extremely high rainfall rates (Doswell et al. 1996).

The MCUF field is not provided in the LBC files of IFS provided by ECMWF. On 1^{st} January 2014 the operational ALADIN forecast in DHMZ has switched to using IFS coupling files. It is possible to compute MCUF field by running ALADIN on the resolution and domain of the coupling fields. Here an analysis is performed of the MCUF field computed by running ALADIN for the common LACE coupling domain for the files provided from IFS since 27^{th} October 2010 until 15^{th} November 2014. Otherwise, it is possible to estimate the error that arises due to linear interpolation of LBC data in time (Termonia 2003) from model tendencies obtained by running ALADIN for one time step. The error was estimated for surface pressure

and mean sea level pressure using coupling data without initialization, or initialized to remove the high frequency noise. Additionally, this work proposes to estimate the magnitude of pressure variations by computing a simple amplitude of oscillations between the successive coupling files.

2.2 Model description and metods of detection of rapidly moving pressure disturbances

2.2.1 Operational forecast model

ALADIN is used for operational weather forecast in DHMZ in 8 km resolution using hydrostatic dynamics, 2-time-level semi-implicit semi-Lagrangian and stable extrapolation two-time-level scheme (Hortal 2002). Operationally, the model uses 37 levels in the vertical and a mass-based hybrid terrain-following vertical coordinate η (Simmons and Burridge 1981).

The initial conditions for the operational forecast are obtained using data assimilation procedure (Stanešić 2011). Details of the operational forecast suite as well as model set-up are provided in Tudor et al. (2013), but there were few changes. The forecast is run up to 72 hours four times a day, starting from 00, 06, 12 and 18 UTC analyses, and coupled to LBC fields from IFS in delayed mode. This means that LBC for 6 hour forecast from 18 UTC run of IFS is used for initial LBC for 00 run of the next day, 9 hour forecast from 18 UTC run of IFS is used for 3 hour forecast LBC for 00 run of the next day, and so on.

The 8 km resolution operational forecast is coupled to a global model on the 8 points wide zone alnog lateral boundaries using relaxation tecnique (Davies 1976) and linear interpolation of LBC data in time (Haugen and Machenhauer 1993; Rádnoti 1995). Each coupling file contains the complete set of fields needed to initialize the ALADIN model forecast.

Digital filter initialization (DFI) is implemented in ALADIN in order to remove high-frequency noise (Lynch and Huang 1992) that arise due to interpolation of the coupling fields from the global model grid to the grid of the coupling files and then again to the resolution of the LAM (and changes in height of topography in different models/resolutions). Since DFI can considerably reduce the depth of the RMPD due to the Doppler effect, alternative scale selective digital filter initialization (SSDFI) was proposed, implemented and tested in the ALADIN model (Termonia 2008).

2.2.2 Global model ARPEGE

ARPEGE is a global sem-lagrangian spectral model run operationally at Meteo France on a stretched and rotated grid (Courtier and Geleyn 1988) with highest horizontal resolution over France and lowest resolution on the opposite side of the Earth. The horizontal resolutions in the model forecast and data assimilation procedure were changing during the 9 years when the MCUF field was computed in the operational ARPEGE forecast. The horizontal resolution of the coupling files also changed twice, see Table B.1.

ARPEGE can use coarser resolution in variational data assimilation procedure than in the forecast run. The fields from the operational forecast are interpolated from the stretched and rotated native model grid to the grid of the limited area LACE domain in Lambert projection of the coupling files.

The fields from operational ARPEGE forecasts are available in the coupling files with 3 hour interval for 4 runs per day (starting from 00, 06, 12 and 18 UTC analyses) and extending up to 72 for the 00, 06 and 12 UTC runs and up to 60 hours for the 18 UTC run. ARPEGE computes the MCUF field operationally according to Termonia (2004) and the field is distributed in the coupling files.

2.2.3 Global model IFS

IFS is also a global spectral model that uses semi-Lagrangian advection. It is run oparationally at ECMWF with uniform horizontal resolution over the globe. The details of the operational set-up in the model forecast and data assimilation have changed over the years used for this study, while the LBC files were available operationally, as did the operational model versions. The model forecast fields are interpolated from the IFS model grid to the LAM grid in Lambert projection and the horizontal resolution of the coupling files remained 15.4 km (see Table B.1).

Following the research studies where LBC data from IFS has been used for studies of severe weather cases (Ivatek-Šahdan and Ivančan-Picek 2006; Branković et al. 2007, 2008), the operational forecast run of the ALADIN model in DHMZ has switched to uding LBC data from IFS on 1^{st} January 2014.

The MCUF field is not computed by the IFS operational suite and therefore not available in the coupling files from IFS provided by ECMWF. Rapid changes in the surface pressure or the mean sea level pressure were detected in the fields provided from IFS operational forecast in the coupling files on the LACE common domain using a number of tools.

- ALADIN was run on the LACE domain (in the resolution of the coupling files) with 600 seconds time step and the MCUF field was computed during the

model run. The computed MCUF field will be referred to as IFSM. However, this means that a different model was run (different dynamics and physics) and the results can be different than when computed in the host model.

- The error function from Termonia (2003) was computed by running one time-step forecast starting from fields in the coupling files (in the same horizontal and vertical resolution), three sets of experiments were performed using initialization without filtering, using DFI or SSDFI.

- The amplitude of the oscillations in the surface pressure (and mean sea level pressure) was computed from three consecutive coupling files.

The last item actually detects situations when the moving pressure disturbance would be missed using $2\Delta t$ (6 hours) coupling update interval not the Δt (3 hours) interval. But the large values of this field can mean that the interval as short as Δt can also be insufficient for proper representation of lateral boundary data by linear interpolation of the LBC fields in time.

2.3 Computing the coupling error from the ECMWF coupling files

2.3.1 Monitoring of the coupling update frequency (MCUF) field from the ECMWF coupling files

ALADIN can compute the MCUF field during the model forecast. The field was computed by running ALADIN on the LACE domain of LBC files from operational IFS with horizontal resolution of 15.4 km (the same resolution and grid as the coupling files) and a time-step of 600 seconds. The output IFSM field is written with 3 hourly interval. The same procedure has been performed on the LBC files provided since 27^{th} October 2010 until 15^{th} November 2014, for 4 runs per day (starting from 00, 06, 12 and 18 UTC analyses) and extending to 78 hours forecast.

The maximum value of the IFSM field on the domain covered by the coupling files has been computed for each forecast output file. The average IFSM has been computed, the number of files when it exceeded the critical value and the maximum value achieved in each grid point for the coupling files for 6 hours forecast and longer.

The same procedure applied to the ARPEGE coupling files

MCUF was also computed by running ALADIN on the domain and resolution of the coupling files from ARPEGE and this fileld is refered to as the ARPM field

to distinguish it from the MCUF field computed in ARPEGE forecast. But the coupling files from the ARPEGE global model are provided in different horizontal resolutions that the files from IFS. There was no period when both coupling files used the same horizontal resolution (Table B.1). It is more important to test the method on both sets of coupling files on the same period in time since the frequency of the occurence of the fast storms can have significant seasonal and annual variability.

2.3.2 The error function

Each coupling file contains the complete set of model fields that can be also used as a initial file to perform a forecast run using ALADIN model. The coupling data are used as initial fields to perform a model integration of one time step forward in time in order to obtain $F(t+\delta t)$ and the tendencies of the model variables. In order to avoid spurious high frequency noise, a filter initialization should be applied before the start of the model run.

When investigating the error due to linear interpolation of surface pressure, Termonia (2003) computes an error function from the surface pressure field and finds that its maximum over the model domain is a good indicator of a RMPD. Each coupling file contains the complete set of fields needed to initialize the model, therefore it can be used as initial fields to perform one time step model integration. Termonia (2003) defines a dimensionless estimate of the truncation error due to linear interpolation in time as

$$e_T = \frac{1}{4}\left|\frac{(F'(t_2) - F'(t_1))\,(t_2 - t_1)}{F(t_1) + F(t_2)}\right|. \tag{2.1}$$

Where $F(t_{1,2})$ are the values of the model field F at times when the LBC data are available in the coupling files and $t_2 - t_1$ is therefore the coupling update interval (3 hours). $F'(t_{1,2})$ is the tendency of the field F at time $t_{1,2}$ and can be computed as $F'(t_{1,2}) = \frac{F(t_{1,2}+\delta t) - F(t_{1,2})}{\delta t}$ where δt is the model time step. The error function of surface pressure and mean sea level pressure was computed for each coupling file. The tendencies can be computed without any filtering of the field in coupling files, using DFI (Lynch et al. 1997) or SSDFI (Termonia 2008).

The error function e_T has been computed for the surface pressure field from IFS coupling files. The maximum values over the model domain are

$$E_T = max(e_T(x, y)) \tag{2.2}$$

where e_T is the error computed in each grid point.

The error estimate E_T revealed cases when linear interpolation of the coupling data in time with 3 hour coupling update interval is insufficient for the Belgian

domain (Termonia 2003). Both E_T computed with or without filtering over the Belgian domain yield a clear signal when there is a intensive RMPD. But the domain of Aladin Belgium used in that work did not contain any strong orography. The Croatian domain (and hence the LACE coupling domain) contains mountains of considerable height (Alps, Apennines etc.).

Digital filter initialization

Coupling files contain already interpolated data (to a lambert conformal grid), not the data from the native global model grid. Horizontal interpolation of the surface pressure field (and other forecast fields) from native IFS grid and topography to the grid and topography of the LBC files also distorts the fields, so there could be spin-up when computing the tendencies. This change in geometry can generate high frequency noise that can be removed using DFI (Lynch and Huang 1992). The DFI was applied using Dolph-Chebyshev filter on 14 time steps adiabatic backward integration and 14 time steps forward integration with a time step of 600 seconds. The time span was 2.333 hours, the stop band edge period was 3 hours, the ripple ratio 0.05 yields minimum time span of 2.07 hours (Lynch 1997) used with the scheme for diabatic DFI in ALADIN (Lynch et al. 1997).

Scale selective digital filter initialization

Doppler effect can shift the frequencies of RMPDs into the range of spurious gravity waves that DFI was designed to remove. Consequently, DFI reduces the intensity of RMPDs (Termonia 2008). Alternative SSDFI is expected to be a better solution for initialize the fields used to compute the error function intended to detect RMPDs.

The SSDFI was applied using Dolph-Chebyshev filter on 8 time steps adiabatic backward integration and 8 time steps forward integration with a time step of 600 seconds. The time span was 1.333 hours, the stop band edge period was 1.5 hours, the ripple ratio 0.05 yields minimum time span of 1.019 hours and the cutoff frequency increases with wave number for 30 m/s (Termonia 2008). This shorter time span and stop band edge period yields less filtering that preserves the storm in Termonia (2008) while still removing the spurious inertia gravity waves generated above mountains. Shorter time span means shorter model run which is also beneficial in the operational context.

Both filtering methods require running the model adiabaticaly backwards for a number of time-steps and then diabatically forward for the same number of time steps for each of the coupling files. The method is therefore computationally expensive if DFI or SSDFI are applied before computing the tendencies (about as expensive

as IFSM).

2.3.3 The amplitude in the pressure variations

All the methods described previously require that all the coupling files (initial and forecast) contain the data necessary to initialize the LAM and run the LAM at least for one time step. Here a very simple method for detecting RMPDs is presented that does not require running LAM.

As a measure of variability in the model field, the following can be computed:

$$A = \frac{1}{2}\left(F(t_1) + F(t_3) - 2F(t_2)\right) \tag{2.3}$$

where $F(t_1)$, $F(t_2)$ and $F(t_3)$ are the values of the model field F at three consecutive times t_1, t_2 and t_3 when the coupling data are available. The differences in times is the coupling update interval $t_2 - t_1 = t_3 - t_2 = \Delta t$ which is operationally equal to 3 hours.

Eq.2.3 describes the changes of the model field F during the $2\Delta t$ period, eg. twice the coupling update period. Therefore, the values of A are largest in points where Δt period is actually enough to describe the evolution of the model variable during the coupling update interval using linear interpolation in time (eg. at the position of the pressure minimum at time t_2). However, A can be used as an indicator of a RMPD, as will be shown in the results of this study. On the other hand, A could miss the evolution of the model variable on a time scale less than Δt, for example when the model variable evolves as the full line in Fig 1 of Termonia (2003).

2.3.4 The effect of linear interpolation

An atmospheric disturbance can enter the domain unnoticed by the coupling scheme. The Figure 2.1 shows mean sea level pressure from the ARPEGE forecast (as provided in the coupling file) and mean sea level pressure from the ALADIN 8 km forecast coupled to it.

Linear interpolation in time distorts the model fields. Figure 2.2 shows the effect of linear interpolation on the mean sea level pressure. The ARPEGE forecast mean sea level pressure from two consecutive coupling files is interpolated linearly in time (as in the operational coupling procedure). In the place of moving storm, LAM sees a dual cyclone structure, one cyclone/storm disappears and another appears. This is why larger coupling zone yields dual cyclone structure, as was shown by Tudor and Termonia (2010).

Other meteorological fields that are used for coupling at lateral boundaries get distorted by linear interpolation in time if they contain high resolution features

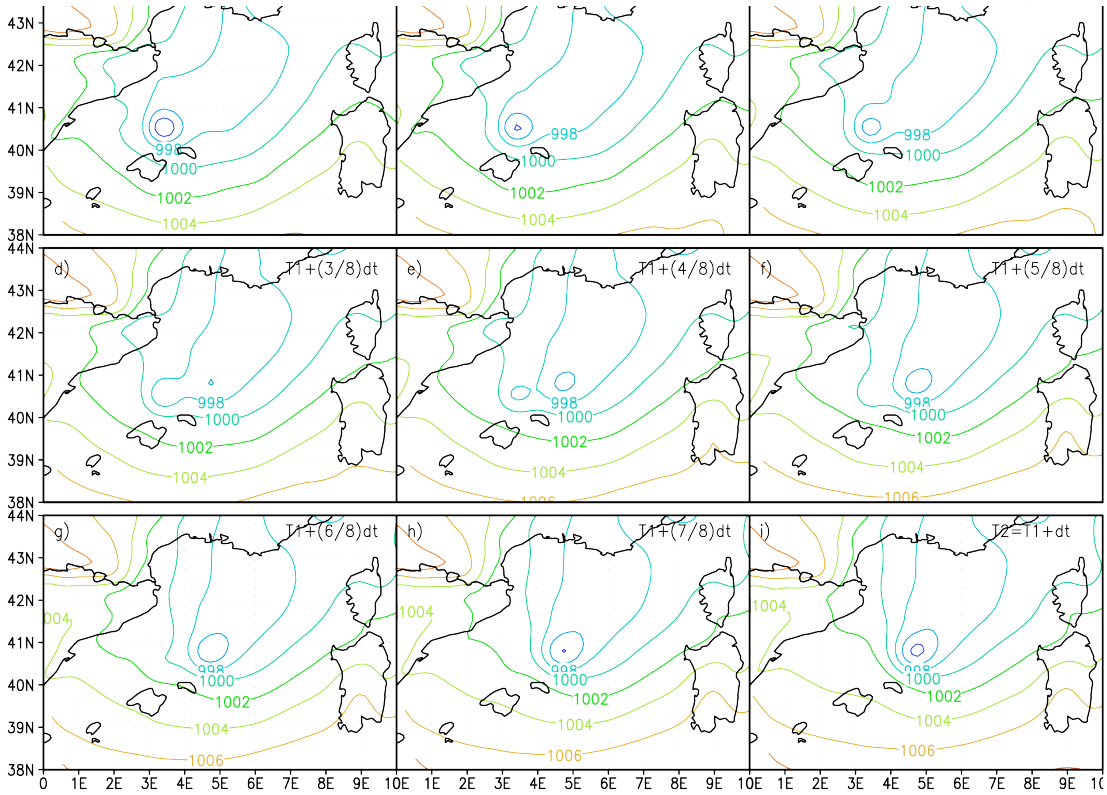

Figure 2.2: Mean sea level pressure (hPa) from ARPEGE operational coupling files starting from 12 UTC analysis on 27^{th} Oct 2008, 57 (a) and 60 (i) hour forecasts, linear interpolation of mean sea level pressure in time to half of the 3 hour coupling period (e), 1/8 of 3h (b), 1/4 (c) 3/8 (d), 5/8 (f), 3/4 (g) and 7/8 (h).

such as storms or meteorological fronts. For simplicity, this chapter will focus on the mean sea level pressure and surface pressure fields.

2.4 Filtered surface pressure field from ARPEGE

2.4.1 The time series of MCUF maxima

The maximum value of the MCUF field as computed in the operational ARPEGE has been extracted from each forecast coupling file available for the whole LACE coupling domain. The time series of MCUF maxima are shown in Figure 2.3. The MCUF maxima from the 3 hour forecast files were omitted in the plot since they had high values due to other phenomena that arose during spin-up following ARPEGE initialization, especially in the period until 6^{th} February 2008. Most of the points with large MCUF values in the 3 hour ARPEGE forecast are close to mountains. This suggests large spin-up of the surface pressure field in the beginning of the ARPEGE forecast. Since these large values of MCUF in the +03 hour forecast mostly do not represent a storm that moves quickly through the domain, analysis has been performed only on fields from +06 hour forecast or larger.

MCUF exceeds the 0.003 value rather often, mostly in successive forecasts of events. For each file where MCUF was larger than this threshold value, a figure was plotted with mean sea level pressure from the coupling file (ARPEGE) and the operational ALADIN forecast in 8 km resolution coupled to it, and the points where MCUF was larger than 0.003 (see example in Figure 2.1). Each time, large MCUF values were associated to a pressure disturbance in ARPEGE that was often less intensive in ALADIN forecast (if covered by the operational ALADIN domain).

The events that yield large values of the MCUF field represent RMPDs that rapidly traverse any part of the LACE domain. These events are more frequent in autumn, but appear throughout the year, least often during summer months. Several large MCUF values can be associated to a single event (one cyclone moving rapidly over the model domain), but they represent maxima from different forecast coupling files and different forecast runs (starting from different initial times corresponding to different ARPEGE analyses). On the whole LACE domain, the critical value of 0.003 has been exceeded 3045 times in 288648 files, more than 1% of the files in the whole period from 23^{rd} January 2006 until 16^{th} November 2014 (see Table B.1). In 878 files, large MCUF values were close to the coupling zone of the operational ALADIN domain in DHMZ (see Figure 2.1). This is only 0.3% of the coupling files and the event can be considered rare. But, as mentioned earlier, these events are perhaps most important to be forecast. In order to properly forecast such events using LAM, one should first detect it and then apply boundary error restarts (Termonia et al.

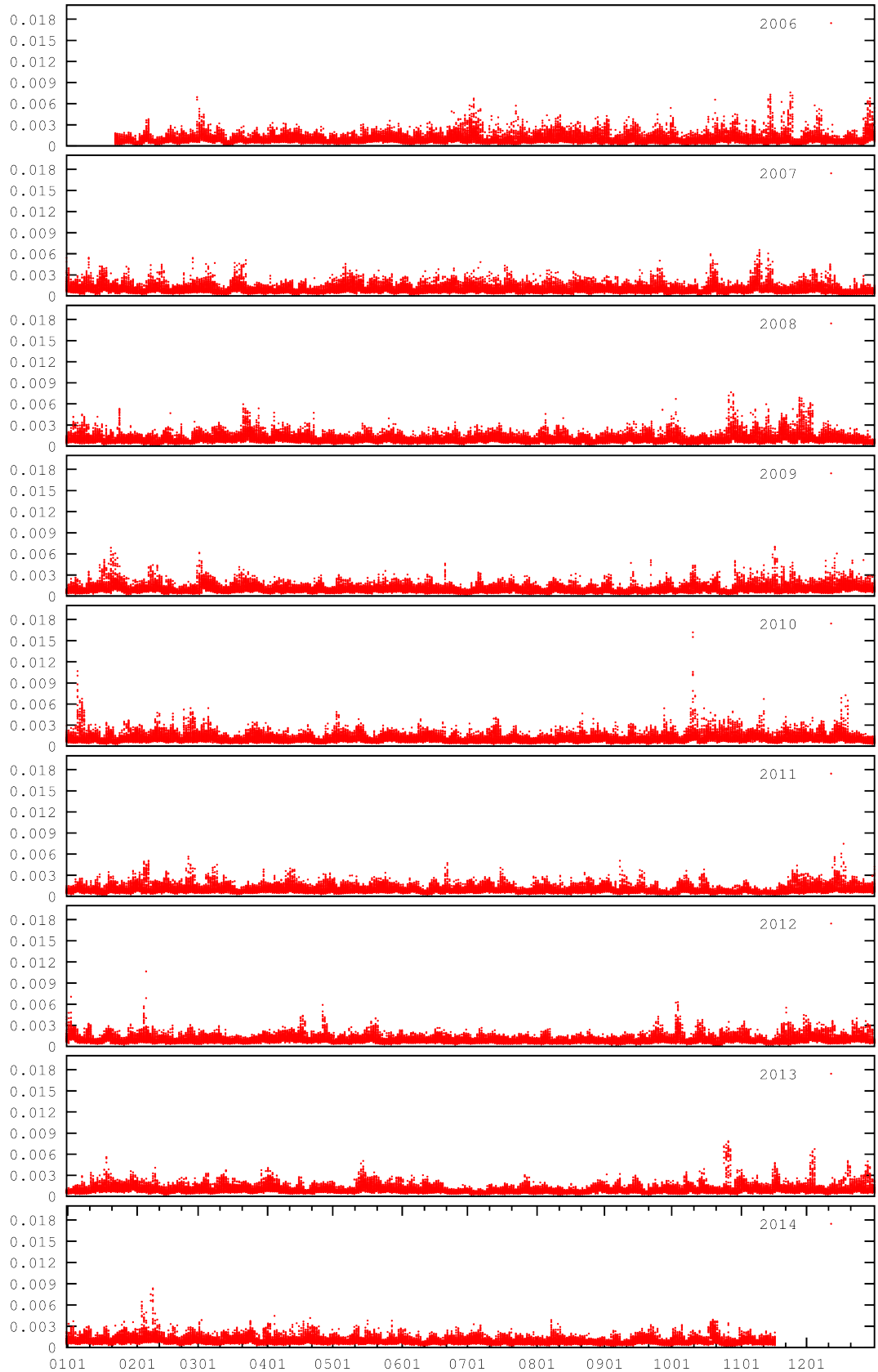

Figure 2.3: Maximum value of the MCUF field (units hPa) on the LACE coupling domain, provided from ARPEGE, from the coupling files for 6 hour forecast up to 72 hours forecast (60 hours for 18 UTC run), starting from 00, 06, 12 and 18 UTC analyses, since 23^{rd} January 2006 until 15^{th} November 2014.

2009) or gridpoint nudging (Termonia et al. 2011).

2.4.2 Spatial distribution of MCUF from ARPEGE

Successfull implementation of the computations of the MCUF field in the operational ARPEGE means that it is not dependent on the horizontal resolution of the global model since ARPEGE is run on a stretched grid. The averaged MCUF fields (Figure 2.4) for different horizontal resolutions (Figure 2.4a for 20.678 km, Figure 2.4b for 15.4 km and Figure 2.4c for 10.51 km) show that it does not depend on the resolution of the coupling files as well as the resolution of the global model where it was computed. Averaged MCUF field is slightly larger over the North Sea in the first period (from 23^{rd} January 2006 until 6^{th} February 2008) for the lowest resolution. The values over the Mediterranean have the highest values in the middle period (from 6^{th} February 2008 until 11th May 2010) for the 15.4 km resolution of the coupling files. This result suggests that the cyclones traversed Mediterranean more often and faster during that period than in the periods before and after.

The maps of number of cases when the MCUF field exceeded the 0.003 threshold (Figure 2.5) show that the number of cases with fast cyclones over the North Sea is the largest in the last period (that is also twice as long as the other two). But over the Mediterranean, MCUF exceeded the critical value most often in the second period, as well as over the area under the influence of the Bay of Biscay.

The absolute maximum values of the MCUF field have large values over most of the western Mediterranean during the second period (Figure 2.6). The overall largest values of MCUF were computed during the third period (and in the highest spatial resolution) close to the coastline of Algeria, but the values are low over the rest of the Mediterranean. On the other hand, the maxima are the highest over the North sea in the last period and over the Black Sea in the first period.

The spatial distribution of the frequency of the events when MCUF exceeded the critical value (Figure 2.5) indicate which areas should be avoided as parts of the coupling zone if one wants to have fewer problems with properly resolving the boundary data in time with 3 hourly coupling update period. When the filtered surface pressure field is larger than a threshold value 0.003, there is a storm rapidly propagating through the area. If the point with the large value is inside the coupling zone of a LAM, it can be expected that the LAM forecast will miss the storm due to time interpolation of boundary data. The analysis of the MCUF field from ARPEGE coupling files for the common LACE coupling domain shows that this field is above the threshold far more frequently than acceptable.

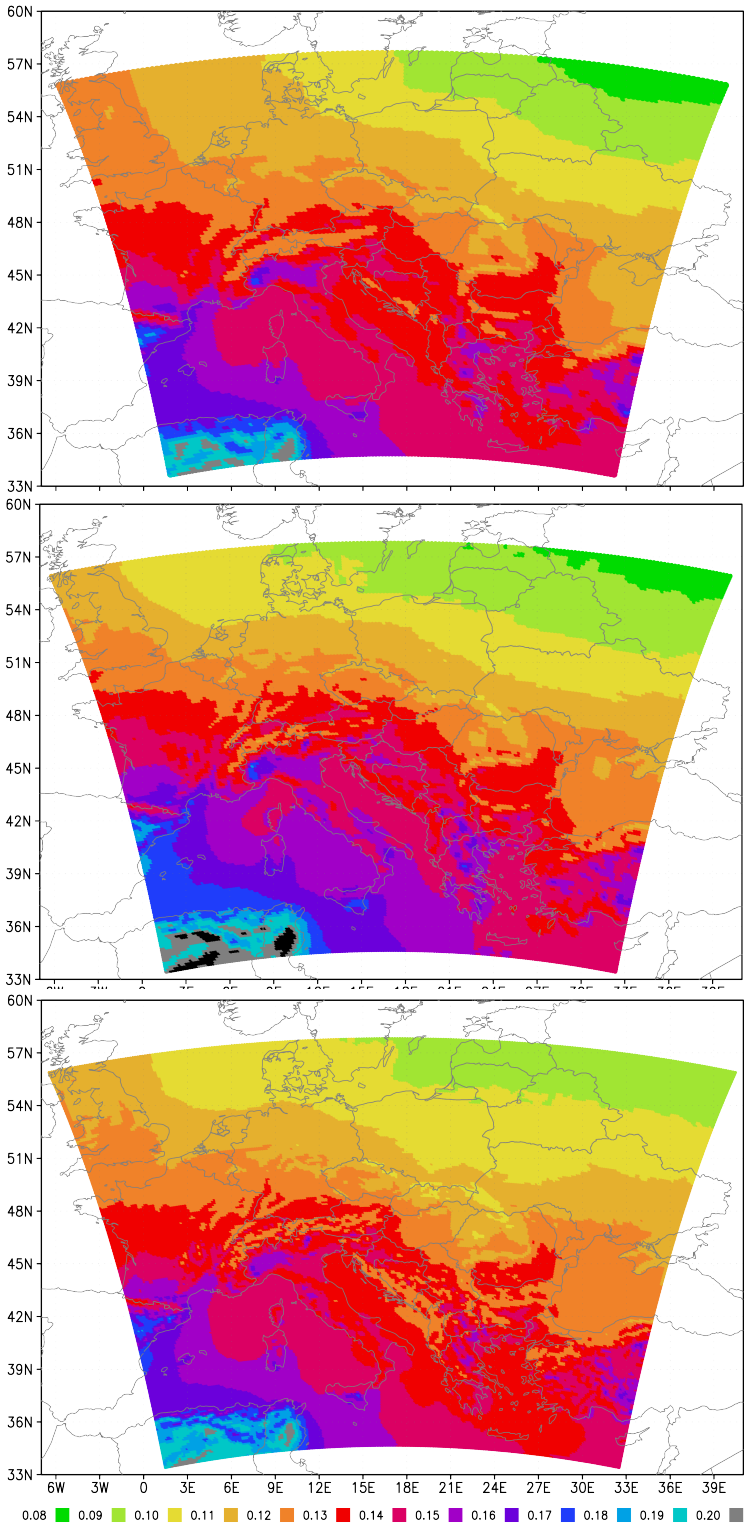

Figure 2.4: Average MCUF field (units 0.001 hPa) from ARPEGE for different resolutions of the LACE coupling files: (a) 20.678 km averaged for the period 23^{rd} Jan 2006 to $6th$ Feb 2008. (b) 15.4 km averaged for the period 6^{th} Feb 2008 to 11^{th} May 2010. (c) 10.51 km averaged for the period 11^{th} May 2010 to 15^{th} Nov 2014.

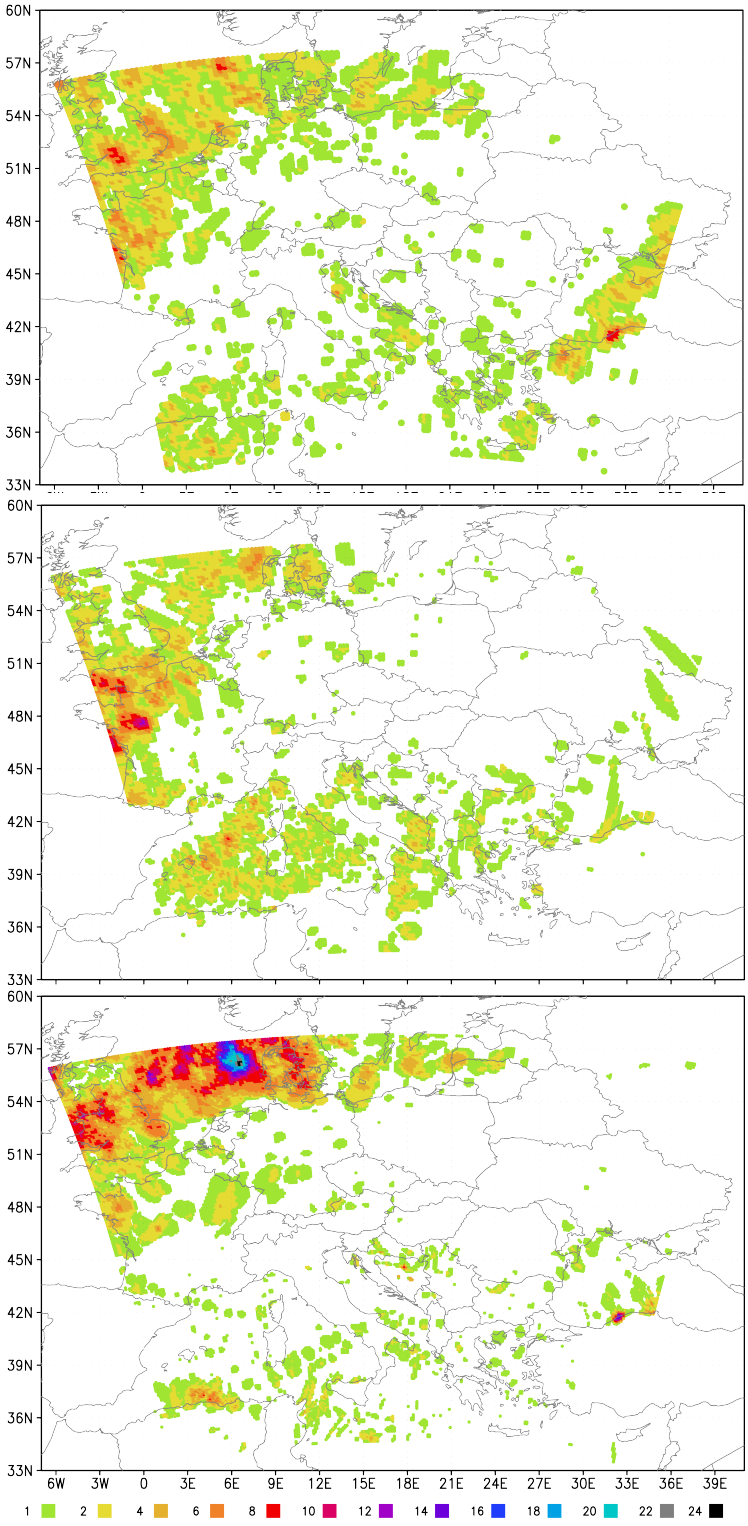

Figure 2.5: The number of times the MCUF field from ARPEGE exceeds 0.003 threshold for different resolutions of the coupling files: (a) 20.678 km averaged for the period 23^{rd} Jan 2006 to $6th$ Feb 2008. (b) 15.4 km averaged for the period 6^{th} Feb 2008 to 11^{th} May 2010. (c) 10.51 km averaged for the period 11^{th} May 2010 to 15^{th} Nov 2014.

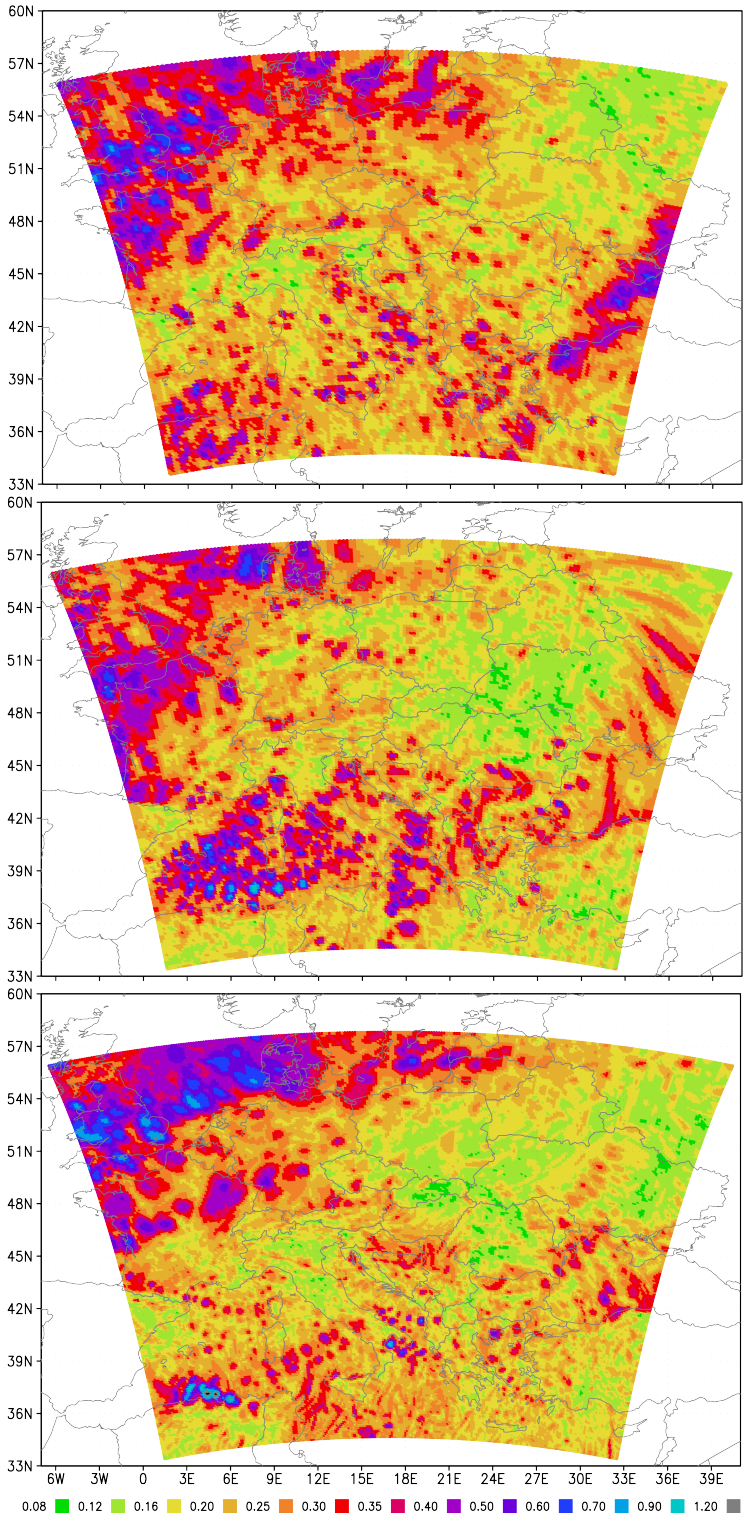

Figure 2.6: Absolute maximum values of the MCUF field (units 0.01 hPa) from ARPEGE for different resolutions of the coupling files: (a) 20.678 km averaged for the period 23^{rd} Jan 2006 to $6th$ Feb 2008. (b) 15.4 km averaged for the period 6^{th} Feb 2008 to 11^{th} May 2010. (c) 10.51 km averaged for the period 11^{th} May 2010 to 15^{th} Nov 2014.

2.5 Detecting rapidly moving pressure disturbances (RMPDs) in the ECMWF coupling files

MCUF is not computed by operational IFS, the alternative methods of detecting RMPDs have been tested on the coupling files received operationally from ECMWF.

2.5.1 Computing MCUF by running ALADIN model on the coupling files from IFS

MCUF computed by running ALADIN in the resolution of the coupling files from IFS using interpolated IFS analysis as the initial conditions (without any filtering) for 4 runs per day up to 78 hours forecast with 3 hourly output. The MCUF field computed this way is referred to as IFSM. The initial IFSM values are zero. IFSM computed during the first 3 hours of forecast has very large values due to model spin-up so only the fields corresponding to the 6 hour forecast and longer are used in the analysis.

The time series of IFSM maxima

The time series of the maximum values of IFSM field from the whole LACE domain for forecast ranges from 6 to 78 hours are shown in Figure 2.7 for the period from 27^{th} October 2010 until 15^{th} November 2014. The critical value is exceeded in 698 files (out of total 147350 files) during the 4 year period and over the whole domain (see Table B.1). This is less often than in ARPEGE, since during the same period MCUF was larger than 0.003 in 995 files (out of 129674 files). The total number of files is larger for IFS than for ARPEGE since ARPEGE forecast LBC files extend up to 72 hours (and only 60 hours for the 18 UTC run), while files from all runs of IFS extend up to 78 hour forecast.

Although the critical value of 0.003 is exceeded less often with IFSM than with MCUF in ARPEGE, there are periods with large values associated to RMPDs during every part of the year, more often in autumn and the least often in summer. A figure with mean sea level pressure from the IFS coupling file and gridpoints with large IFSM values were plotted for each coupling file for which IFSM exceeded the critical value in order to estimate if the large IFSM values are associated to the cyclones in the IFS files (and not only in the ALADIN forecast run used to compute the IFSM field). Inspection of this set of figures lead to a conclusion that large values of IFSM are connected to a pressure low in IFS fields.

One should keep in mind that the MCUF values are computed by running ALADIN using IFS coupling files (initial and forecast). ALADIN model can yi-

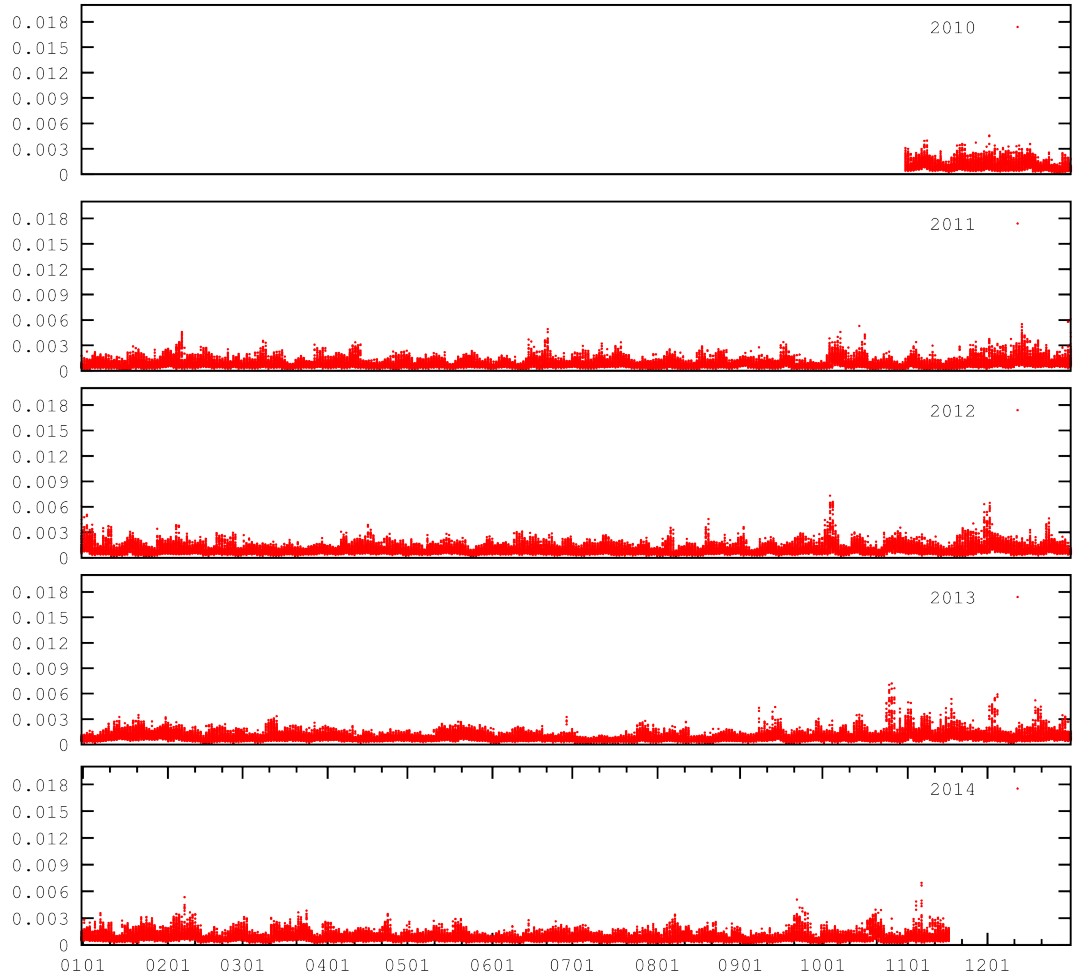

Figure 2.7: Time series of maximum value of IFSM field (units hPa) on the coupling LACE domain for 6 hour forecast up to 78 hours forecast, computed by running ALADIN, starting from 00, 06, 12 and 18 UTC analyses, since 1^{st} November 2010 until 15^{th} November 2014.

eld different evolution of model variables, including surface pressure, so that large MCUF values correspond to a cyclone that moves quickly in the ALADIN forecast, not neccessarily in the IFS forecast. On the other hand, a RMPD in the IFS forecast might be less intensive or slower in the ALADIN forecast due to differences in the model set-up, choices in physics and dynamics.

Spatial distribution of IFSM

MCUF was computed by running ALADIN forecast on a limited area domain in 15.4 km resolution. Coupling zone was 8 points wide. The procedure could have missed a cyclone entering the LACE domain during the coupling interval. It is also expected to get unwanted phenomena in the IFSM field in the coupling zone of LBC files.

In the figure 2.8, a small dot is plotted in the position of each model grid-point in the colour corresponding to the average IFSM value multiplied by 1000 as shown in the colour scale below. Average IFSM field and average MCUF from ARPEGE for the same period (Figure 2.8) have substantially different spatial distributions. The differences are most pronounced over the Baltic area, where IFS yields more fast cyclones and over Mediterranean, where ARPEGE forecasts more RMPDs.

Maximum MCUF has larger values than IFSM (Figure 2.9). The average values are low along lateral boundaries, but the maxima do not decrease towards the lateral boundaries (Figure 2.8). The differences in the maximum MCUF and IFSM values are much less pronounced than for the averaged fields.

In most of the domain, MCUF and IFSM exceeded the critical value less than once in the 4 year period (Figure 2.10). The most critical part is in the north, where cyclones apparently traverse rather quickly and the number of files where IFSM s larger than threshold threshold exceeds 20. Both MCUF and IFSM show areas where pressure disturbances move more rapidly and/or frequently than elsewhere, such as the North Sea, the Baltic, western Mediterranean and west coast of the Black Sea. The critical value of 0.003 is exceeded more often for IFSM than in ARPEGE (Figure 2.10), over the North Sea, western Black Sea and the Baltic, but less often over the western Mediterranean. This suggests that IFSM field could be missing some of the RMPDs approaching Adriatic Sea and Croatia over the western Mediterranean.

Computing MCUF by running ALADIN model on the coupling files from ARPEGE

ARPM was computed by running ALADIN on the domain and resolution (10.61km) of the ARPEGE coupling files with 450 seconds time step starting from

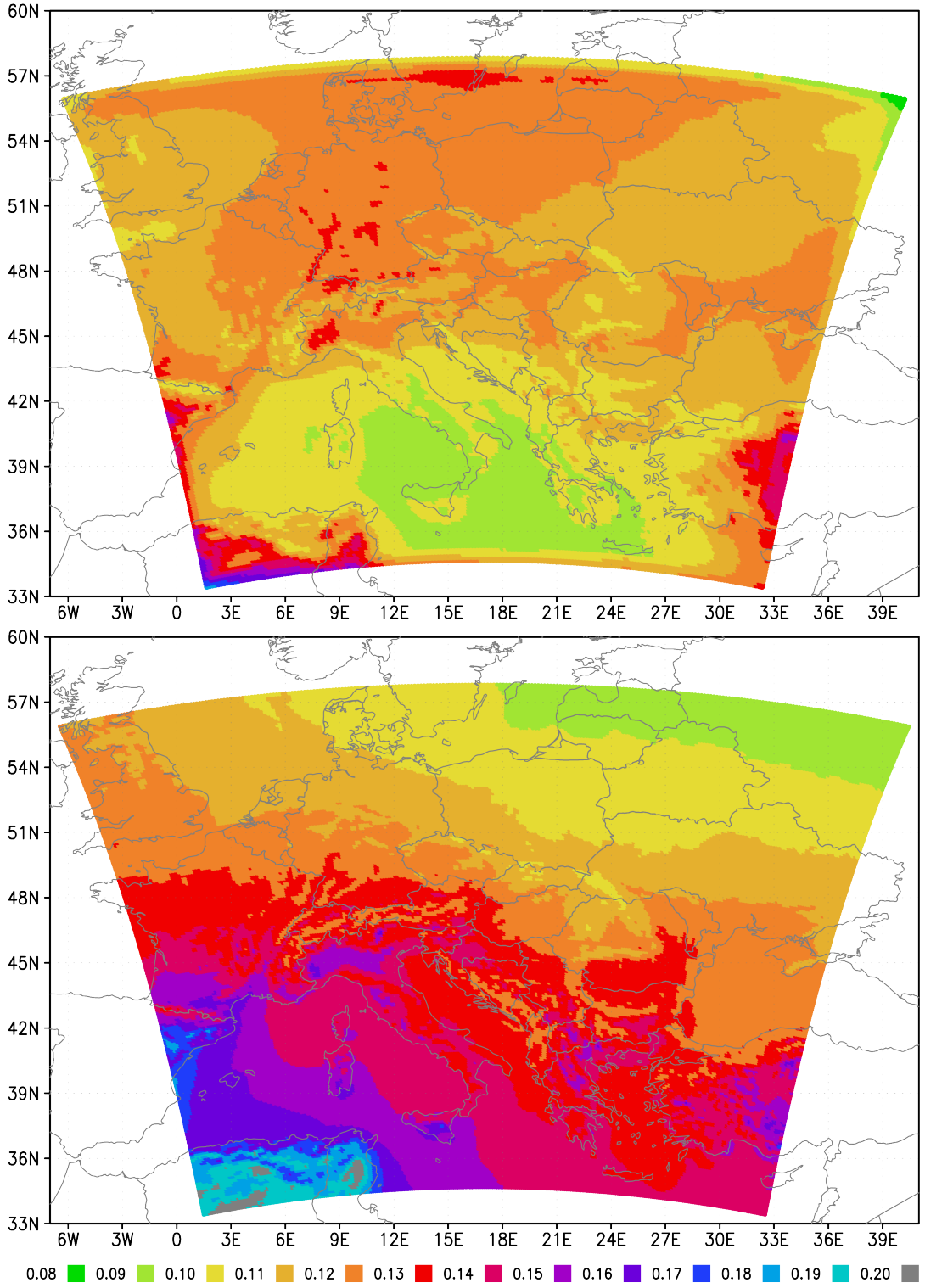

Figure 2.8: Spatial distribution of the average IFSM (top) and MCUF (bottom) values (units 0.001 hPa) for forecast hour greater than or equal to 06 hours for the period since 1^{st} Nov 2010 until 15^{th} Nov 2014.

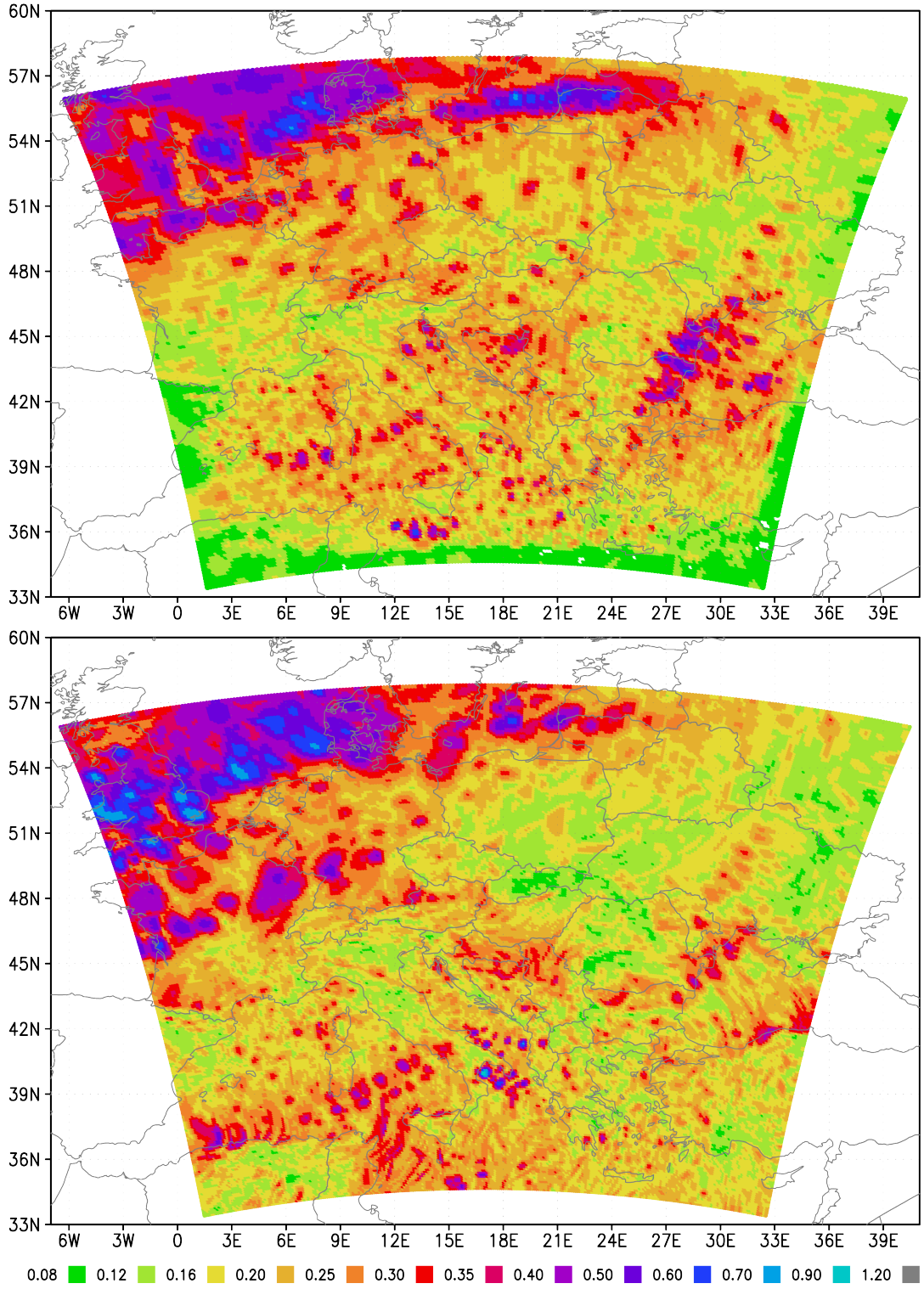

Figure 2.9: Spatial distribution of the maximum of absolute IFSM (top) and MCUF (bottom) (units 0.01 hPa), for forecast hour greater than or equal to 06 hours for the period since 1^{st} Nov 2010 until 15^{th} Nov 2014.

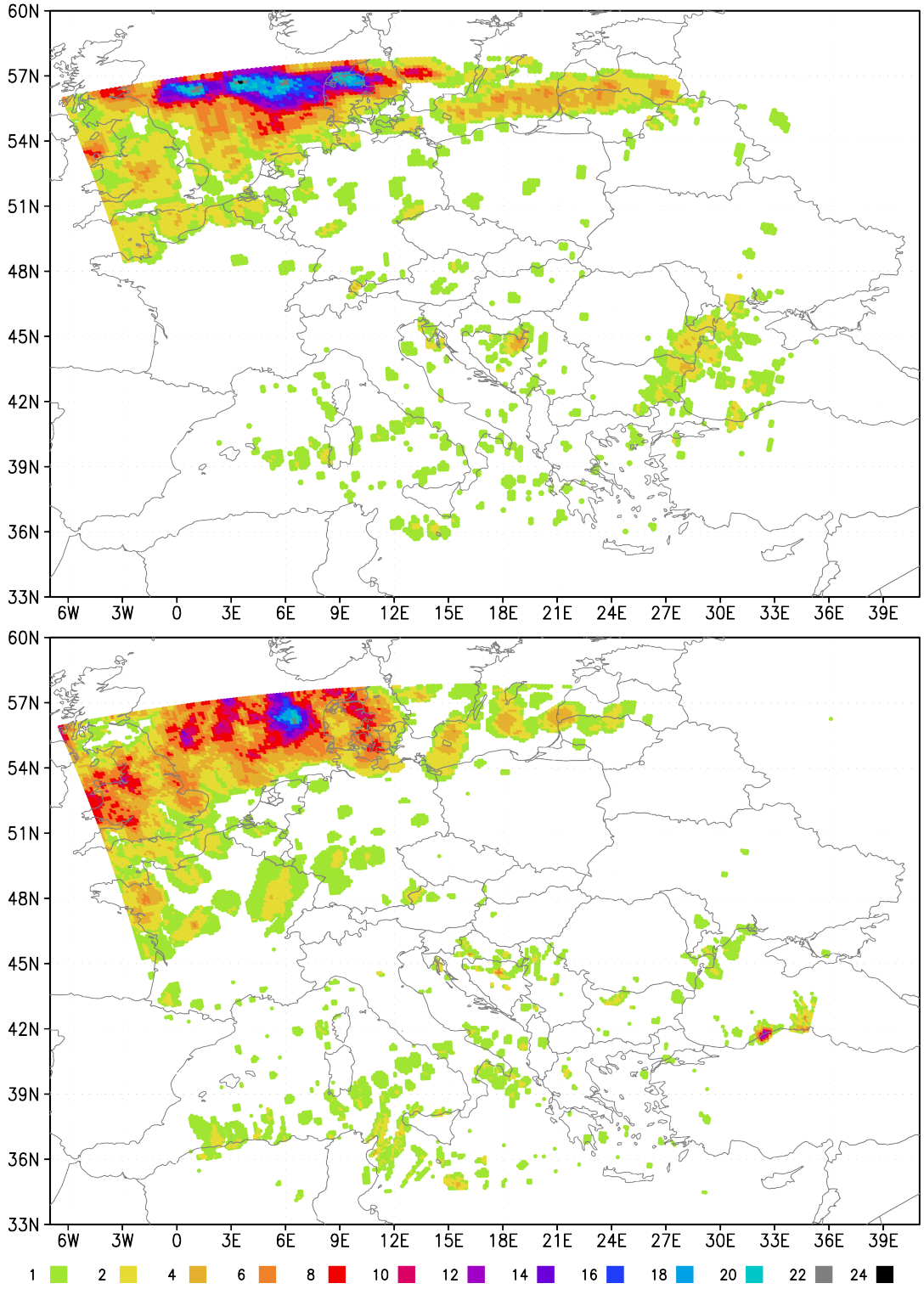

Figure 2.10: Spatial distribution of the number of occurences when IFSM (top) and MCUF (bottom) values exceed the value 0.003, for forecast hour greater than or equal to 06 hours for the period since 1^{st} Nov 2010 until 15^{th} Nov 2014.

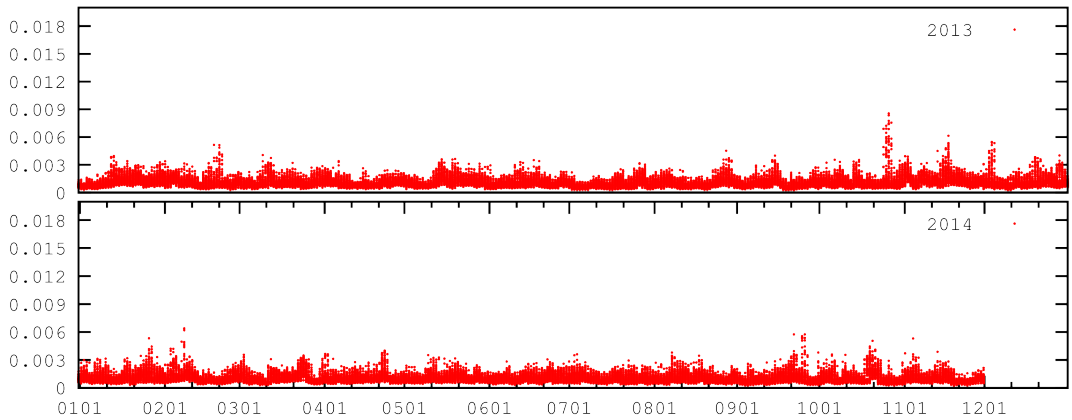

Figure 2.11: Time series of maximum value of ARPM (MCUF computed by running ALADIN on the coupling LACE domain from ARPEGE (the domain and resolution of LBC files) with 450 sec time-step).

the ARPEGE analysis without initialization. The time series of ARPM maxima over the LBC domain are shown in Figure 2.11. There is a good agreement with MCUF computed in ARPEGE. But ARPM gives additional strong signal for the storm that hit Turkey on 27^{th} September 2014. MCUF did not show a signal for the same case.

2.5.2 The error function values using mean sea level pressure from ECMWF coupling files

ALADIN was run for one time step using fields from the coupling files from IFS as initial conditions in order to estimate the tendency of the model variables (in particular the surface pressure). The run is performed on the grid of the coupling files using 600 second time step. The error is estimated according to equation 2.1 and its maximum over the model domain according to the equation 2.2. The error function was computed for the period since 27^{th} October 2010 until 15^{th} November 2014 for experiments without initialization and initialized with SSDFI, and for the period since 1^{st} January 2013 for the experiment with DFI.

Tendencies computed without filtering initialization

The time series of E_T computed without initialization is plotted in Figure 2.12. The noise is more intensive than with IFSM, but the signal of RMPDs can be seen. The level of noise is lower in summer than in winter and it is lower when the error function is computed using mean sea level pressure than for surface pressure. Due to rather high level of noise, a critical value larger than 0.003 should be defined in order to avoid false alarms. The method using error estimate sometimes yields large

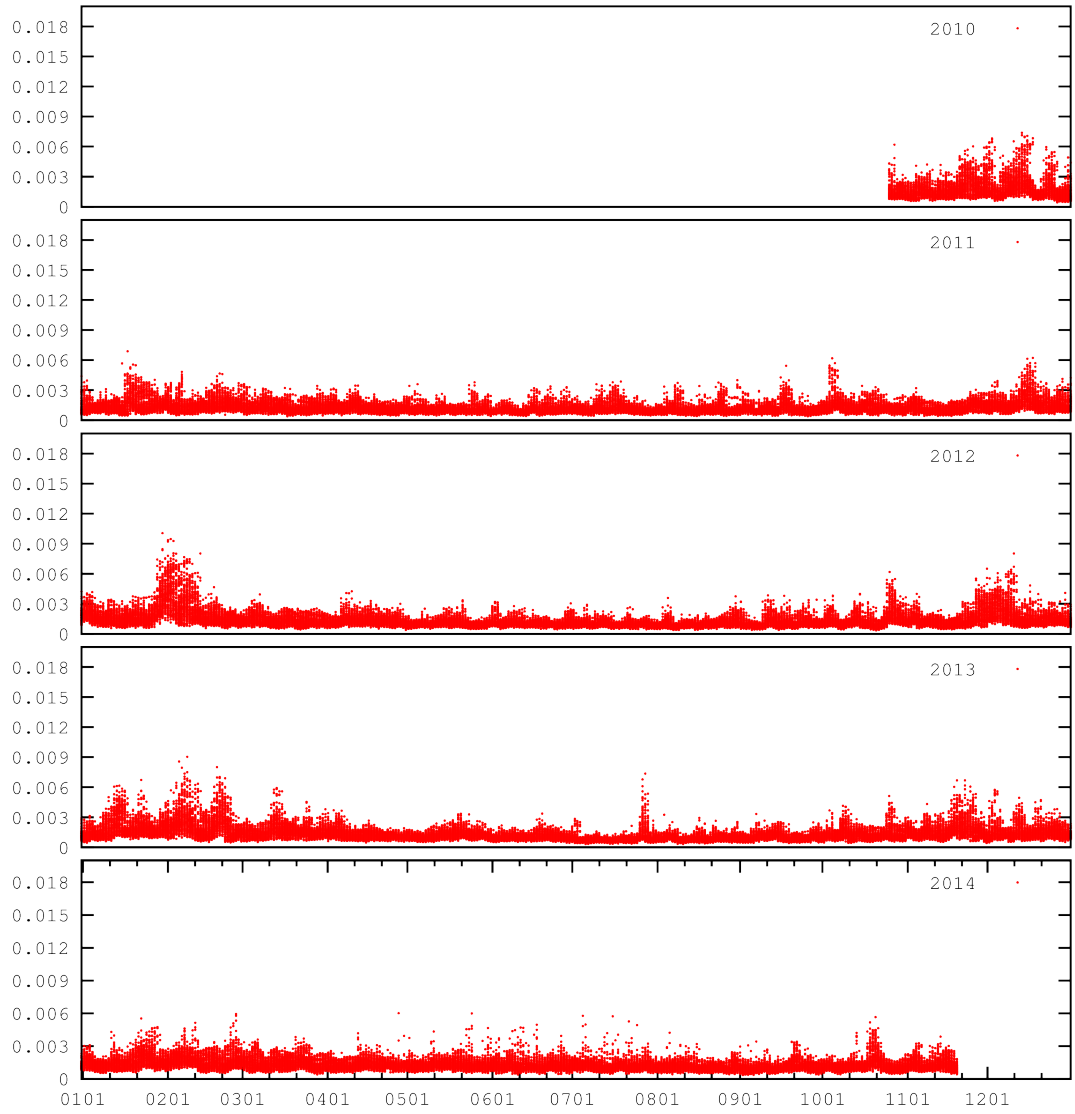

Figure 2.12: Time series of maximum value of error function (E_T, Eq. 2.2) without any filtering initialization.

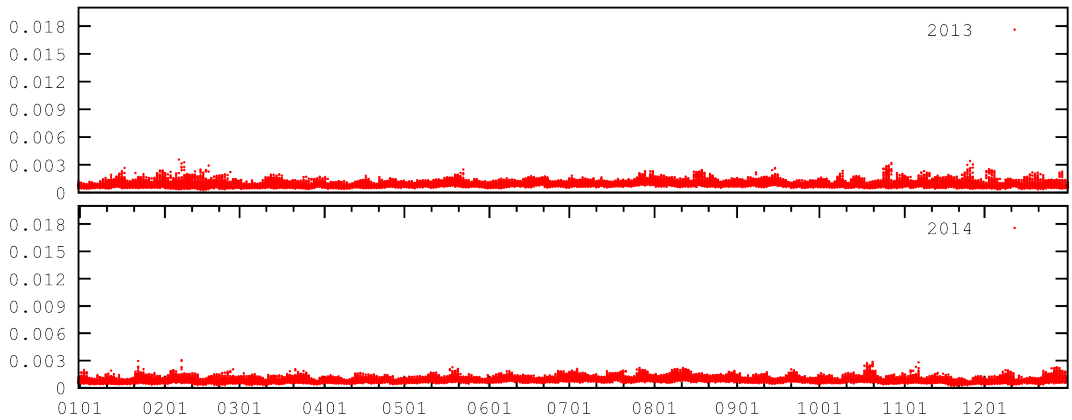

Figure 2.13: Time series of maximum value of error function, fields are initialized with DFI.

values over mountainous areas. If the model domain is defined so that the mountains are not in the intermediate zone (close to lateral boundaries), these events could be ignored by the operational procedure and would not be false alarms.

Tendencies computed with digital filter initialization

The time series of E_T computed for fields initialized with DFI is plotted in Figure 2.13 for the period from 1^{st} January 2013 until December 2014. The noise is much lower than for the test without initialization, but the signal of RMPDs is also weaker. There is more noise in E_T computed for mean sea level pressure than for surface pressure in winter and spring, but less in the autumn. The signal of the RMPDs is removed almost completely from the error function computed for surface pressure, especially in winter and spring.

There is a signal for RMPD in E_T computed from mean sea level pressure on 27^{th} November 2013 that does not exist in the time series of E_T for the surface pressure. The peak is located over the Alps and shows preristently for model runs from successive analyses about the same time (9 to 15 UTC that day). The satellite figures of the area for that date show clouds associated to mountain waves (not shown).

Tendencies computed with scale selective digital filter initialization

Similarly, the error function was computed after the fields in the coupling files have been initialized using SSDFI for the period since 27^{th} October 2010 until December 2014. The time series of the maxima of the error function is ploted in Figure 2.14. The level of noise and the intensity of the signal of approaching RMPDs are similar to tose computed with DFI. But there are subtle differences. Several cases

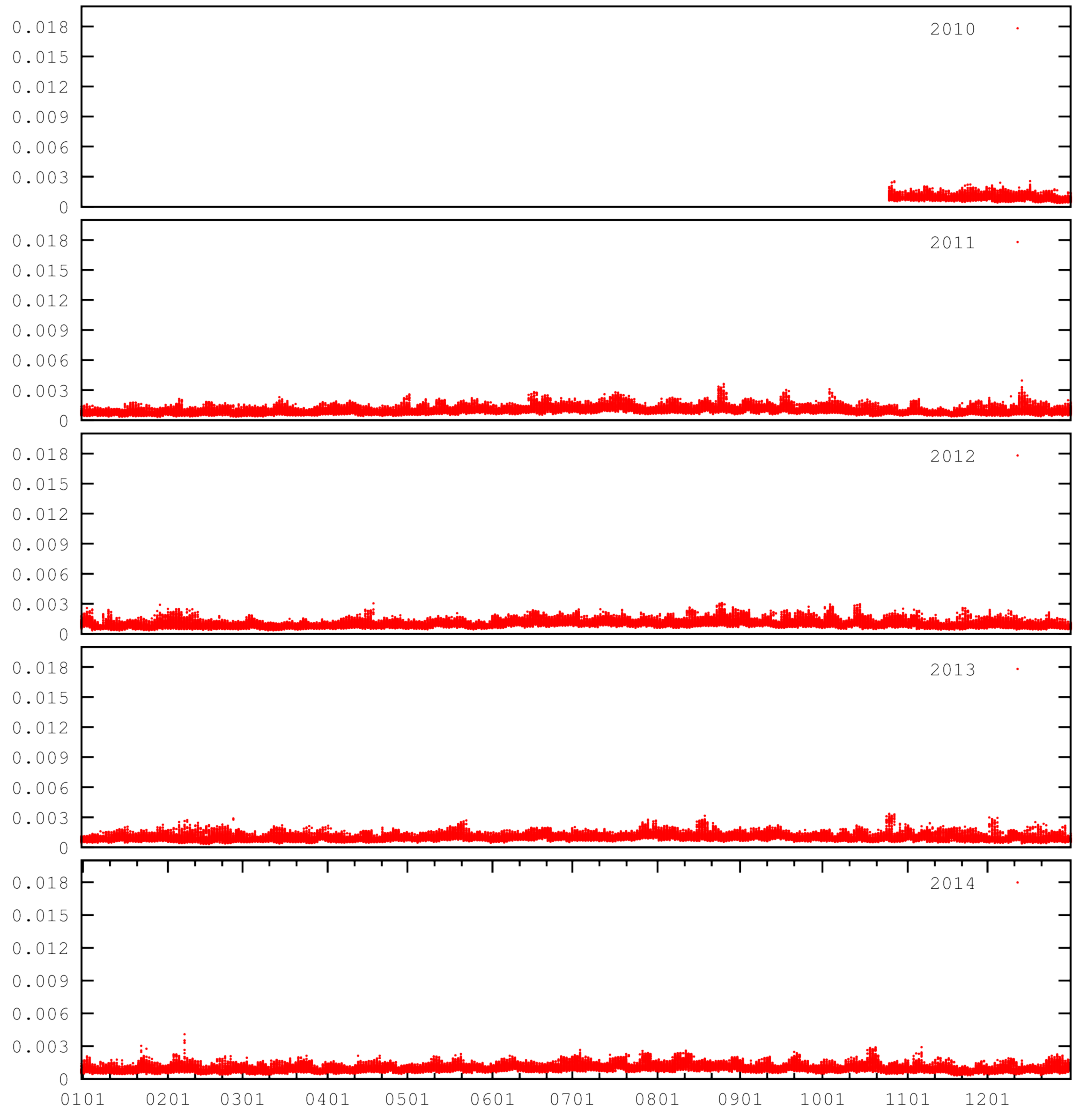

Figure 2.14: Time series of maximum value of error function, fields are initialized with SSDFI.

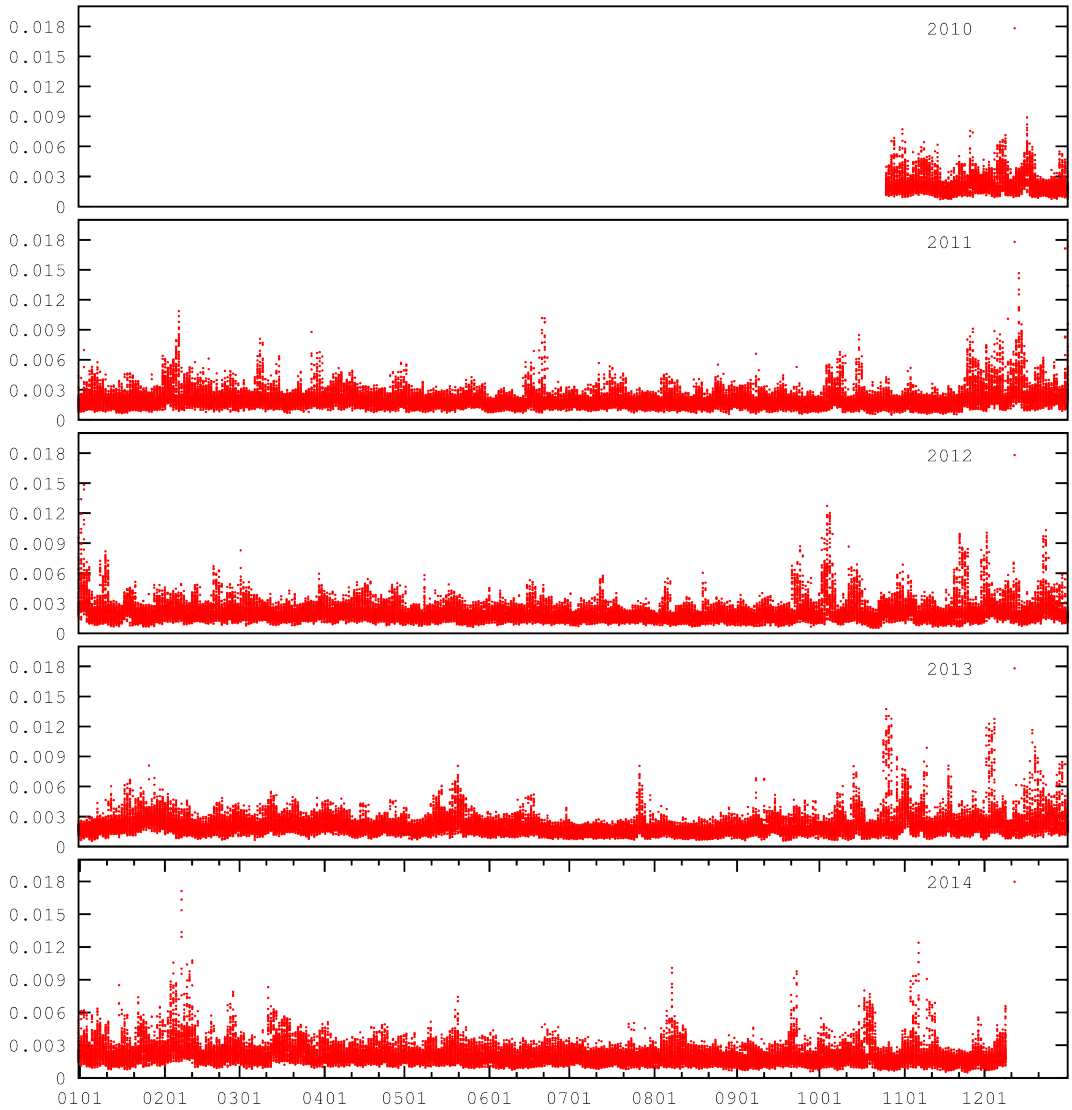

Figure 2.15: Time series of the maximum value of the amplitude in the mean sea level pressure variations (Eq. 2.3) computed from the coupling files from IFS.

of RMPDs are more pronounced and there is no signal on 27^{th} November 2013 that occured when DFI was used.

2.5.3 Amplitude of oscillations in mean sea level pressure

The amplitude of oscillations in mean sea level pressure was computed for the coupling files from IFS for the period since 27^{th} October 2010 and for the coupling files from ARPEGE since 1^{st} January 2013, both until December 2014. The time series of the maxima in the amplitude of the mean sea level pressure variations from IFS is displayed in Figure 2.15 and for ARPEGE in Figure 2.16.

Although the amplitude maxima achieve large values during periods without

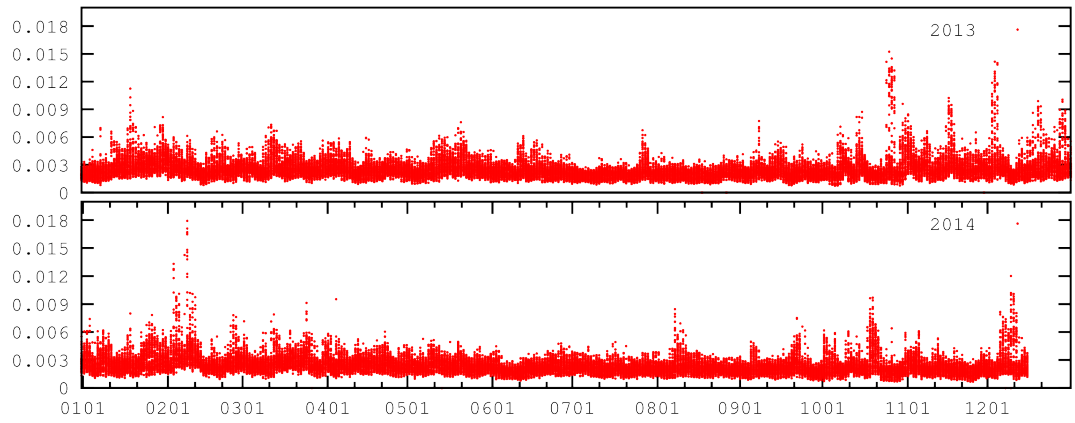

Figure 2.16: Time series of the maximum value of the amplitude in the mean sea level pressure variations (Eq. 2.3) computed from the coupling files from ARPEGE.

RMPDs (the periods without RMPDs are those when MCUF and IFSM are low), the amplitude is so much larger in a case with RMPD that there is a signal that can be distinguished in the noisy pattern.

A figure was plotted with mean sea level pressure from the coupling file from IFS and all points with large values of A ($A > 0.003$) for each case when this threshold was exceeded. The majority of the cases are related to propagating cyclones and pressure throughs and are usually associated to the large values of IFSM. However, there are cases when A is larger than the threshold in mountainous regions of Alps, Atlas mountains and Turkey, but these are associated to an atmospheric front approaching the area so the large values could not be dismissed as false.

There is also a number of cases when IFSM did not indicate a RMPD, while A did reach values above the threshold in points close to the edge of the coupling domain. The subsequent coupling times also had large values of A in the vicinity. In these cases, the cyclone entered the coupling domain too quickly to be detected by the procedure used to compute the IFSM field.

2.6 Conclusions

The three hourly coupling update interval is insufficient for resolving the storm in lateral boundaries as presented for the Lothar storm case (Termonia 2003). Davies (2014) recommends choosing carefully the resolution and fequency of large scale LBCs. However, meteorological services that depend on LBCs from elsewhere might have little choice. A coupling update frequency is sufficient if the large scale model data contains only features that are large enough and slow enough to be resolved by the coupling update period (Denis et al. 2003). Therefore, the coupling update frequency is determined by the properties of the global model, not the LAM that

uses it for LBCs.

Termonia (2004) developed a strategy to monitor rapid changes in surface pressure in ARPEGE by producing a diagnostic output field for the filtered surface pressure (MCUF). This field is provided in the coupling files since 06 UTC run on 23^{rd} January 2006 for the LACE coupling domain.

When MCUF is larger than a threshold value of 0.003 (Termonia 2004), there is a rapid development in the surface pressure suggesting that a fast cyclone has moved through the area. If the point with the large value is inside the coupling zone of the ALADIN domain, it can be expected that the ALADIN model run will miss the cyclone strength and development due to time interpolation of boundary data. When the time series of MCUF data has been analysed for the Belgian domain (Termonia et al. 2009), it was found that such events occurred only several times per year.

The analysis of the MCUF field in this chapter shows that this field is above the threshold more frequently for the whole LACE coupling domain as well as for the coupling zone of the Croatian operational domain (it covers larger area than the operational Belgian domain in (Termonia 2003), but the event can still be considered rare. There are changes from one season to another (more ot less 'stormy'), but there is no apparent increase in the number of fast propagating storms with an increase of the ARPEGE resolution (at least in the range of resolutions available for this study).

The spatial distribution of MCUF reveals that RMPDs favour the sea surfaces, especially the North Sea and the western Mediterranean. Analysis of the MCUF and IFSM fields for a longer period can show which areas favour quickly moving storms that could be missed by the coupling procedure if the 3 hourly coupling period is used. Maps with number of occurrences when the filtered pressure field is larger than the 0.003 threshold show that there are not to many places where to put the coupling zone in order to avoid LAM forecast failure in the case of a RMPD. The problem would be only made worse in higher resolution LAM. The coupling zone on the lateral boundaries is 8 grid points wide and shrinks with the resolution increase. The storm needs less time to cross the narrow coupling zone. Higher resolution global model can yield more intensive pressure changes.

The spatial distribution can be viewed as a map of the fast cyclone tracks and areas that support rapid changes in cyclone development. Not surprisingly, this study shows that not only North Sea, but also the western Mediterranean is an area where storms frequently propagate with high velocities and can not be resolved in LBCs of a 8 km resolution LAM when provided with 3 hour interval. In LAM with roughly 3 times larger horizontal resolution, even 1 hour coupling interval would be insufficient.

There is no field similar to MCUF provided in the coupling files of IFS from ECMWF. Therefore an experiment has been performed in order to compute the field locally from the coupling files. The forecast needed to compute MCUF was run using ALADIN model and the resulting field IFSM can be used for detecting RMPDs in the operational forecast. It requires running the ALADIN forecast in low resolution up to 78 hours (same range as the coupling files are provided). It is more computationally expensive than reading the field already provided in the LBC files but it is feasible. However, the results contain some detrimental effects:

- different model dynamics could lead to different developments in the surface pressure field and hence different MCUF values,
- a quickly moving storm can enter the LBC domain undetected and consequently be missed by the MCUF,
- rather low cyclone activity on the western Mediterranean comapred with results using ARPEGE.

The error function (Termonia 2003) were computed using tendencies estimated by running ALADIN for one time step, using fields from the coupling fields without initialization, initialized with DFI and with SSDFI. No initialization yields a signal of RMPDs but also a lot of noise. Clearly a higher threshold value should be used, but it should be chosen carefully. DFI reduces the level of noise and the magnitude of the signal and many RMPDs are removed from the time series (Figure 2.13) but there are still evidences of large values related to mountains. SSDFI reduces the level of noise and the signal of RMPDs, but more of the signal is preserved.

Finally, RMPDs are detected by simple computations of variations in the mean sea level pressure from three consecutive coupling files. Apparently, this rather simple method can be used for detecting RMPDs. The noise is more intensive than for error function computed without initialization, but so is the signal for RMPDs. This method can be used on any variable and it does not require running any model using coupling data as initial conditions. Mean sea level pressure is less sensitive to the reduction in the coupling update frequency than precipitation and vorticity (Denis et al. 2003).

Climate LAMs could benefit from a large domain (Žagar et al. 2013). It takes several days for the cascade of variance to fill the small scales (Laprise 2008). Loosing small scale features, arriving from the global model at lateral boundaries, certainly does not help. If the domain of the climate LAM is small and the flow over the area is strong, it could move over the domain too quickly to develop small scales (Žagar et al. 2013), and if the temporal interpolation of LBC data filters high resolution data from a global model, there might not be enough space (in the domain) nor time (before the flow leaves it) for LAM to recreate these small scales.

On the other hand, NWP models that have small scale data in the initial conditions through blending (Brožkova et al. 2001) or data assimilation cycle (eg. Stanešić (2011)) need RMPDs that enter the domain during the model forecast. It took ALADIN 66 hours to develop a small scale feature in the 2 km resolution nonhydrostatic run (Tudor and Ivatek-Šahdan 2010) coupled to 8 km operational forecast that was run without data assimilation at the time (Ivatek-Šahdan and Tudor 2004).

As there are plans to increase the resolution of the operational ALADIN to 4 km and ECMWF announced plans for the increase in the horizontal resolution of operational IFS, the problem of resolving RMPDs in LBC data available with 3 hourly interval will become more frequent and it is questionable if hourly coupling data would be sufficient in some cases. Boundary error restarts (Termonia et al. 2009), gridpoint nudging (Termonia et al. 2011), computing corrected interpolation in time with time derivatives (Termonia 2003) and alternative methods of interpolating LBC data in time (Tudor and Termonia 2010) are computationally expensive and should be used only when needed. Therefore such cases should be detected by a reliable method since any missed case means that LAM would not forecast severe weather conditions. The error function computed without initialization and the amplitude method (Section 4.3) are cheap methods that could be applied in a straightforward manner. MCUF from IFSM seems reliable for most of the LACE domain. The error function computed from the initialized fields does not improve the results enough to justify the extra computational cost. The alternative is to compute MCUF in operational IFS.

Chapter 3

An introduction to: Alternative formulations for incorporating lateral boundary data into limited area models

3.1 Introduction

Limited area models (LAMs) are used as an alternative to global numerical weather prediction (NWP) models for a wide variety of research and operational forecast applications. Particularly LAMs are subject to different sources of forecast error: the parameterizations of physical processes, the initial conditions, the numerical algorithms and surface forcing. These also affect various global NWP models, but LAMs have one additional source of error related to their lateral boundary conditions (LBCs). The most popular scheme for LBC treatment is the the one proposed by Davies (1976), used almost exclusively for one-way coupled operational LAMs (McDonald 1999). There are problems that are linked with the nature of various lateral boundary schemes (Davies 1983) but LBC problems can also be of a different source, for example the quality of the large scale data. An overview of the weaknesses of the LAM forecast caused by the LBCs was provided by Warner et al. (1997).

LBCs are obtained from models with a coarser mesh in the horizontal and the vertical that usually use simpler (different) parameterizations of physical processes. The coarse grid of the host model smooths the information supplied at the lateral boundaries (Caian and Geleyn 1997). The numerical procedures used on the interface of the two grids also generate errors (McDonald 1999). Termonia et al. (2009) showed that commonly used temporally interpolating lateral-boundary data may

lead to errors in the surface field of up to about 10 hPa in case of fast propagating storms.

Model errors due to LBCs can be significant since it propagates into the domain interior during the forecast (Nicolis 2007). It propagates and amplifies as it enters the domain of integration depending on the intensity of the cross-boundary flow and spreads further through the domain with longer time of integration (Nutter et al. 2004). This problem is becoming more important as LAM forecasts tend to be longer, up to 72 hours and in higher resolution, covering smaller area and with narrow coupling zone. Enlargement of the domain to move the edges far from the area of interest does not prevent the LBC error from eventually contaminating the solution (Vánnitsem and Chome 2005).

Juang and Kanamitsu (1994) developed a regional spectral model that predicts deviations from the global model forecast and find that shorter coupling intervals allow more noise in the mean sea level pressure field along lateral boundaries, but not in the precipitation field. In order to force the perturbations to zero along lateral boundaries and reduce the aforementioned noise, they apply lateral boundary relaxation for the dynamical part of the total tendency and a blending of the total tendency over the entire regional model domain. The second procedure was found unnecessary for noise removal. The subsequent study (Juang and Hong 2001), using the same model, revealed that it is not necessary to have large domain in order to avoid lateral boundary influence and multi nesting is not necessary for a very fine resolution forecast over a small domain. Assignment of lateral boundary values at the boundaries is found essential for representing scales too large to be periodic on LAM domains (Laprise 2003), which represents a large scale closure.

The schemes for lateral boundary conditions used in NWP usually specify every field at all the lateral boundaries making the initial-boundary problem mathematically ill-posed (McDonald 1999). Unfortunately, Oliger and Sundström (1978) found that local pointwise boundary conditions cannot be well-posed for hydrostatic equations and open boundaries. There are solutions in simplified models (see e.g. McDonald 2000; Termonia 2008) that allow well-posedness and to control the gravity waves, but the extension of the gravity wave control mechanism from one to more dimensions leads to fundamental difficulties (Durran 1999). The search for the well-posed solution continued, e.g. for the problem in semi-Lagrangian models when the origin point of the trajectory lies outside of the model domain (McDonald 2000), the application of this work in spectral models (Termonia and Voitus 2008; Voitus et al. 2009), and improved schemes for overspecified LBCs such as for instance Navon et al. (2004). Spurious gravity waves that occur due to the ill-posedness of the LBCs are filtered by the coupling procedure itself and/or the horizontal diffusion scheme and it is supposed that the remaining spurious waves are acceptable. Even

when the problem is well-posed, waves can still be reflected from the boundary. Boundaries that transmit waves in and out without spurious reflections are said to be transparent (McDonald 2002). Such set has been tested in a nested environment on a simple set of shallow water equations (McDonald 2003) on a single level without diffusive terms. However, the results still depend on the quality of the large scale data used for coupling.

The quality of the LBC data for operational as well as research purposes is severely restricted since its amount is limited by storage and data-transfer capacities. Large scale fields are usually available in temporal resolution of several hours, but they are needed at each LAM time step which is usually on the order of several minutes. Consequently, LBCs are obtained at every LAM time-step using large scale fields that are interpolated in time. This interpolation procedure corrupts the fields, especially the features that have time scales shorter than the coupling interval. The situation can be made even worse when the large scale fields are taken only from the narrow area close to the domain lateral boundaries. Consequently, small scale features that are quick enough to enter the domain during one coupling interval are not suitably represented by the interpolated data, see Termonia (2003).

In Termonia (2004) it is shown that it is possible to detect boundary errors coming from such deficiencies in the interpolation. Termonia et al. (2009) proposed a solution that relies on a restart of the forecast after the storm has entered the domain and the error is detected by the boundary error procedure. This proposal improves the forecast itself, but still exhibits two weaknesses that may be subject for improvements. The first is that a standard initialization like the popular digital-filtering initialization (DFI) may weaken the depths of the large-scale storms present in the data of the coupling model. This can be controlled by using a scale-selective digital filter (SSDFI) as proposed in Termonia (2008). Secondly, any small scale information that has been built up in the limited-area model since the beginning of the forecast run is lost. In that paper it is also suggested that this method may be improved in spectral models by relying on spectral nudging of the type proposed in Waldron et al. (1996), von Storch et al. (2000), Radu et al. (2008), and Guidard and Fischer (2008). In those papers the spectrally nudged information was used over the entire domain. Possible benefits of spectral nudginig have been noticed by Meinke et al. (2006). The present chapter makes a first feasibility study of such methods to improve the LBC temporal resolution problem, in particular investigating its use within the buffer zone at the lateral boundary of the domain only. As a comparison the spectral nudging over the entire domain will also be included in the present chapter.

The aim here is to develop a simple coupling procedure that could be used operationally as a supplement or as an alternative to the flow-relaxation one either

always, or when the quality of the LBCs is found insufficient by the monitoring procedure of Termonia (2004). Alternative time-interpolation schemes for LBC data are proposed. Alternative time-interpolation schemes for LBC data are proposed. Different coupling procedures are implemented and tested using a simple one-dimensional model. This enables the identification of the errors linked to a particular LBC schemes, that could hardly be identified using a realistic model (Robert and Yakimiw 1986).

This chapter is organized as follows. Section 3.2 outlines the problem by discussing the time evolution of spectral coefficients produced by an operational run of a realistic three dimensional LAM. The one-dimensional model used for the testing of the alternative formulations, is also briefly the described in this section. Results obtained using the flow-relaxation scheme are presented in Section 3.3. The method of spectral coupling is described in Section 4.1. Section 4.2 describes the time interpolation done in spectral space in combination with the usual gridpoint coupling scheme. The final part of this chapter brings discussion and conclusions.

3.2 Data and experimental setup

This section analyses spectral data of a forecast for the operational ALADIN limited-area numerical weather prediction model developed and maintained by the ALADIN International team (1997). The obtained results will then be used as a basis for proposing improved temporal interpolation schemes in sections 4.1 and 4.2.

Figures 3.1a and 3.1b show the evolution of the mean-sea level pressure (mslp) of the Lothar storm (Wernli et al. 2002) in an operational forecast of the ALADIN model between 0900 UTC and 1200 UTC 26 December 1999. This model was run with a resolution of $\Delta x = \Delta y = 9.5km$ and 300 grid points in the zonal and meridional directions and a time step of $\Delta t = 300s$. Fig. 3.1c shows the mslp in the middle of this time interval at 1030 UTC. When linearly interpolating this storm within the 3-h time interval between $t_0 = 0900$ UTC and $t_1 = 1200$ UTC,

$$\mathcal{L}\, c\,(t) = \frac{t_1 - t}{t_1 - t_1}\, c\,(t_0) + \frac{t - t_0}{t_1 - t_0}\, c\,(t_1)\ . \tag{3.1}$$

one gets at $t = 1030$ UTC not one, but a "dipole" of two depressions, as can be seen from Fig. 3.1d. In most operational applications such interpolated data is used as coupling data for the Davies scheme. If, for instance, the configuration in Fig. 3.1d would happen in the fictitious Davies zone shown in the panels c and d, some completely spurious information might enter the physical domain of interest.

ALADIN is a spectral model following the work of Haugen and Machenhauer (1993), so the Fourier components of the fields can be easily obtained. The spectral

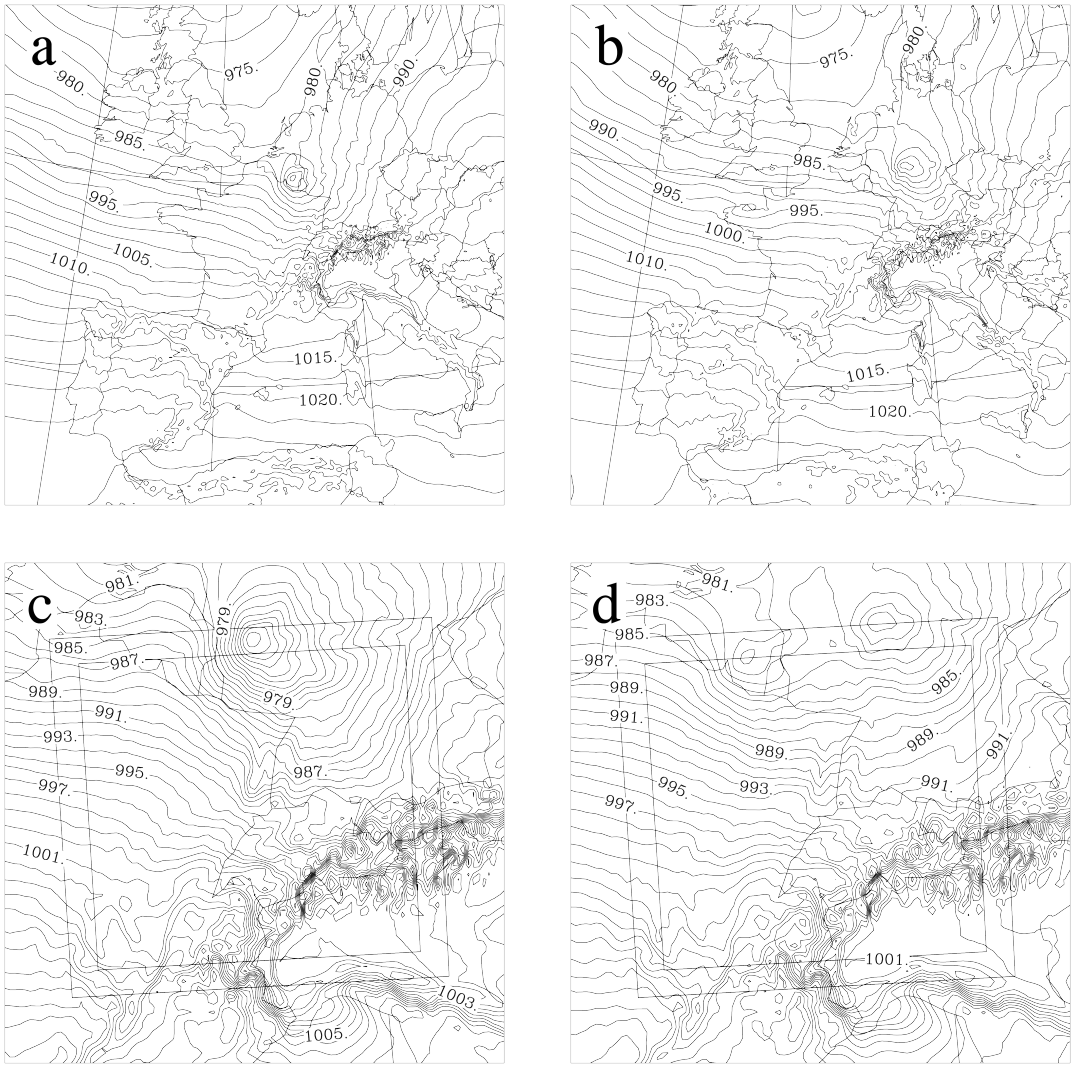

Figure 3.1: ALADIN-France forecast of the Christmas storm on 26 December 1999: (a) the MSL pressure at 09 UTC (contour interval is 2.5 hPa), (b) MSL pressure at 12 UTC (contour interval is 2.5 hPa), (c) the MSL pressure at 10h30 UTC, (zoom of the domain with contour interval of 1. hPa), and (d) the linear interpolation at 10h30 UTC between the MSL pressure at 09 UTC and the MSL pressure at 12 UTC (zoom of the domain with contour interval of 1. hPa). The frame on the Figs. c and d is a fictitious Davies relaxation zone containing the "dipole" structure of the interpolated field in Fig. d.

coefficients are computed on an extension of the physical domain of the limited-area model, where the fields on the extension zone are constructed in such a way as to make the fields periodic using splines. During a time step computation the spectral information is present at the beginning of the time step and during the inversion of the Helmholtz equation, as explained in table II of Termonia and Hamdi (2007). It is our aim here to investigate whether the spectral information may be useful to improve *the proposals made in Termonia et al. (2009)*.

Within the ALADIN model a fast Fourier transform is applied twice in the two spatial horizontal directions I and J of the grid-point field F_{IJ} with gridpoint indices $I = 0, \ldots, M-1$ and $J = 0, \ldots, N-1$ by

$$c_{KL} \;=\; FFT\left[F_{IJ}\right]_{KL} \frac{1}{MN} \sum_{I=0}^{M-1} \sum_{J=0}^{N-1} F_{IJ}\, e^{-\frac{2\pi i}{M} I K} e^{-\frac{2\pi i}{N} J L}\,, \tag{3.2}$$

for the indices $K = -\frac{M}{2}, \ldots, \frac{M}{2}$ and $L = -\frac{N}{2}, \ldots, \frac{N}{2}$, corresponding to waves with wave lengths $l_{KL} = [(K/M\Delta x)^2 + (L/N\Delta y)^2]^{-\frac{1}{2}}$.

The spectral coefficients are available for each model time step in the interval $[t_0, t_1]$,

$$c^{\alpha}_{KL} = c_{KL}\left(\alpha \Delta t\right)\,, \tag{3.3}$$

for $\alpha = 0, \ldots, n_t$ corresponding to $t = t_0 + \alpha\Delta t$, with Δt the model integration time step. It can be easily verified that applying $\mathcal{L}$ to the grid-point field F_{IJ} is equivalent to applying it to the spectral coefficients c_{KL},

$$FFT\left[\mathcal{L}F_{IJ}\right]_{KL} = \mathcal{L}c_{KL}\,, \tag{3.4}$$

so the effect of the linear interpolation in Eq. (3.1) can be studied by investigating its effect on each separate spectral coefficient.

Fig. 3.2 shows the time evolution of the three coefficients $c_{11,-15}, c_{1,0}$, and $c_{18,3}$, for the surface pressure between time $t_0 = 9h$ and $t_1 = 12h$ forecast range of the forecast run presented in Fig. 3.1. It can be seen from the time evolution of $c_{11,-15}$ in Fig. 3.2a that even though the linear interpolation may be quite good in the middle of the interval (indicated by the diamonds), it can completely miss the rotating part of the time evolution of the spectral coefficient. So the interpolation should be considered in all points in the interpolation interval. Fig. 3.2b shows for the large scales, illustrated here by $c_{1,0}$ with a wave length of $2850\,km$, that the linear interpolation is a good approximation. On the other hand for the small scales, exemplified here by $c_{18,3}$ with wave length $l_{18,3} = 156\,km$, the interpolation is entirely wrong.

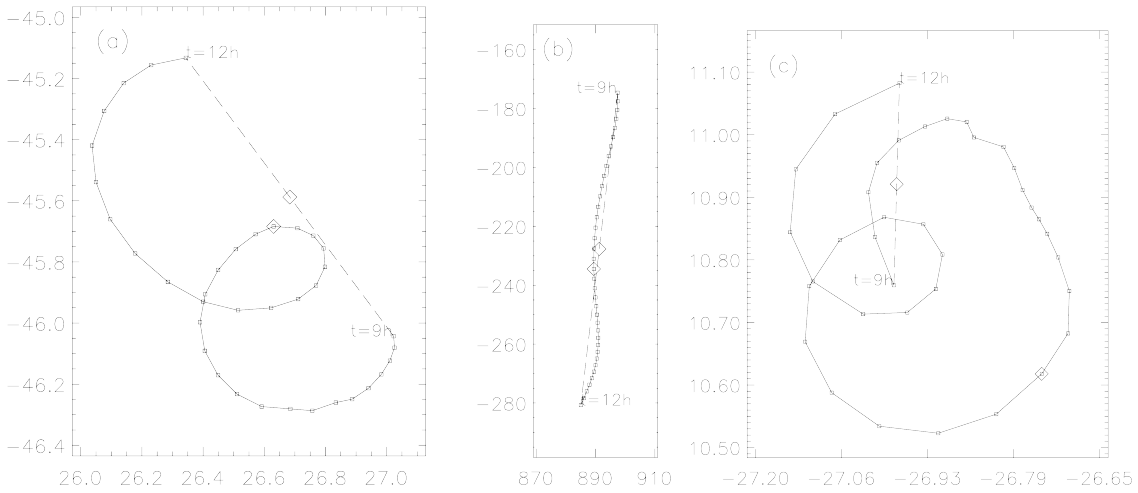

Figure 3.2: Example of the time evolution of three spectral coefficients: (a) $c_{11,-15}$, (b) $c_{1,0}$, and (c) $c_{18,3}$. The x axis and the y axis indicate the real and the imaginary part respectively, in units of Pa.

The time evolution of the spectral coefficients c^{α}_{KL} in Fig. 3.2 can be seen as a superposition of a linear trend and a rotation in the complex plane

$$F_{KL}(t) = \Phi_{KL}(t) + \mathcal{A}_{KL}(t)\,, \tag{3.5}$$

with the linear trend given by

$$\Phi_{KL}(t) \;\; = \;\; \phi_{KL}(t_0) + (t - t_0)\, v_{KL}\,, \tag{3.6}$$

and the complex rotational part given by

$$\mathcal{A}_{KL}(t) \;\; = \;\; M_{KL}\, e^{i\,[\Omega_{KL}(t-t_0)+\lambda_{KL}]}\,. \tag{3.7}$$

The term Φ_{KL} can be interpreted as the part of the field that is locally growing (both positively or negatively) with tendency v_{KL}. The term $\mathcal{A}_{KL}$ represents the moving part of the wave.

Fig. 3.3 shows some examples of the time evolution of selected spectral coefficients of the ALADIN forecast of the Christmas storm between 0900 UTC and 1200 UTC to formula (3.5). Each time step is represented by a small rectangle. A fit of the function (3.5)-(3.7) is superposed on each panel (solid lines)[1]. This fit quantifies the validity of the hypothesis that the evolution can be decomposed into a rotating

[1] The fit was taken as the optimal estimate for the parameters in F_{KL} by minimizing the cost function

$$I\,[\Omega_{KL}, M_{KL}, \lambda_{KL}, v_{KL}, \phi_{KL}] = \tfrac{1}{2} \sum_{\alpha=0}^{n_t} \overline{(F_{KL}(t_0 + \alpha\Delta t) - c^{\alpha}_{KL})}\; (F_{KL}(t_0 + \alpha\Delta t) - c^{\alpha}_{KL})\,,$$

and a linear part.

From Fig. 3.3 we see that within time intervals of a few hours (3 h in this case) and for the large scales, i.e. the scales of the storm (100 km and more), at the level of the spectral coefficients, the time evolution manifests itself as a combination of a linear trend and a rotation in the complex plane. Note that the fit is is better for larger length scales. For instance in panels (j) and (l) corresponding to wave lengths $l_{16,-3} = 175km$, and $l_{19,19} = 106km$, the fits are of lower quality.

The aim of the present chapter is to test whether this behavior of the spectral coefficients can be exploited to improve the LBC temporal resolution problem. As mentioned above this will be studied in a one dimensional spectral shallow-water model on a single horizontal level. It uses velocity and geopotential as model fields and it can run on global or limited area domains. The term global domain herein describes a periodic domain where a signal that exits on one end re-enters on the opposite side. Use of the limited-area domain implies a coupling procedure on the domain edges. It is integrated with two time level semi-implicit semi-Lagrangian scheme with a second order accurate treatment of the non-linear residual (Gospodinov et al. 2001).

A shallow-water spectral limited-area model that applies Fourier spectral representation on the model variables requires usage of time-dependent periodic LBCs (Haugen and Machenhauer 1993). Semi-implicit time integration and solving the Helmholtz equation in spectral space constrains the coupling procedure to be applied at the very beginning or end of the gridpoint computations (Rádnoti 1995). Another solution would be to develop a simple and cheap procedure that can be applied in the spectral space. The width of the extension zone is determined by the fact that the extended boundary fields should be well represented by the used truncation (Haugen and Machenhauer 1993). The non-linear terms of the model equations are computed without aliasing if the number of grid points in the whole integration area is chosen so that $N_x > 3M + 1$ where M is the truncation wavenumber. Weak numerical diffusion is applied in spectral space at the end of the time step to alleviate accumulation of energy at the smallest scales due to spectral blocking.

The large scale model is a periodic low resolution model that provides LBCs and will be referred to as the global model henceforth. In the tests, two sets of model runs are performed, the global and the LAM. The global model and LAM are using the same initial conditions that consist of a Gaussian shape depression that propagates from west to east with constant speed through the whole domain.

The global model is run on 200 grid points with Δx=40km and the truncation

by a conjugate gradient method (following Gilbert and Nocedal 1992). The bar denotes the complex conjugate.

wavenumber 66. The LAM run is on 200 grid points 11 of them are the extension zone on east and the 8 points on the eastern and western edge of the remaining 189 points are the relaxation zones. The horizontal resolution of the LAM was Δx=10km and the truncation wavenumber is equal to the one used in the global model since the number of grid points is the same. Both models use the same time step of 150 seconds.

Time steps when the large scale data are available will be referred to as the coupling steps. They are separated by the coupling interval. The coupling procedure is done at each time step. It consists of spatial and temporal interpolation and the coupling scheme, e.g.. the Davies (1976) scheme. The large scale data are interpolated in space onto the LAM grid and then interpolated in time to be used at each LAM time step. The 3h coupling interval is 72 time steps of the LAM.

3.3 Gridpoint coupling

This section demonstrates the capability of the simple model described in the previous section, to reproduce problems associated with interpolation of LBC in time on narrow lateral zones. The flow-relaxation coupling scheme proposed by Davies (1976) relaxes the interior flow to the prescribed exterior flow consuming gravity wave energy and fine spatial scale potential vorticity in a narrow zone near lateral boundaries representing adequately the outgoing gravity waves as well as geostrophic flow through the boundary. This zone is called the relaxation zone and its width will be 8 grid points of the LAM domain in the following tests. On the lateral boundaries, the LAM is forced with the large scale solution. The value of the model variable in the relaxation zone (X_C) is computed from the large scale (X_{LS}) and the small scale (X_{SS}) values by

$$X_C = \alpha X_{LS} + (1-\alpha) X_{SS}\,, \tag{3.8}$$

using the relaxation coefficient α

$$\alpha = (p+1)Z^p - pZ^{p+1}\,, \tag{3.9}$$

where p is the order of the polynomial (tuning parameter), $Z = \frac{|x-x_e|}{x_c-x_e}$ is the distance of the gridpoint x from the domain edge x_e relative to the width of the coupling zone $(x_c - x_e)$. The relaxation coefficient $\alpha = 1$ in the extension zone and $\alpha = 0$ in the central zone of LAM.

The large scale solution is known only at coupling steps t_0, t_1, t_2, ... where t_0 is usually the initial time and the coupling intervals usually kept constant, e.g. in operational applications 3 hours, which is much longer than the typical time step

used in operational LAM (5-10 minutes). The large scale model state X used in the relaxation zone is interpolated in time linearly:

$$X(t) = w_1 X_{t_1} + w_2 X_{t_2} \quad \text{where} \quad w_1 = \frac{t_2 - t}{t_2 - t_1} \quad \text{and} \quad w_2 = \frac{t - t_1}{t_2 - t_1}, \tag{3.10}$$

or quadratically

$$\begin{aligned} X(t) = w_1 X_{t_1} + w_2 X_{t_2} + w_3 X_{t_3} \quad \text{where} \quad w_1 &= \frac{(t_2 - t)(t_3 - t)}{(t_2 - t_1)(t_3 - t_1)} \quad , \\ w_2 = \frac{(t_1 - t)(t_3 - t)}{(t_1 - t_2)(t_3 - t_2)} \quad \text{and} \quad w_3 &= \frac{(t_1 - t)(t_2 - t)}{(t_1 - t_3)(t_2 - t_3)} \quad , \end{aligned} \tag{3.11}$$

or using the tendency of the model state Termonia (2003)

$$X(t) = w_1 X_{t_1} + w_2 X_{t_2} - w_1 w_2 (t_2 - t_1) \left[\left(\frac{\partial X}{\partial t} \right)_{t_2} - \left(\frac{\partial X}{\partial t} \right)_{t_1} \right] \quad . \tag{3.12}$$

where w_1 and w_2 are computed as in linear interpolation scheme. Another solution can be to increase the size of the coupling zone to include the area where the depression appears at the coupling step.

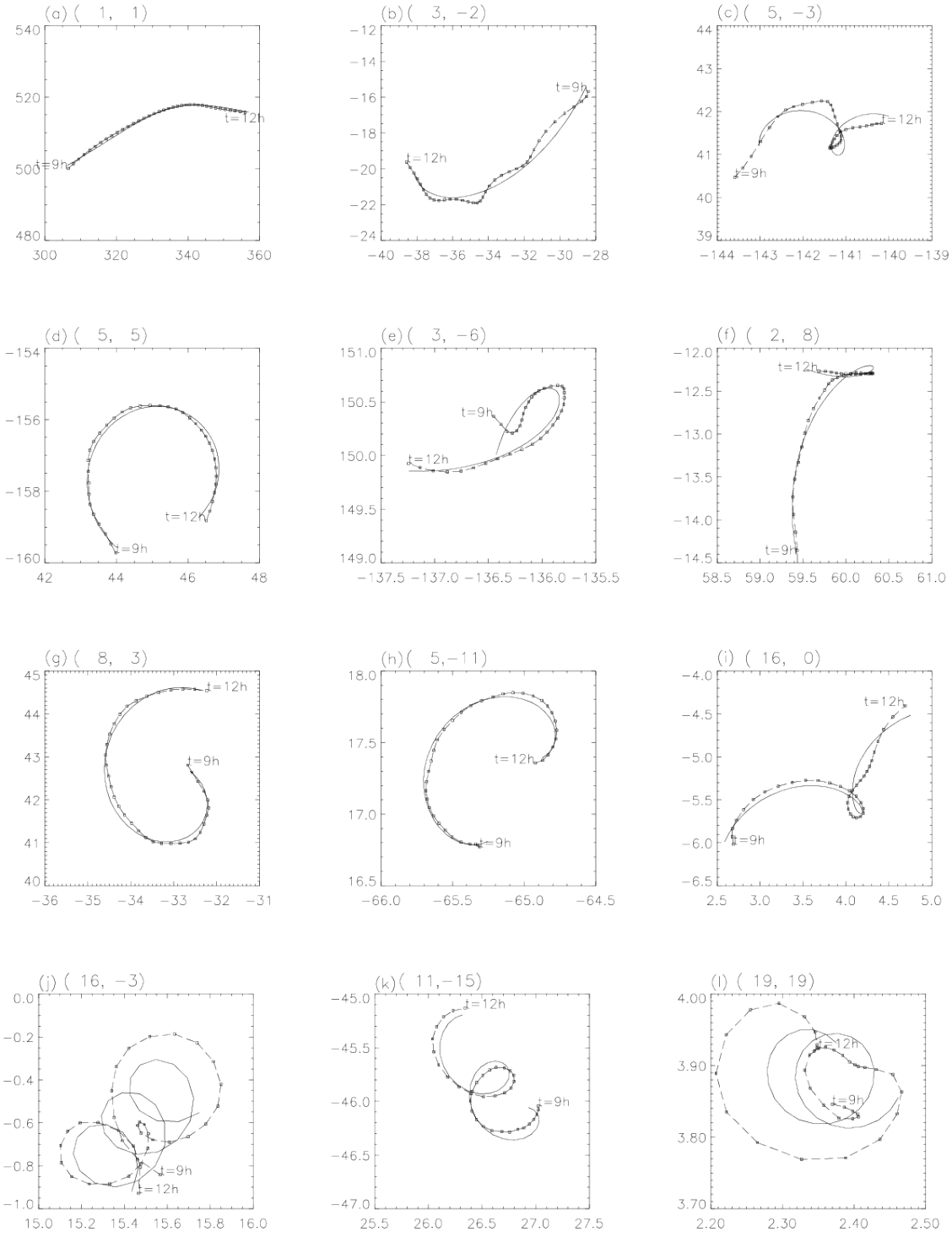

Figure 3.3: Fits (solid lines) of selected spectral coefficients of the ALADIN forecast of the Christmas storm between $09h$ and $12h$ forecast range, compared to the forecast data (a) $c^{\alpha}_{1,1}$, (b) $c^{\alpha}_{3,-2}$, (c) $c^{\alpha}_{5,-3}$, (d) $c^{\alpha}_{5,5}$, (e) $c^{\alpha}_{3,-6}$, (f) $c^{\alpha}_{2,8}$, (g) $c^{\alpha}_{8,3}$, (h) $c^{\alpha}_{5,-11}$, (i) $c^{\alpha}_{16,0}$, (j) $c^{\alpha}_{16,-3}$, (k) $c^{\alpha}_{11,-15}$, (l) $c^{\alpha}_{19,19}$ (points). The x and y axis indicate the real and imaginary part respectively (in Pa).

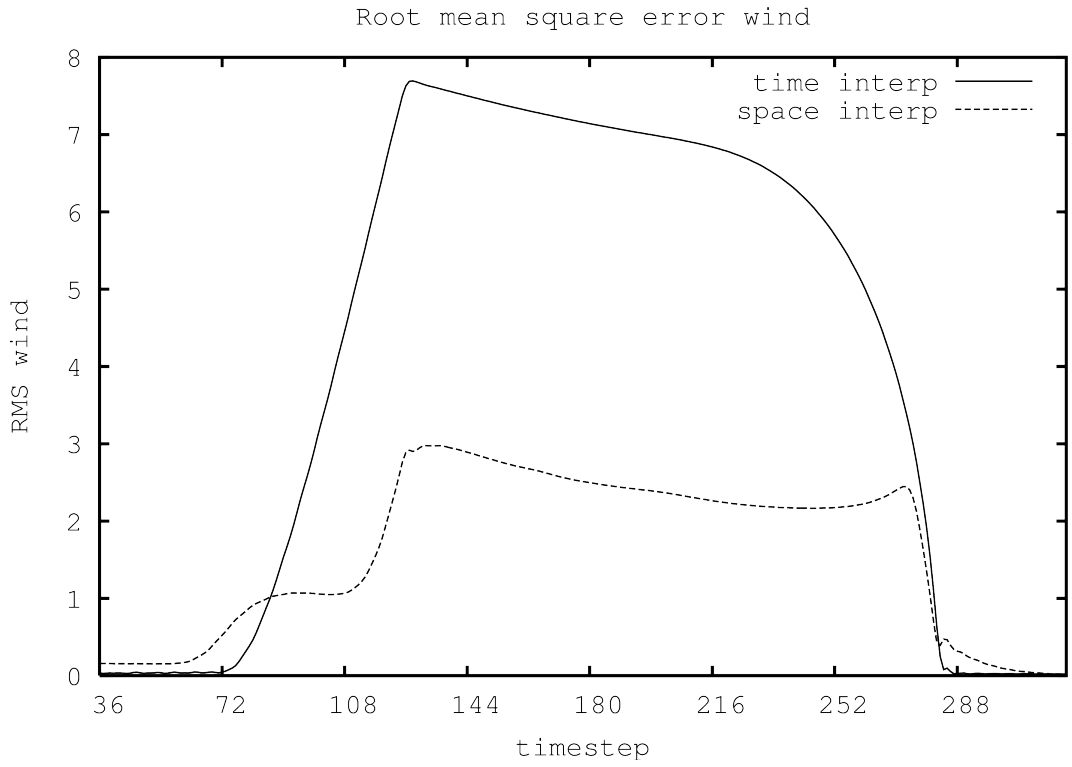

Figure 3.4: Root mean square error of wind variable computed over the LAM domain using the LAM coupled to high resolution global model as reference, for LAM coupled to high resolution global data with 3h interval (line) and coupled to low resolution global data from every time step (dashed).

Chapter 4

Alternative formulations for incorporating lateral boundary data into limited area models

We need to determine the appropriate reference simulation to be used as reference for computation of error introduced by the coupling or time interpolation scheme. The effectiveness of the boundary updating was first tested using the method of Baumhefner and Perkey (1982).

Test 1 The global model was run using the same horizontal resolution as the LAM, on 800 grid points with Δx=10km and the truncation wavenumber 264. The LAM was run on the same domain as usual, but coupled to the high resolution global model using the flow relaxation scheme. In the first test, output from the high resolution global model was used from every time step so interpolation in time or space was not needed.

Test 2 In the second test, the output from the high resolution global model was taken with a 3 hour interval and interpolated in time only.

Test 3 In the third test the output from the low resolution global model was used from every time step so the LBC data were interpolated in space only.

There was no difference between the global and the LAM solutions in the first test when the flow relaxation scheme was used, as was expected (McDonald 1999). The difference between the results from the first and the second test represents the error due to the temporal interpolation procedure. The difference between results of the first and the third test represents the error due to spatial interpolation (Figure 3.4) and different global model resolutions. The results of the global model run with different spatial resolutions are different. Consequently, LAM is coupled to the different global model data and the error is large. In other words, the disturbance

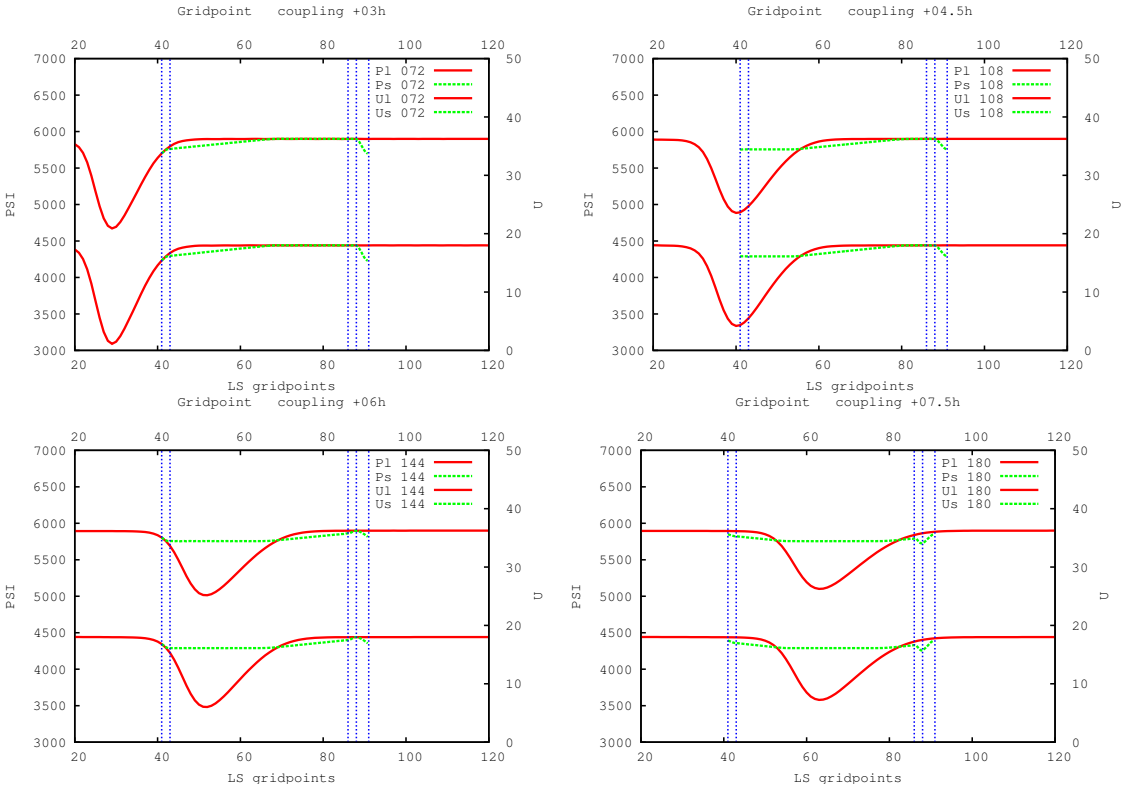

Figure 4.1: Results for coupling using Davies scheme with 3 hour interval between input large scale data, before the depression enters the domain, 3 hour forecast (a) and after, 6 hour forecast (b). Global model (full line) and limited area model (dashed) results for geopotential are shown above the results for the wind variable. Vertical lines are, from left to right, left edge of the LAM domain, right edge of the left coupling zone, left edge of the right coupling zone, right edge of the right coupling zone (also left edge of the extension zone) and the right edge of the LAM domain.

that enters the domain is different so the error is not only due to spatial interpolation but it is still lower than the error due to temporal interpolation. This is why the result of the third test will be used as reference in the rest of the chapter.

Using gridpoint coupling with large scale data available with only 3 hourly interval allows for the depression to enter the domain area almost unnoticed (Figure 4.1). When the same computational scheme is used but with new large scale data available at every LAM time step (Test 3), the disturbance is detected by the coupling scheme and further developed by the LAM (Figure **??**a). This result represents our ideal goal of "perfect coupling" to be reached by the modified or new coupling scheme. Unfortunately, such perfect conditions of data availability are hardly ever met by LAM users, so other options are tested. Quadratic interpolation in time does not improve the results (not shown) while using the tendencies as well as values of the model variables with 3 hourly interval does improve the results (Figure **??**b) but unfortunately, this is still far from the desired ideal. When the LAM domain

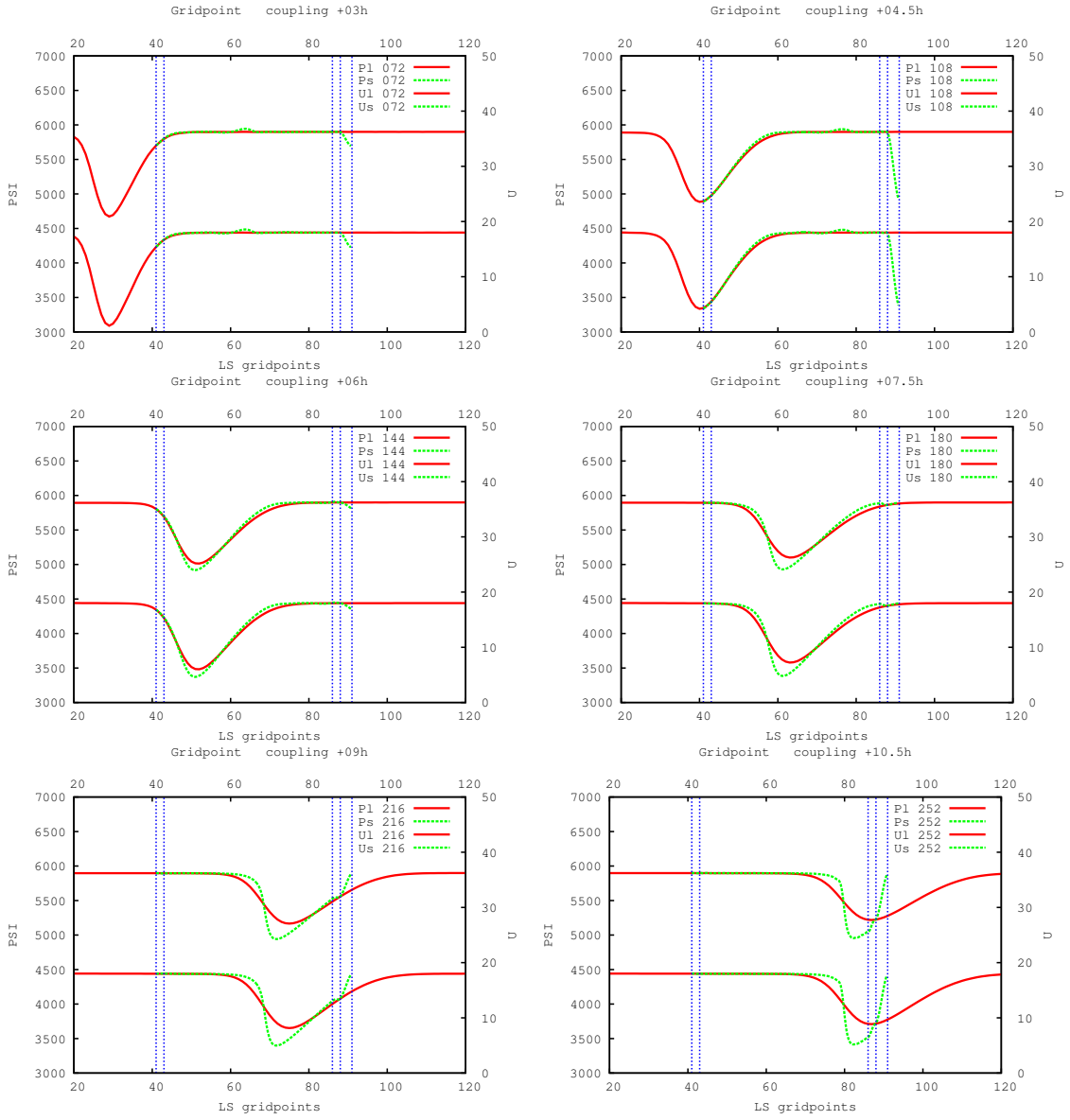

Figure 4.2: Results for coupling using Davies scheme with 1 time-step interval between input large scale data ... Lines have the same meaning as in Figure 4.1.

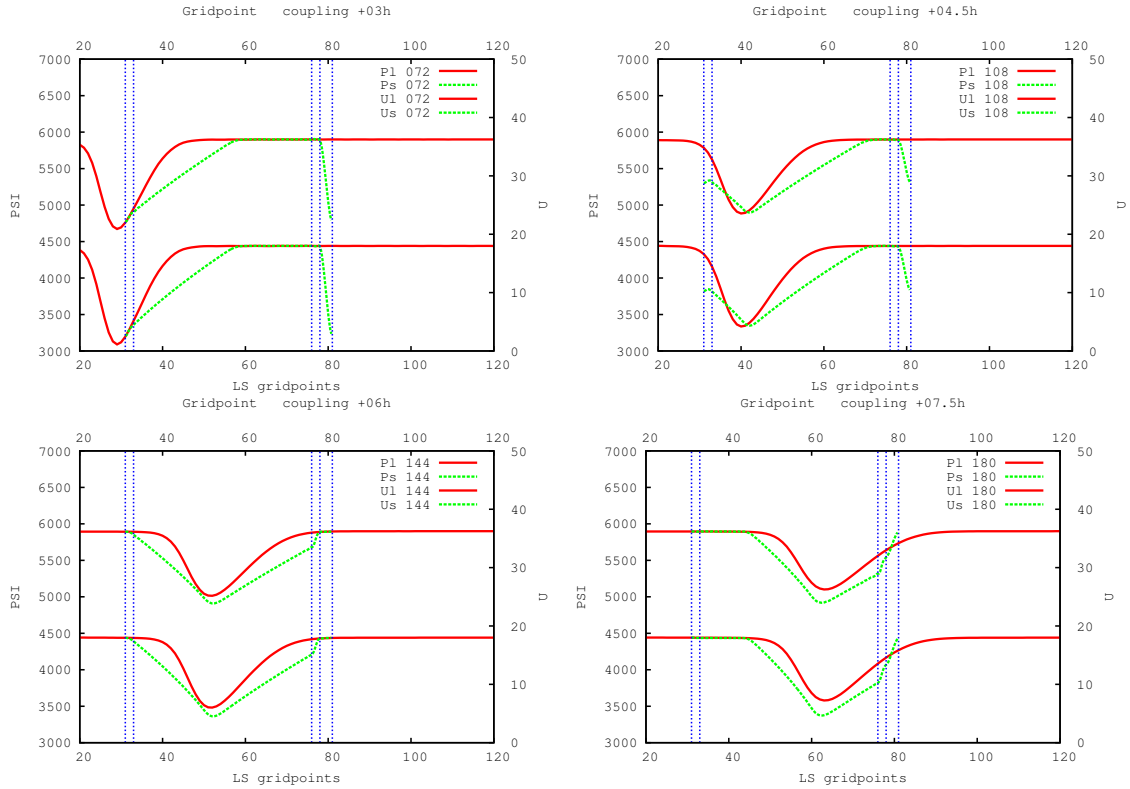

Figure 4.3: Results for coupling using Davies scheme with 3 hour interval between input large scale data and LAM domain shifted so that the depression enters the domain at the time large scale data are known .... Lines have the same meaning as in Figure 4.1.

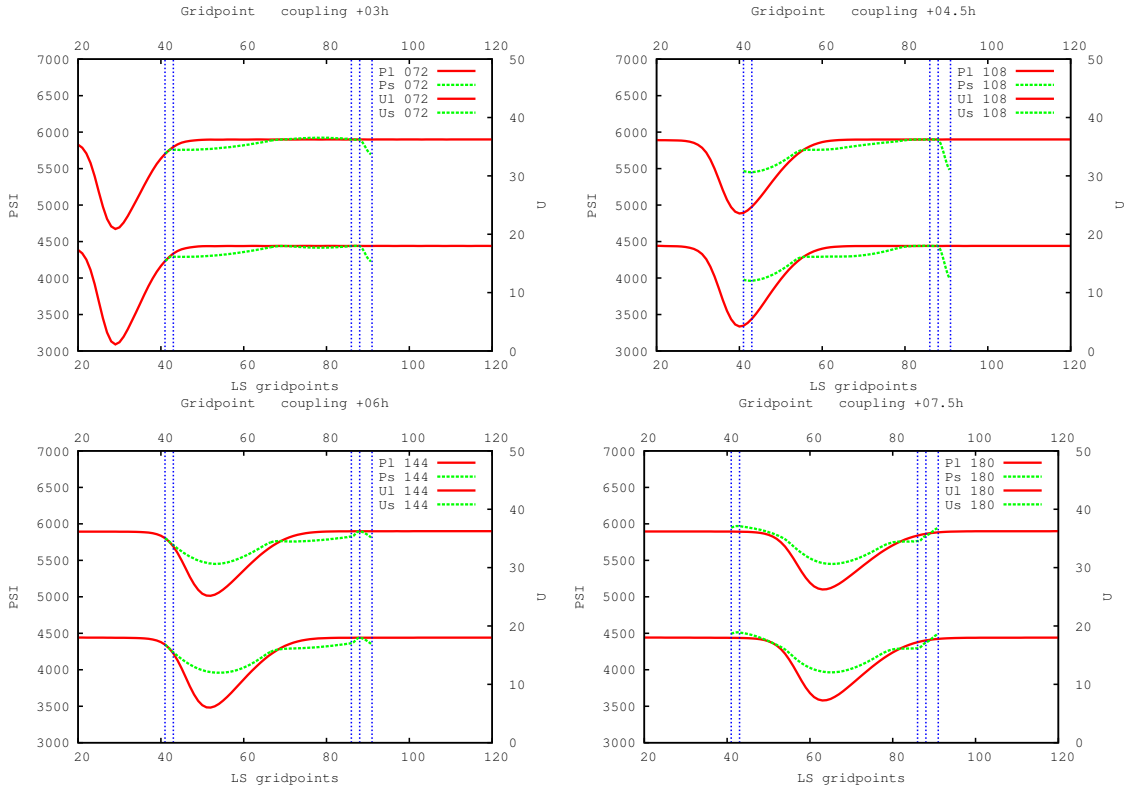

Figure 4.4: Results for coupling using Davies scheme with 3 hour interval between input large scale data and using tendencies of the large scale fields for coupling Lines have the same meaning as in Figure 4.1

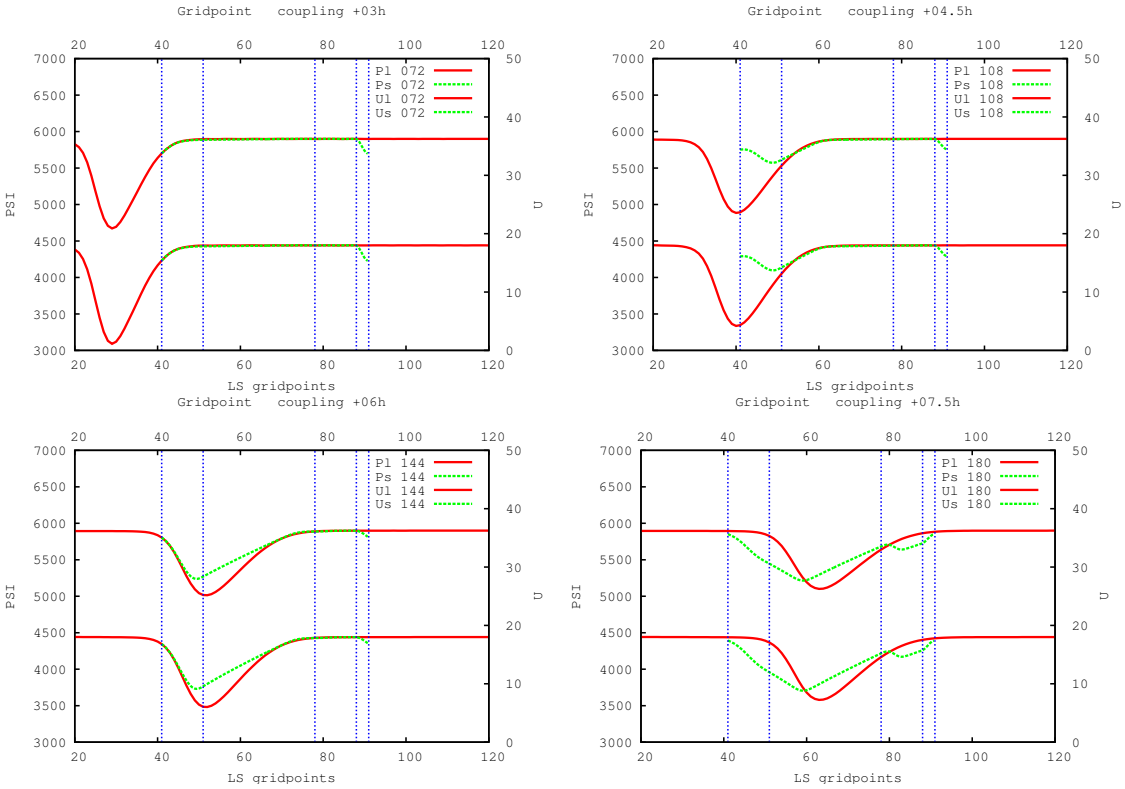

Figure 4.5: Results for coupling using Davies scheme with 3 hour interval between input large scale data and the coupling zone is increased 5 times: using 40 instead of 8 points Lines have the same meaning as in Figure 4.1

was shifted so that the depression minimum enters the domain at the moment when the large scale data are available, the depression was recognized, but its shape was distorted by the time interpolation of the large scale data (Figure **??**a). Another simple geometry solution would be to increase the size of the coupling zone. When its width was five-fold its usual (Figure **??**b) the depression was recognized, but it also produced some spurious phenomena when the disturbance was leaving the domain.

Figure 4.6 shows the evolution of the model error due to the time-interpolation procedure (McDonald 1999) of the wind variable using Test 3 as reference. The error increases as the disturbance enters the domain, between 72 and 144 time steps and decreases when it leaves the LAM domain, between 216 and 288 time steps. These last two results show that there is an error inherent in the temporal interpolation and/or the coupling scheme since it misinterprets or spoils the features that enter the domain giving more incentive for finding an alternative coupling or more suitable time interpolation scheme.

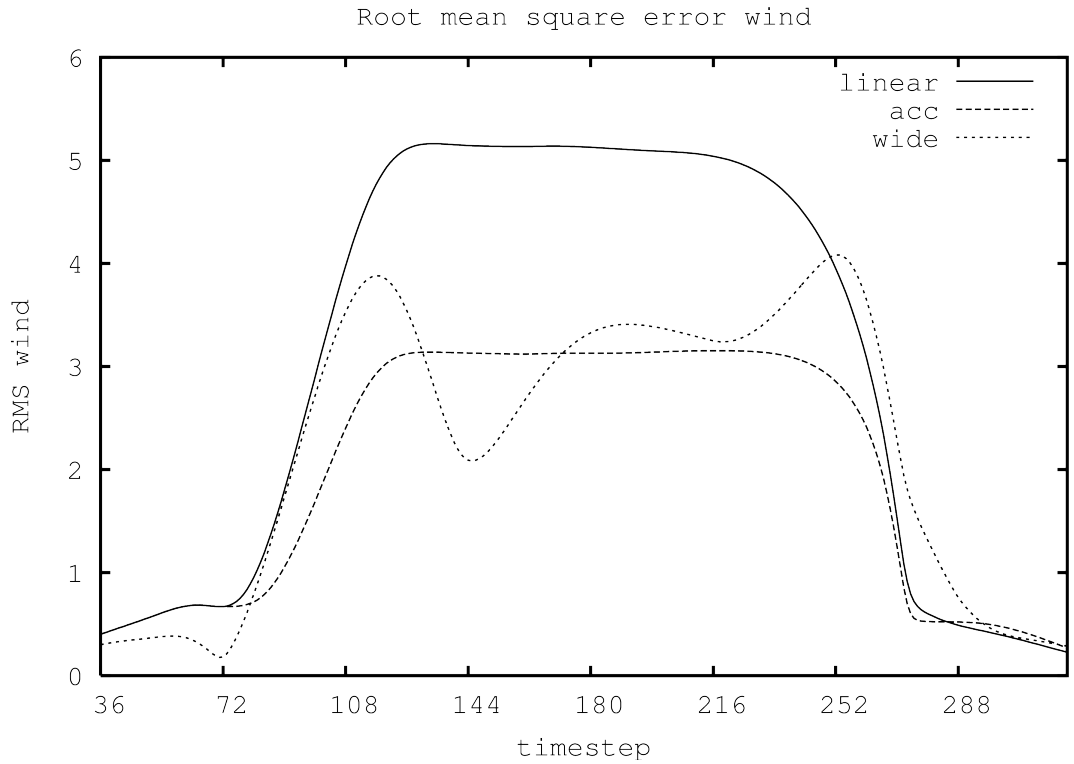

Figure 4.6: Root mean square error of wind variable computed over the LAM domain using the LAM coupled to low resolution global model for each time step as reference, for LAM coupled using flow relaxation scheme to low resolution global data with 3h interval interpolated linearly in time (line), using acceleration (long dash) and wider coupling area (short dash).

4.1 Spectral coupling

As mentioned in the introduction, the coupling of LAM to a global model can be achieved using a procedure similar to spectral nudging that will be referred to as spectral coupling. This coupling is done ovet the whole domain area, not onls the boundaries. The spectral coupling scheme was built using similar mechanism as the flow-relaxation scheme. Small wavenumber state (long waves) is taken from the large scale, large wavenumber state (short waves) is taken from LAM with a smooth functional transition in between. In other words, the large scale solution is spectrally filtered and blended with the LAM solution. The coupling scheme was developed on a basis of a spectral model used with a Fourier transform. The details are described in the following subsection.

4.1.1 The coupling method

For wave numbers lower than some threshold k_0 we take spectral coefficients from the large-scale model. For the wave numbers larger than another threshold value k_1, the spectral coefficients are taken from the LAM. The spectral coefficients for wave numbers between k_0 and k_1 are computed as

$$SP_C = \alpha SP_{LS} + (1-\alpha)SP_{SS}\,, \tag{4.1}$$

where the subscript C denotes the coupled values, LS denotes the values from large scale model and SS denotes values from small scale model. In analogy with the flow-relaxation scheme, the dependency of the α coefficient on the wave number k can be linear

$$\alpha = \frac{k_1 - k}{k_1 - k_0}\,, \tag{4.2}$$

or have a polynomial dependence on k

$$\alpha = (p+1)z^p - pz^{p+1} \qquad for \qquad p > 0 \tag{4.3}$$

$$\alpha = 1 - (-p+1)(1-z)^{-p} - pz^{-p+1} \qquad for \qquad p < 0 \tag{4.4}$$

where $z = \frac{k_1 - k}{k_1 - k_0}$ is the relative distance of the wave number k from the small scale wave number k_1 and p is the order of the polynomial. The boundary wave numbers (k_0 and k_1) are tunable parameters, set according to the model resolutions and the size of the LAM domain. The choice of $k_0 = 2$ and $k_1 = 8$ address the need to describe the scales that are too large to be periodic in LAM (Laprise 2003) using lateral boundary data. The polynomial dependence of α on wave number did not bring much improvement over the linear one in the tests using the simple one dimensional

model, so the linear dependence will be kept in the following experiments.

The spectral coupling scheme is scale selective, as the large scales are dominated by the spectra of the large scale model and only small scales are dominated by the spectra of the LAM. Its advantage is that the large scale solution is forced to LAM on the whole domain area. Unfortunately, spectral coupling scheme alone cannot eliminate spurious wave propagation from the lateral boundaries inward. Due to biperiodization, a necessity of a spectral LAM, without the gridpoint flow relaxation at the boundaries, all the waves that exit on one side of the domain freely enter on the opposite side. This is why we still need to use the gridpoint flow-relaxation scheme simultaneously to provide the damping on the domain edges. In other words, both coupling methods are combined. The relaxation takes place at the end of the gridpoint computations simultaneously with the flow-relaxation scheme.

4.1.2 Coupling without interpolation of large scale fields in time

As shown in previous sections, time interpolation can introduce significant errors to the model results. These errors could be avoided by not doing the time interpolation at all. The large scale fields are known only at discrete time intervals. In the gridpoint coupling scheme the coupling is done every time step and the large scale fields on the boundaries are interpolated in time. Spectral coupling forces the large scale solution LAM over the whole domain and could be done only at the coupling steps, when the large scale data are available, or more often, up to every LAM time step.

First several options were tested of introducing large scale data into the LAM without being interpolated in time. The large scale spectral coefficients are inserted to the LAM and the gridpoint part of the coupling scheme is left unchanged. If the LAM solution is forced by the large scale one only at the coupling steps, the depression appears suddenly, during one time step. Such result suggests that this method is not good for a real LAM with more sophisticated dynamics and physics parameterization package.

Instead of introducing large scale data suddenly, in one time step, an attempt was made to introduce it gradually during the coupling interval, so that coupling coefficient α was multiplied by a time dependent β function

$$\beta = \left(max \left[0, \frac{1}{1 - t_s} \left(\frac{t - t_1}{t_2 - t_1} - t_s \right) \right] \right) \tag{4.5}$$

where t_s is the time when the large scale solution from the second coupling time starts to be used, t_1 is the time of the first coupling file, t_2 is the time of the second

coupling file. The time t is from the coupling interval $t_1 < t < t_2$. This way the large scale data are not interpolated in time, but the data from the second coupling step are gradually introduced to the model during the coupling interval.

Unfortunately, such method leads to an unphysical solution of a false rapid generation of depression that develops in the domain, not an undisturbed transfer of a depression into the model domain. Therefore, we need to accomplish a different type of smooth transition between the coupling steps that would allow more physical representation of the model evolution on the lateral boundaries.

4.1.3 Temporal interpolation of spectral coefficients

The model uses spectral coefficients, so the first attempt was to use them in the time interpolation and avoid additional computations or transformations. The spectral coefficients of the large scale fields are interpolated in time before being used by the coupling procedure. Regarding the spectral coefficients in a realistic LAM such as the ALADIN model, this corresponds to the assumption that they evolve in time linearly according to (3.6) and that the component in (3.7) is zero. This interpolation in time can be linear, but in analogy with the gridpoint coupling procedure above, also a quadratic interpolation has been investigated and the one that uses tendencies of the spectral coefficients. We use similar formulas as the ones in Eqs. (3.11) and (3.12) for gridpoint coupling when the values of the model fields are replaced by its spectral coefficients.

Results for linear interpolation of spectral coefficients in time is shown in Figure 4.7. Instead of advection of the depression, a dipole is obtained. The depression develops and then dissolves only to develop on another position simultaneously. But even this unnatural model behavior led to improvements in the model error (see Fig. 4.8). Similar results were obtained for quadratic interpolation of spectral coefficients in time as well as when their tendencies (acceleration) were used. As shown in section 2, the time evolution of spectral coefficients is better represented with time interpolation of the linear trend and rotation in the complex plane. These can be seen as amplitude and phase of waves that constitute the field in spectral space. Since interpolation spectral coefficients in time also led to unrealistic model behavior, an attempt was made using amplitude and phase of spectral components.

4.1.4 Temporal interpolation of amplitude and phase of spectral coefficients

Amplitude and phase are first computed from the spectral components and then interpolated in time. The interpolated amplitude and phase are used to compute the

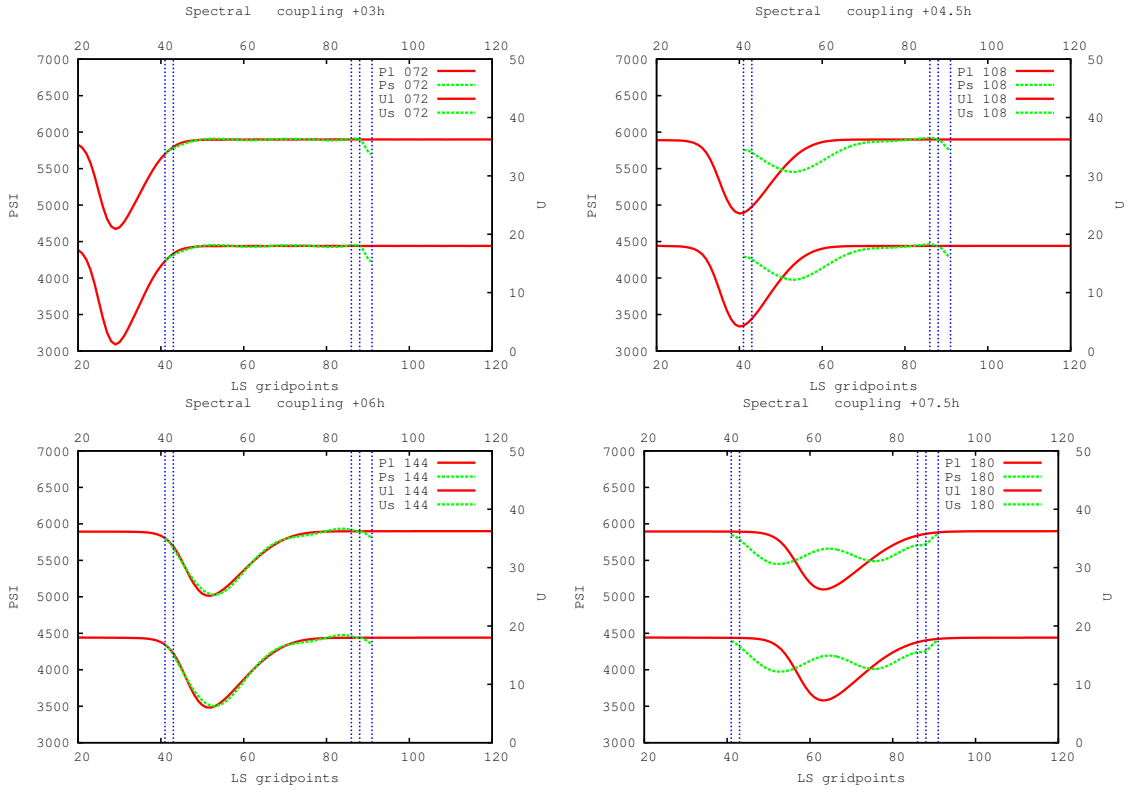

Figure 4.7: Results using spectral coupling scheme with 3 hour interval between input large scale data, when the spectral coefficients are interpolated linearly in time, after 3 (a) 4.5 (b), 6 (c) and 7.5 (d) hours. Lines have the same meaning as in Figure 4.1

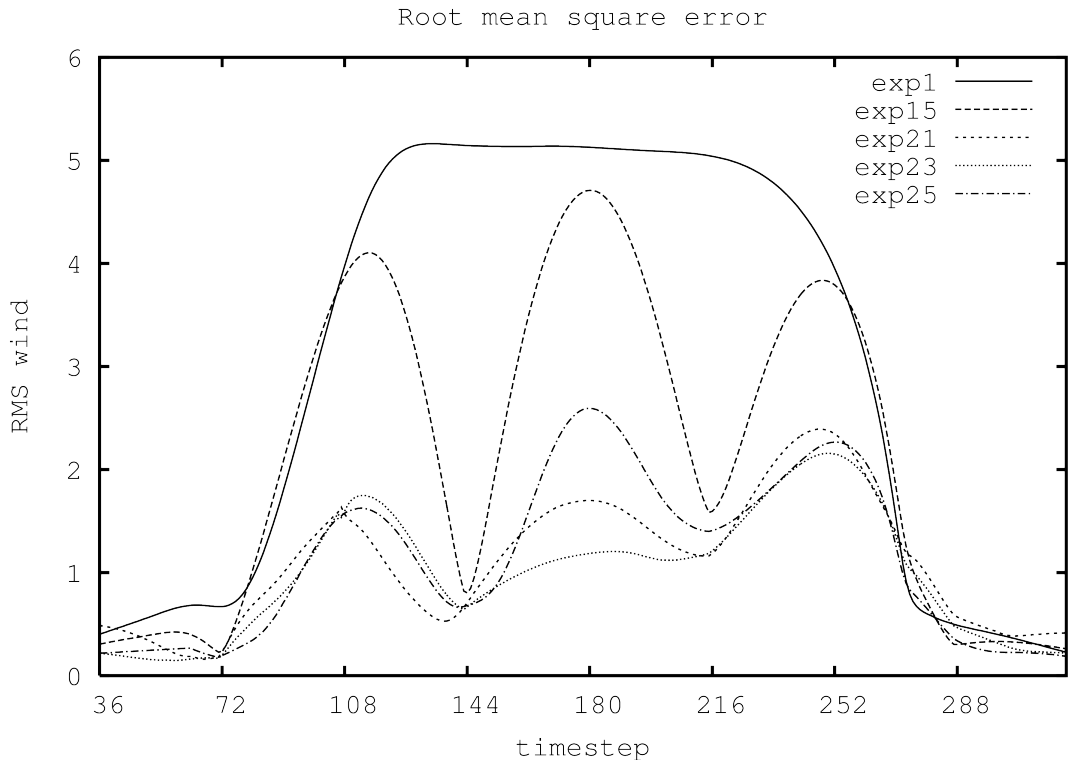

Figure 4.8: Root mean square error of wind variable computed over the LAM domain using the LAM coupled to low resolution global model for each time step as reference, for LAM coupled using flow relaxation scheme to low resolution global data with 3h interval interpolated linearly in time (full line), coupled using spectral coupling scheme when spectral coefficients are interpolated linearly in time (long dash), when the amplitude and phase of the spectral components are interpolated in time using extrapolation (short dash), integration between coupling steps (dots) or polynomial interpolation in time (dot dash).

large scale spectral components used for coupling at a given time step. Linear and quadratic time interpolation of amplitude and phase is done using same formulas as in gridpoint coupling schemes and acceleration is accounted for in analogous way (Termonia 2003). This approach takes into account the fact that, in realistic LAMs such as the ALADIN model, also the phases corresponding to Eq. (3.7) evolve in time. The resulting model run showed significant improvements compared to the run when spectral coefficients were interpolated. The depression was mostly advected and the dipole problem almost disappeared. This result encouraged searching for alternative schemes for interpolation of amplitude and phase in time.

Average of extrapolated values

An alternative time interpolating scheme has been introduced that estimates the value of the model variable X at time t by extrapolating it from the coupling steps. Assume that model variable X at one coupling step at time t_1 has known value X_1 and a time derivative $\left(\frac{\partial X}{\partial t}\right)_{t_1}$ and in the next coupling step at time t_2 has value X_2 and derivative $\left(\frac{\partial X}{\partial t}\right)_{t_2}$. The simplest way of accounting for the tendency in the interpolation scheme is to compute the forward extrapolated value from time t_1

$$X_1(t) = X_1 + \left(\frac{\partial X}{\partial t}\right)_{t_1} (t - t_1) \tag{4.6}$$

and backward extrapolated value from time t_2

$$X_2(t) = X_2 + \left(\frac{\partial X}{\partial t}\right)_{t_2} (t - t_2)\,, \tag{4.7}$$

and finally compute their weighted average

$$X(t) = w_1 X_1(t) + w_2 X_2(t), \tag{4.8}$$

where w_1 and w_2 are the same as for the linear interpolation. Usage of this interpolating scheme allows the depression to smoothly enter the domain, to be advected through it and exit (Figure 4.11). Unfortunately, there are a few spurious waves generated on top of the simulated depression that spoil the solution slightly. Another drawback is that the LAM contribution to the resulting model evolution is suppressed by the spectral nudging of the spectral components towards the large scale solution. In other words, the LAM does not bring useful contribution to the evolution of the model variables or this contribution is hidden with spurious waves that are consequence of the temporal interpolation of the large scale fields.

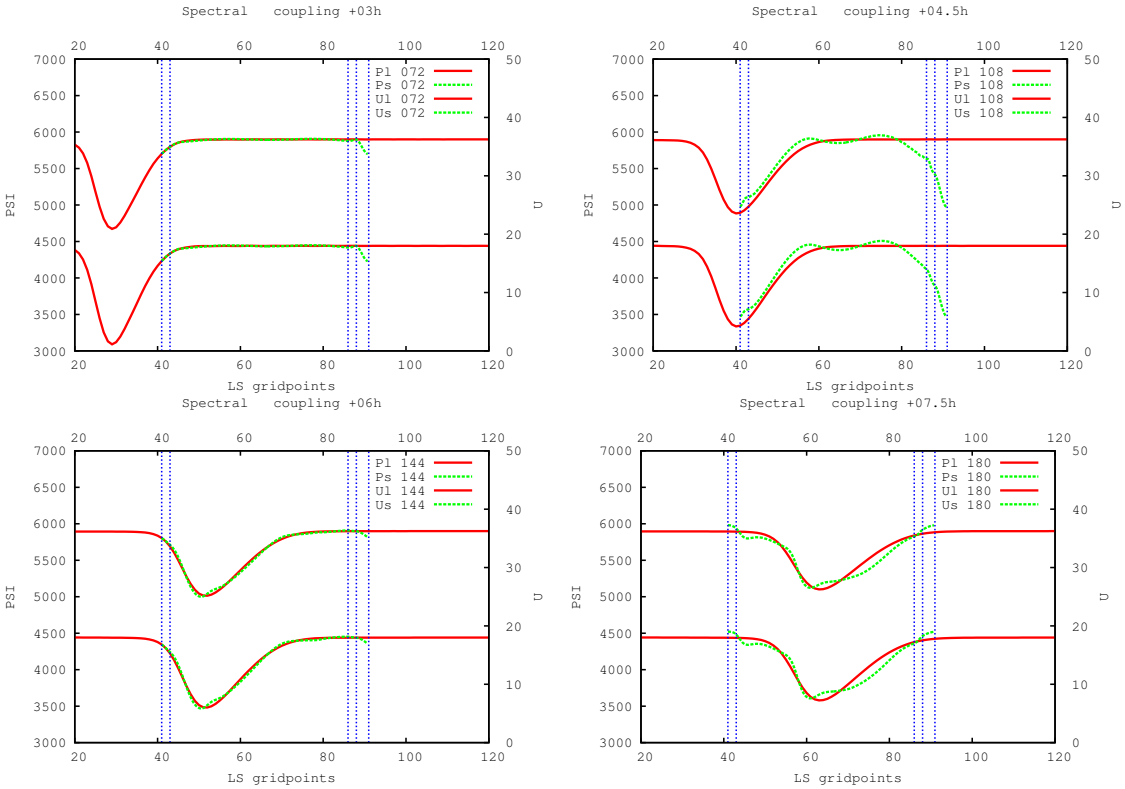

Figure 4.9: Results using spectral coupling scheme with 3 hour interval between input large scale data, when amplitude and phase are interpolated in time using the extrapolated values after 3 (a), 4.5 (b), 6 (c) and 7.5 (d) hours. Lines have the same meaning as in Figure 4.1

Integrated weighted tendencies

Instead of using fixed value for the tendency for the whole $(t - t_1)$ or $(t_2 - t)$ period, we can use a weighted average of the two tendencies at each time step and then compute the integral from t_1 to t or from t to t_2 respectively.

The value of the model variable X at time t can be estimated by forward integration of the following expression

$$X_1(t) = X_1 + \int_{t_1}^{t} \left(w_1 \left(\frac{\partial X}{\partial t} \right)_{t_1} + w_2 \left(\frac{\partial X}{\partial t} \right)_{t_2} \right) dt \,, \tag{4.9}$$

where $w_1 = \frac{t_2 - t}{t_2 - t_1}$ and $w_2 = \frac{t - t_1}{t_2 - t_1}$ are functions of time t. The obtained function of time is

$$X_1(t) = X_1 + \left(\frac{\partial X}{\partial t} \right)_{t_1} (t - t_1) + \frac{1}{2} \left(\left(\frac{\partial X}{\partial t} \right)_{t_2} - \left(\frac{\partial X}{\partial t} \right)_{t_1} \right) \frac{(t - t_1)^2}{t_2 - t_1} \tag{4.10}$$

or alternatively, a similar expression can be obtained when integrating from time t_2 backward

$$X_2(t) = X_2 - \int_{t}^{t_2} \left(w_1 \left(\frac{\partial X}{\partial t} \right)_{t_1} + w_2 \left(\frac{\partial X}{\partial t} \right)_{t_2} \right) dt \,, \tag{4.11}$$

yielding alternative function of time

$$X_2(t) = X_2 - \left(\frac{\partial X}{\partial t} \right)_{t_2} (t_2 - t) + \frac{1}{2} \left(\left(\frac{\partial X}{\partial t} \right)_{t_2} - \left(\frac{\partial X}{\partial t} \right)_{t_1} \right) \frac{(t_2 - t)^2}{t_2 - t_1}. \tag{4.12}$$

The final interpolation function is the linear combination of the two

$$X(t) = w_1 X_1(t) + w_2 X_2(t) \,. \tag{4.13}$$

This interpolation scheme generates far less spurious waves (Figure **??**) and apparently there is some benefit of the higher resolution LAM run since it contributes to the evolution of the disturbance.

Polynomial interpolation

Another interpolation function can be computed using the values of the model variable X and its derivative at times t_1 and t_2 to evaluate coefficients in a 3rd order polynomial. First assume a polynomial dependence of the variable X in time,

$$X(t) = a + bt + ct^2 + dt^3 \,, \tag{4.14}$$

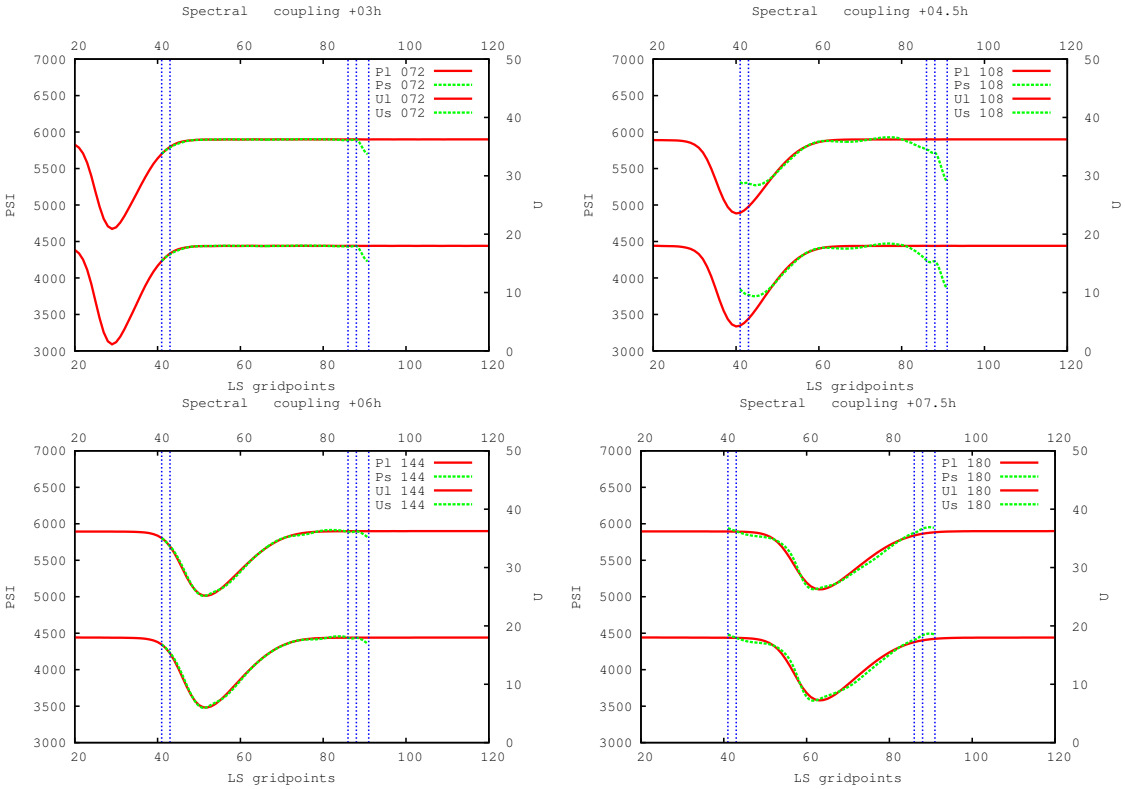

Figure 4.10: Results using spectral coupling scheme with 3 hour interval between input large scale data, when amplitude and phase are interpolated in time using the integrated values after 3 (a), 4.5 (b), 6 (c) and 7.5 (d) hours. Lines have the same meaning as in Figure 4.1

and compute the coefficients assuming $t_1 = 0$ for simplicity

$$
\begin{aligned}
a &= X(t=0) = X_1 \,, \\
b &= \left(\frac{dX}{dt}\right)_{t=0} \left(\frac{\partial X}{\partial t}\right)_{t_1} \,, \\
c &= \frac{3}{t_2^2}\left[X_2 - X_1 - \frac{1}{3}\left(2\left(\frac{\partial X}{\partial t}\right)_{t_1} + \left(\frac{\partial X}{\partial t}\right)_{t_2}\right) t_2\right] \,, \\
d &= -\frac{2}{t_2^3}\left[X_2 - X_1 - \left(\left(\frac{\partial X}{\partial t}\right)_{t_1} + \left(\frac{\partial X}{\partial t}\right)_{t_2}\right) t_2\right] \,.
\end{aligned} \tag{4.15}
$$

This interpolation scheme also allows for the depression to smoothly enter the domain, but unfortunately it also amplifies several wave components more than it should so spurious waves appear in the LAM solution (figure not shown, results qualitatively similar to those in Figure 4.11).

The spectral coupling procedure using temporal interpolation of amplitude and phase instead of spectral coefficients has reproduced the model evolution in more physical way yielding results that are similar to the test with gridpoint coupling using large scale data from each time step - the "perfect coupling" test (Figure **??**a). The spectral coupling alone allows for waves to re-enter the domain upon exiting on the opposite side due to biperiodization of the large scale fields. Therefore it still requires simultaneous usage of the gridpoint coupling procedure on the domain edges to filter the waves that would otherwise re-enter the domain.

The model error evolution (Figure 4.8) shows the minimum values at coupling steps and maxima in the time between, when the error of the interpolation in time is largest. This is consistent with results from Nutter et al. (2004) who found largest errors in the boundary zone near the midpoint of the LBC update cycle. The results suggest that integrated weighted tendencies give the least spurious waves while allowing for the disturbance to enter and leave the LAM domain.

Unfortunately, the temporal interpolation scheme in combination with the spectral coupling procedure and biperiodization might generate spurious waves that could spoil the solution or mask the LAM contribution to the model evolution. It is also possible that these spurious waves are partly a consequence of double coupling on the domain edges where the spectral coupling procedure could push the model fields in a different way than the gridpoint procedure. Therefore another alternative is sought in the next section, that could potentially allow for physical evolution of LBC conditions and enable evolution of the LAM solution in the central part of the domain undisturbed by the spectral nudging toward the large scale data.

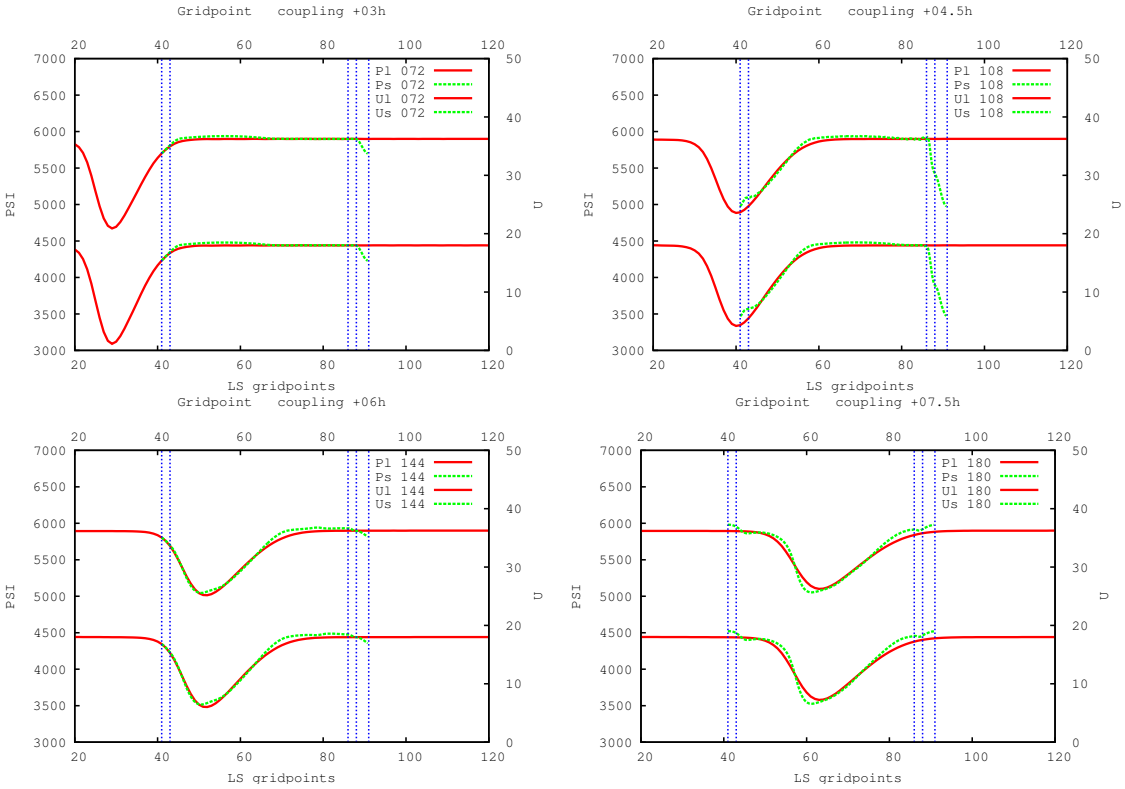

Figure 4.11: Results using spectral coupling scheme with 3 hour interval between input large scale data, when amplitude and phase are interpolated in time using the extrapolated values but coupled in gridpoint space only in the narrow area close to the domain boundary, after 3 (a), 4.5 (b), 6 (c) and 7.5 (d) hours. Lines have the same meaning as in Figure 4.1

4.2 Gridpoint coupling using amplitude and phase angle interpolation in time

The large scale model state X_{LS} is transformed from gridpoint to the spectral space, and the spectral coefficients are obtained. Then the amplitude and the phase angle of the complex spectral coefficients are computed and interpolated in time using the same procedures as when doing the spectral coupling. The time interpolated amplitude and phase angle are used to compute the time interpolated spectral coefficients which are transformed back from spectral to gridpoint space. This way we obtain the large scale fields used for gridpoint coupling.

The time interpolation of amplitude and phase can also be linear or quadratic, use acceleration, tendencies for integral or polynomial interpolation. When the amplitude and phase are interpolated linearly in time, the simulated depression is significantly weaker than with the perfect coupling scheme, but recognized. Unfortunately, when the depression leaves the domain, it is followed by a strong false positive signal (not shown). Results using quadratic coupling are very similar to the linear one. When the acceleration of amplitude and phase is used, the simula-

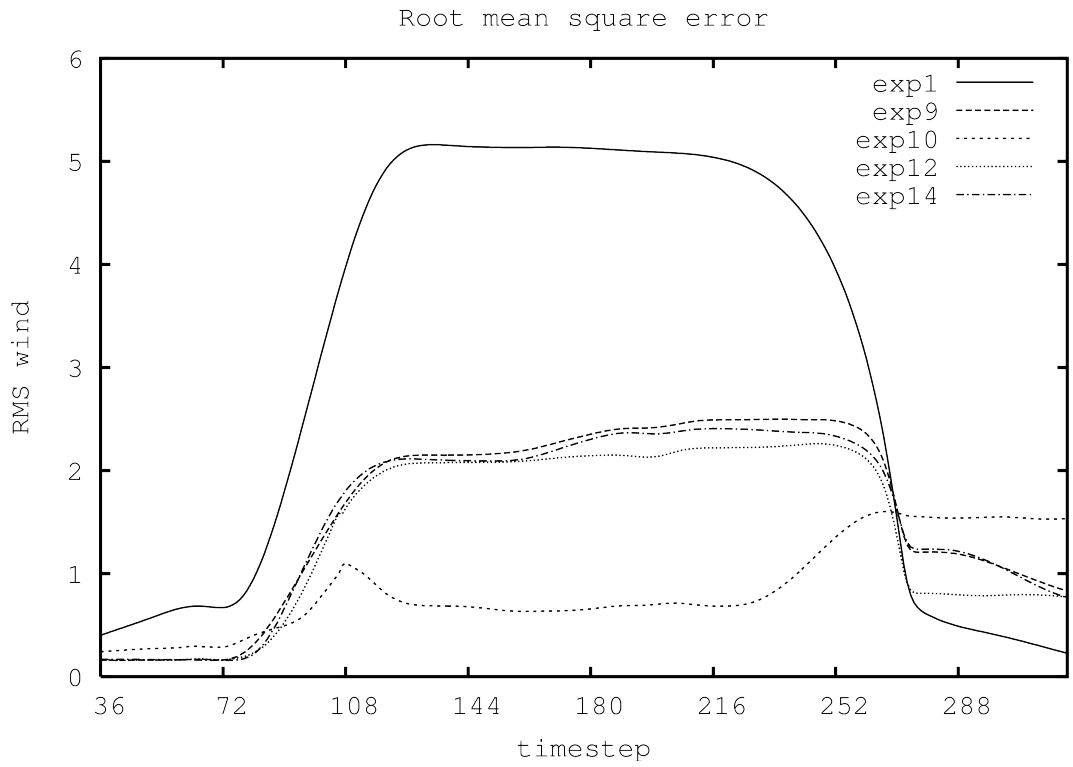

Figure 4.12: Root mean square error of wind variable computed over the LAM domain using the LAM coupled to low resolution global model for each time step as reference, for LAM coupled using flow relaxation scheme to low resolution global data with 3h interval interpolated linearly in time (full line), coupled in gridpoint space but the large scale data are interpolated in spectral space: when the amplitude and phase of the spectral components are interpolated in time using amplitude (long dash) extrapolation (short dash), integration between coupling steps (dots) or polynomial interpolation in time (dot dash).

ted depression is stronger and the false anticyclone is reduced. Using the average of extrapolated values gives satisfactory depth of the depression but the amplitude of few short modes is a bit too strong (Figure **??**). Other results using tendencies of the model fields, either integrated between coupling steps or using polynomial interpolation give similar results as the simplest case shown in Figure **??**. The depression enters the domain, although it is less deep than in the large scale model. But since this scheme relaxes the LAM solution to the large scale one only in the narrow area close to the domain edge, the LAM can contribute to the development of the disturbance. Unfortunately, the other benefit of the gridpoint coupling is lost since the longest modes also re-enter the domain, although much weaker. This is a consequence of the biperiodization of the large scale fields. The evolution of the model error (Figure 4.12) shows an increase after the depression leaves the domain, due to these excessive waves.

4.3 Disucussion and conclusions

The present chapter aims to improve the LBC temporal resolution problem. A LAM that uses LBC data from a storage utility or remote center usually has the data available with a coupling interval of several hours. LBC data are interpolated in time and used in LAM each time-step of several minutes. The features with time-scales shorter than the coupling interval are corrupted or even removed by the time-interpolation procedure. The problem has encouraged the research on the coupling procedure that would enable a better representation of such features using the available LBC data.

It was shown (Figure 3.1d) that linear interpolation of LBC within 3h interval distorts the model fields. The interpolation procedure created two cyclones instead of one. The time evolution of the large scale model fields is poorly represented by the time-interpolated fields on the domain edges. The evolution of model fields in time is better represented by a linear trend and a rotation of spectral coefficients in the complex plane (Figure 3.4). This data obtained for a realistic 3D model served as inspiration to improve the temporal interpolation, in particular of the spectral coefficients. And these alternatives for the commonly used linear interpolation were tested using a simple 1D model. The tests reveal what error can be expected when using the different coupling and time-interpolation schemes.

Gridpoint coupling using standard Davies scheme on a narrow area close to the edges of the LAM domain with a coupling interval of several hours misses a signal that enters the domain. Two possible alternatives to the standard Davies coupling are presented in the framework of a simple one-dimensional model. The first one does the coupling in the spectral space. This method is also known as spectral nudging and has shown benefits in other models (eg. Meinke et al. (2006)). The second one only interpolates the large scale fields in time in spectral space but does the coupling in gridpoint space. Both of them are able to represent the missed signal in the LBC, but the second one could be the first step further from the "standard" gridpoint coupling using fields interpolated linearly in time.

Usage of the spectral coupling alone supports spurious waves that could re-enter the domain as a consequence of biperiodization. These waves can be filtered by the gridpoint coupling scheme, as was done in previous studies when the boundary relaxation scheme was found necessary for LBC noise removal (Juang and Kanamitsu 1994).

Time interpolation in spectral space improves the representation of fast small-scale disturbances in LBC data. LBC coupling scheme can benefit from the boundary relaxation scheme used in combination with the improved time-interpolation. Both schemes could be used either always or they could be applied only when the

monitoring procedure proposed by Termonia (2004) detects that some signal has entered the LAM domain without being properly sampled by the standard 3-h linear temporal interpolation.

Dodatak A

When does NH dynamics matter?

Operational forecast in Meteorological and hydrological service of Croatia uses ALADIN model for 2km resolution dynamical adaptation procedure that provides high resolution forecast of 10m wind. It was found reliable for bura cases by previous studies, although the model uses hydrostatic dynamics, crude vertical resolution above the surface layer and only turbulence parametrization.

The two cases of strong and severe bura that were not predicted by the operational forecast occured in the night from 1st to 2nd February and in the late afternoon and evening on 3rd February (Figures A.2 and A.3). The cases were analyzed using wind and pressure measurements from two automatic stations situated in locations hit by these bura episodes and ALADIN model runs in high resolution. Vertical soundings were used from both Croatian stations where this measurements are done. These are relatively far from the area hit by bura episode, but are the closest available to estimate the quality of the modelled vertical structure of the atmosphere and allow insight into the real vertical profiles.

The full 72 hour ALADIN forecast was run on 2 km resolution on 37 levels using the complete set of physics parameterizations. Two sets of experiments were done, using hydrostatic and nonhydrostatic dynamics. Only the least diffusive set-up of horizontal diffusion scheme is shown here. The problem of horizontal diffusion in high resolution is beyond the subject of this case study so it is not analyzed here in more detail. Non-hydrostatic effects become more important for narrow mountains. This can be seen in the model results since the largest differences between the hydrostatic and nonhydrostatic model forecast can be observed for Makarska for the first bura case but almost none in the second case.

Although the NH model did predict short episode of strong bura in Split during the first bura case, the peak was too early in the afternoon, and the predicted wind speed reaches lowest values when the measured ones are the highest. Obviously, one could say that the vertical structure of the atmosphere was not predicted well since it misses the temperature inversion that was close to the mountain height.

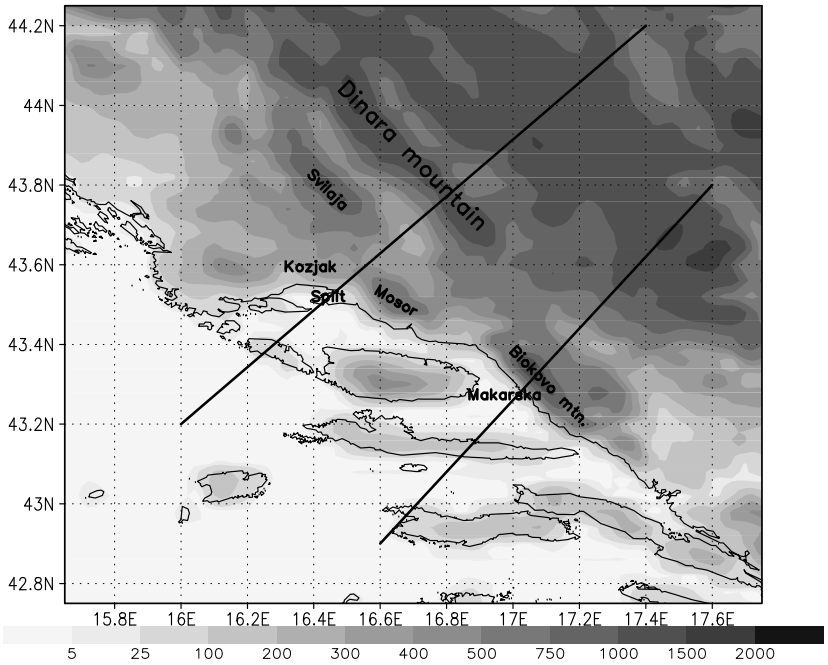

Figure A.1: Terrain height in 2 km resolution. Split and Makarska are locations where the measurements from the automatic stations are taken. The vertical cross-sections are shown as full lines.

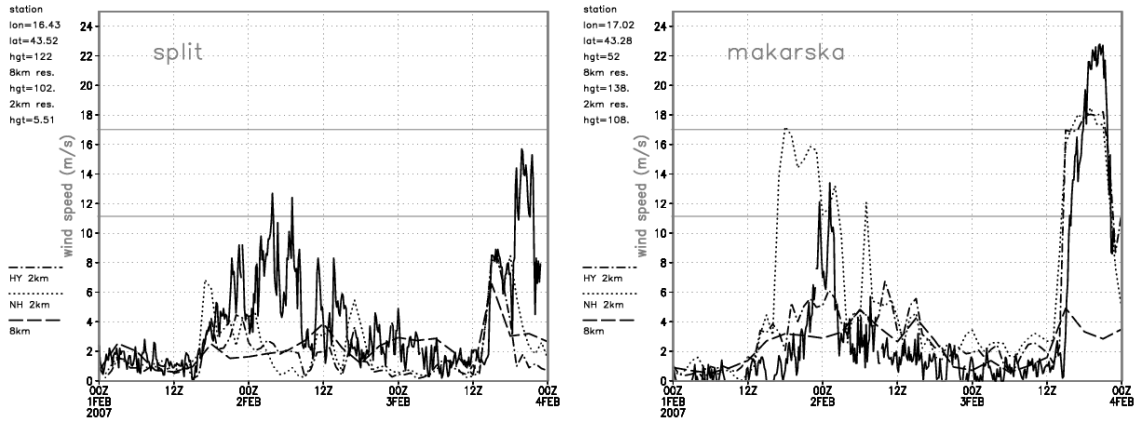

Figure A.2: 10 minute measurements (full line) of wind 10 meters above ground, the 72 hour forecast runs starting from 00 UTC 1st February 2007 in 8 km resolution (dashed line), 2 km resolution full run with hydrostatic (dot dash line) and non-hydrostatic (dotted line) dynamics for Split (left) and Makarska (right) locations. The longitude and latitude of the measuring station locations as well as height above the sea level are also shown.

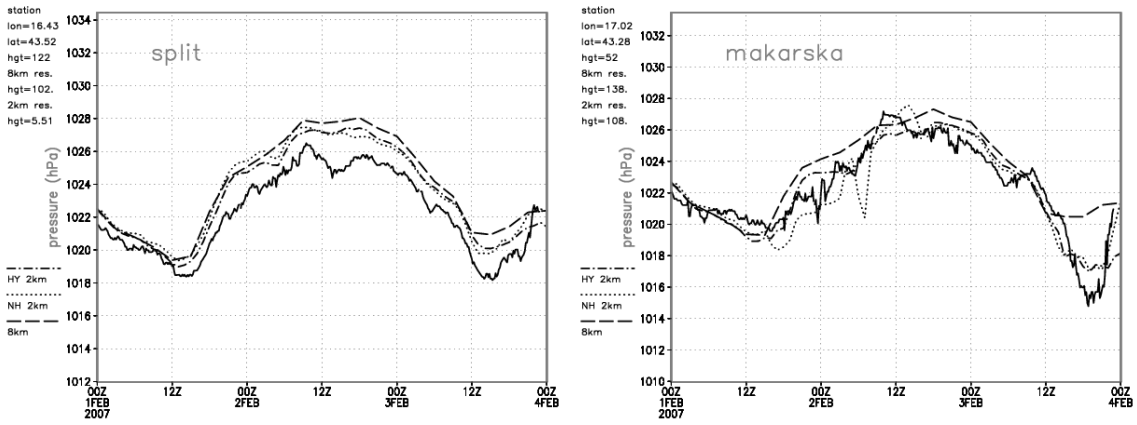

Figure A.3: As Figure A.2 but for pressure reduced to mean sea level.

The formation of rotors and low-level turbulent zones is favoured when an inversion resides just above the mountaintop level. A deep and stable layer with horizontal wind speed that increases with height above the mountain leads to trapped lee waves. Rapid changes in wind speed could be the consequence of the rapid rotor evolution and shifting of the wavelength or amplitude of the mountain waves above. Individual rotors form and advect downstream before dissipating. On the other hand, the same model run overpredicted wind speed for Makarska in the first bura case, as a consequence of too strong variations in pressure. Finally, the second case of bura was predicted well for the same location by both hydrostatic and nonhydrostatic model runs.

Dodatak B

Impact of horizontal diffusion, radiation and cloudiness parameterization schemes on fog forecasting in valleys

Fog and low stratus forecasting experiments have been carried out with the numerical weather prediction model ALADIN on a case of long lasting fog. The model has been used with different radiation, cloud diagnosing and horizontal diffusion schemes, different representation of orography, increased vertical resolution and with or without prognostic condensates and turbulent kinetic energy (TKE). Some of the numerical set-ups are able to reproduce the fog (low stratus) field as seen in the satellite images as well as the measured 2m temperature and relative humidity diurnal cycles. The results show that cloud diagnosing schemes and overlap assumptions play a more important role than a more sophisticated radiation scheme, or introduction of prognostic cloud water, ice, rain, snow or TKE. More realistic orography representation and a more physical horizontal diffusion scheme significantly improve the modelled low stratus and 2m temperature in the areas with variable orography.

The numerical weather prediction model ALADIN had difficulties in predicting correctly the low stratus and fog. During the first half of December 2004, low stratus and fog covered the valleys in inland Croatia. These clouds were not predicted by the operational ALADIN forecast. Since this was not an isolated incident of the model failure in such a weather situation, it was important to find out if there is a model set-up that would predict the development of low stratus and fog.

The initial and boundary conditions were obtained from the global host model ARPEGE. These contained the atmospheric state without fog and low stratus as well. There is data assimilation, but, when the model forecast is wrong, the gu-

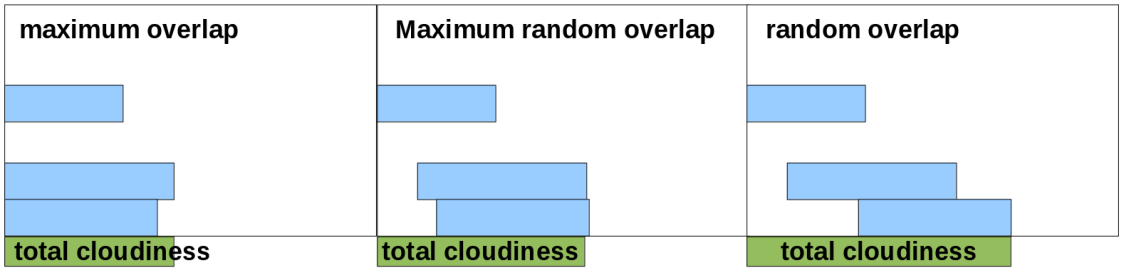

Figure B.1: The effect of overlap assumption on the diagnosed cloudiness (and exchange of fluxes in the atmosphere). The diagnosed cloudiness for maximum overlap yields lowest amount of total cloudiness and maximizes the cloud to cloud and cloudless to cloudless exchange. The random overlap yields the largest diagnosed total cloudines and maximizes the exchanges from cloud to cloudless layers. The maximum random overlap is an intermediate solution.

Table B.1: List of experiments (Exper.=Experiments, Xu-Ran=Xu-Randall, Rad.=Radiation, Prog.=Prognostic, cond.=condensate, Cloud=Cloudiness)

Exper.	Cloud scheme	Overlap	Horiz diff	Rad. scheme	Prog. TKE	Prog. cond.	Cloud figure	Fig 2m temp
Oper	Oper	Random	Num	RG90	No	No	No	B.3 full line
Exp1	Xu-Ran	Random	Num	RG90	No	No	Fig B.2a	Figs B.3a dashed, B.3b full line, B.4a full line
Exp2	Xu-Ran	Maximum	Num	RG90	No	No	No	B.3a dotted
Exp3	Xu-Ran	Random	Num	RG90NER	No	No	Fig B.2b	B.3b short long dash
Exp4	Xu-Ran	Random	Num	FMR 3h	No	No	No	B.3b dashed
Exp5	Xu-Ran	Random	Num	FMR 1h	No	No	Fig B.2c	B.3b dotted
Exp6	Xu-Ran	Random	Num	RRTM 3h	No	No	No	8 dot dash
Exp7	Xu-Ran	Random	Num	RRTM 1h	No	No	Fig B.2d	B.3b dot dot dash
Exp8	Xu-Ran	Random	SLHD	RG90	No	No	Fig B.2e	B.4a dashed
Exp9	Xu-Ran	Random	SLHD	RG90	Yes	No	No	B.4a dotted
Exp10	Xu-Ran	Random	SLHD	RG90	Yes	Yes	Fig B.2f	B.4a dot dash, B.4b full line
Exp11	Xu-Ran	Random	SLHD	RG90	Yes	Yes	Envelope orography	B.4b dashed
Exp12	Xu-Ran	Random	SLHD	RG90	Yes	Yes	73 levels	B.4b dotted

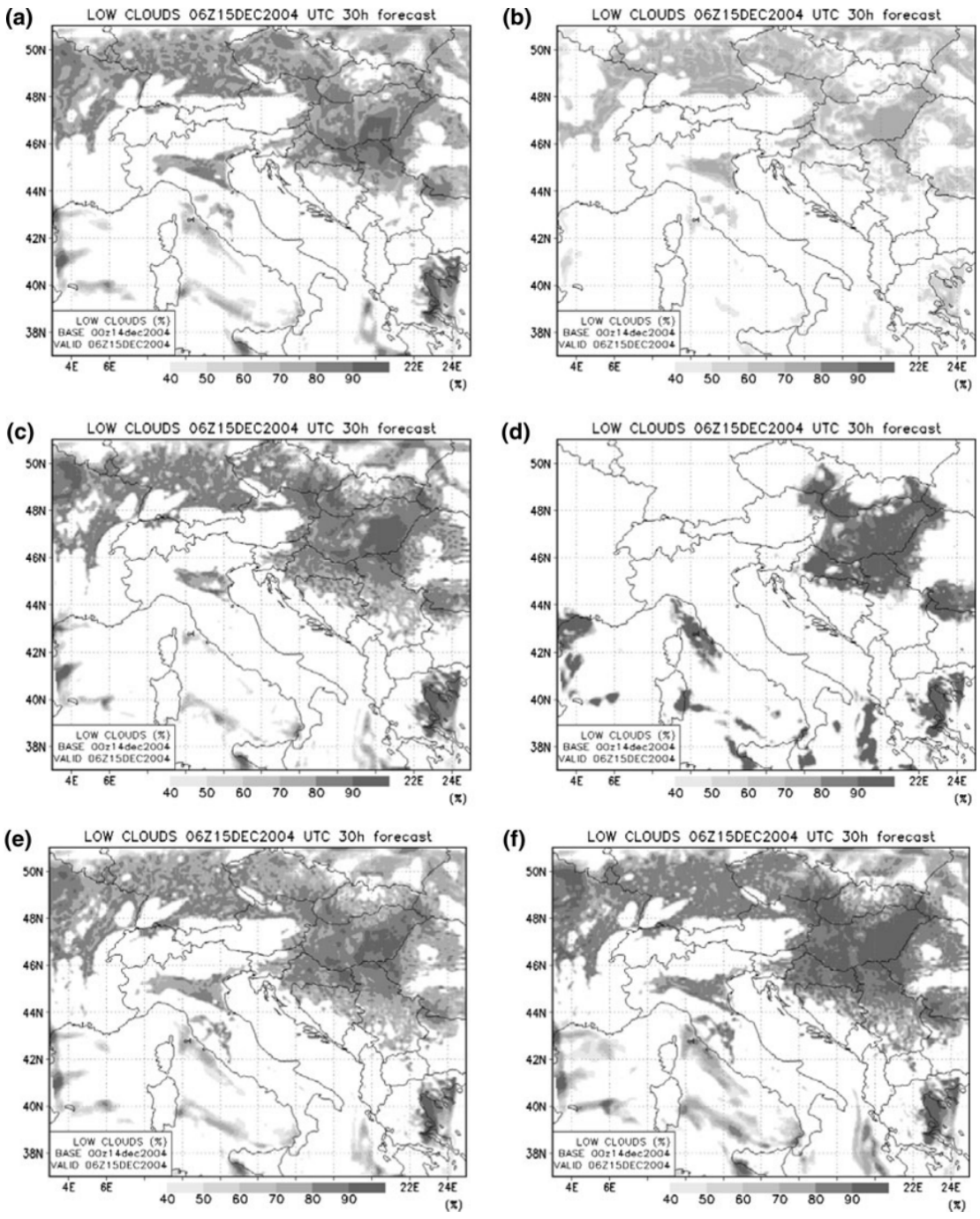

Figure B.2: Low cloudiness (02 km agl) 30-h forecast starting from 00 UTC analysis 14th December 2004 to 6 UTC 15th December 2004 for the experiments: exp1 (a), exp2 (b), exp5 (c), exp7 (d), exp8 (e) and exp10 (f). Additional explanations may be found in the Table B1 and text.

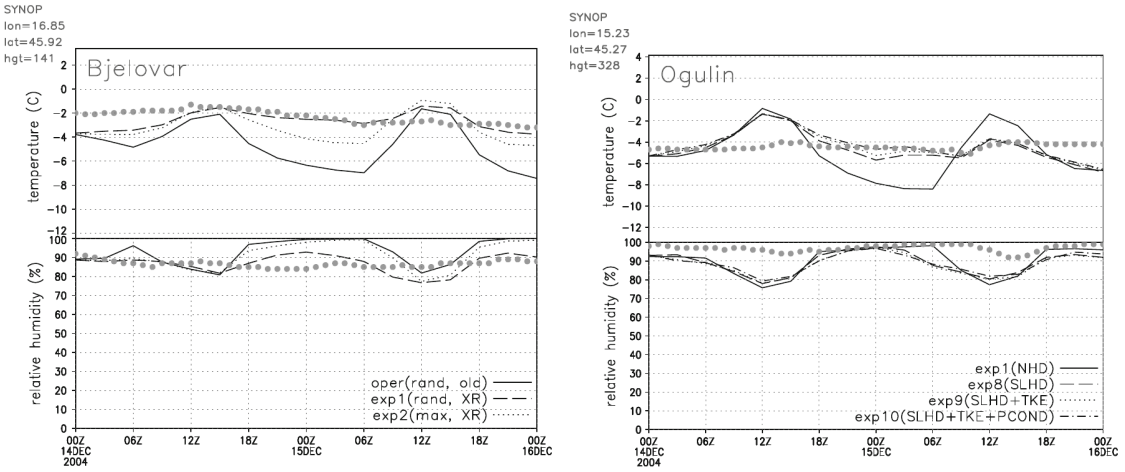

Figure B.3: Comparison of the modelled 2m temperature and relative humidity evolution with measured data (large grey dots) for Bjelovar SYNOP station, the following experiments: (a) oper (full line), exp1 (dashed) and exp2 (dotted) and (b) exp1 (full line), exp4 (dashed), exp5 (dotted), exp6 (dash dotted) and exp7 (dash dot dotted).

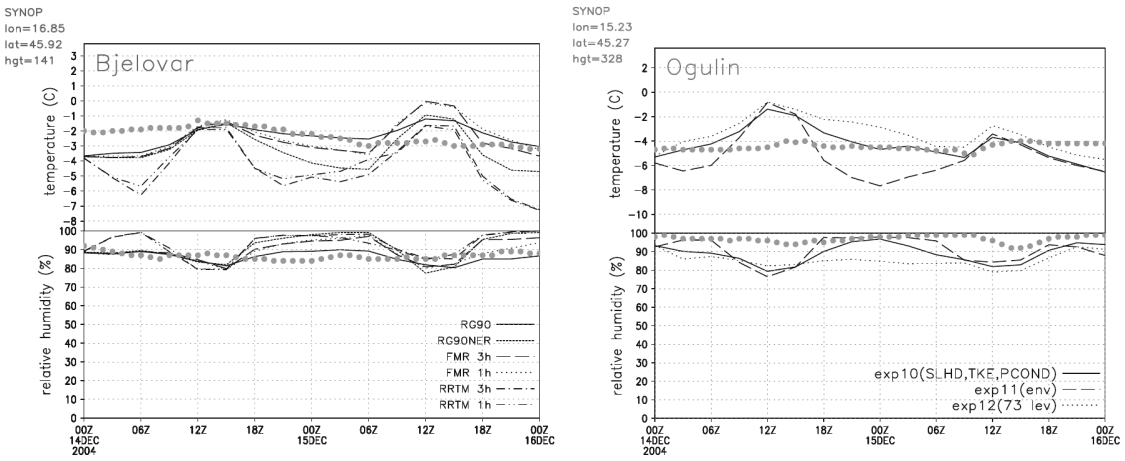

Figure B.4: Comparison of the modelled 2m temperature and relative humidity evolution with measured data (large grey dots) for Ogulin SYNOP station and the following experiments: (a) exp1 (full line), exp8 (dashed), exp9 (dotted) and exp10 (dash dotted) and (b) exp10 (full line), exp11 (dashed) and exp12 (dotted).

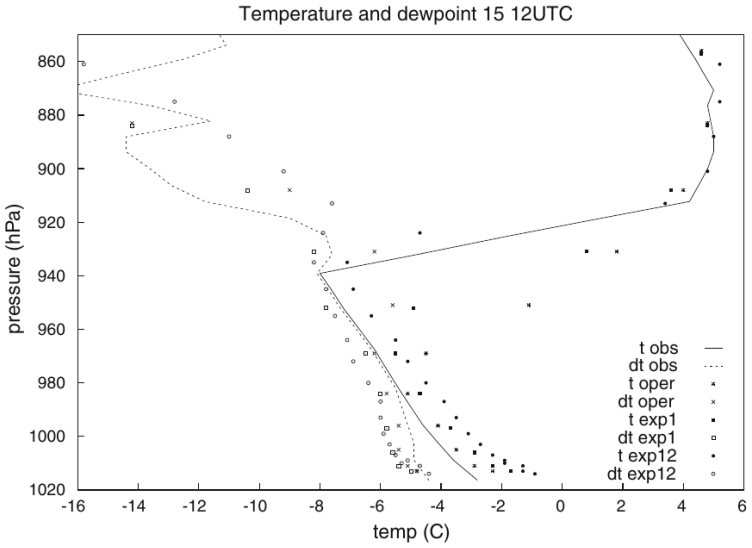

Figure B.5: Measured and forecast vertical profiles of temperature (t) and dewpoint temperature (dt). The pseudo-TEMP messages were created extracting data on the model levels for the location Zagreb- Maksimir where vertical sounding measurements are available. The model output is shown for operational run (star for temperature, times symbol for dewpoint temperature) and exp1 are run on 37 levels (full square for temperature, open square for dewpoint temperature) and exp12 that is run on 73 levels (full circle for temperature, open circle for dewpoint temperature). Measured temperature is shown as full line and dewpoint temperature as dashed.

ess is far from observations, the observations are not assimilated. Consequently, the analysis does not contain the atmospheric state details essential for the cloud formation and development. The problem persists in the consecutive operational forecast runs. This problem has inspired development of an empirical sub-inversion cloudiness scheme that initiates the positive feedback of radiation flux divergence, turbulence and cloud formation. This scheme overcomes the problem of wrong initial profiles in temperature and humidity and allows for the development of stratus and fog.

This study compares influences of different parameterizations in the ALADIN model on cloudiness forecast in a fog and low stratus case. The cloud overlap assumption plays a very important role, as well as the formula used to diagnose cloudiness. Both are needed to establish the correct cloud input for the radiation scheme that supports further cloud development. Although fog is not a rapidly developing phenomenon, it seems necessary to compute radiation at least on an hourly basis to allow fog to develop in the model. Otherwise, old radiative transfer coefficients computed in a cloud free atmosphere are used. This prevents the feedback process that leads to cloud development. Other phenomena, as well as transient fog cases might require new radiative transfer coefficients more often. Infrequent calculation of radiative heating rates can produce numerical instability (Pauluis and

Emanuel 2004) and degrade the forecast in cases where radiative balance between the cloud and the rest of the atmosphere is important in the cloud development.

Numerical horizontal diffusion acts along model levels that follow the terrain and consequently mix (or smooth) the model fields between the valley bottom and a mountain ridge nearby. Its intensity is the same in all weather situations. The new scheme for horizontal diffusion, SLHD, is dependent on the flow deformation field, so that the intensity of horizontal mixing is weak when the wind is low. A more physically based horizontal diffusion scheme allows the development of fog in relatively narrow valleys (for the horizontal resolution of 8 km used in this study). Introduction of prognostic condensates and TKE scheme has a positive impact in the valleys and close to the mountain slopes, but only in combination with SLHD. The terrain complexity stresses the importance of the correct representation of the unresolved terrain height variations. Different representation of orography, with or without the envelope, can lift certain areas (in the model) within or above the fog layer (in the real atmosphere) and therefore have a significant impact on the correct forecast of the 2m temperature and humidity. The persistent fog layer in this case was thick, so increased vertical resolution has a low impact on cloudiness forecast, once the parameterizations are set to produce fog. However, increased vertical resolution improves the temperature inversion forecast.

Very high horizontal resolution has been found necessary (but not sufficient) for the correct modelling of boundary layer structure over complex terrain of some phenomena as the valley flows and foehn. This was not necessary for this study where both large scale and local circulations are almost non-existent and the valleys considered are wide enough to be resolved with 8 km horizontal resolution. Higher horizontal resolution would allow higher slopes and the effect of mountain shadows on solar radiation would become important. Therefore, a case of transient fog in a narrow valley would require high horizontal resolution that would resolve local flow patterns that develop due to differential heating of the slopes.

Study of other fog and low stratus cases, especially for more narrow valleys, might require higher horizontal resolution as well as the parameterization of the shadow in the valley produced by the surrounding mountains. Case studies of more transient phenomena would give better insight into the longwave radiative balance and heating by shortwave radiation. These studies would also require better initial conditions and surface analysis as well as data assimilation in higher resolution. This study has revealed which model configurations allow the prediction of fog and low stratus. Before introducing it into the operational forecast suite, one should also verify that the proposed configuration is suitable for operational use on a large number of cases covering various types of weather phenomena.

!

Sažetak na hrvatskom jeziku

Modeli na ograničenom području se koriste u nacionalnim službama brojnih zemalja prvenstveno za operativnu prognozu lokalnih vremenskih prilika do 3 dana unapred te su često podešeni u skladu s time. Takvi modeli trebaju prognozu nekog modela na većem području, obično globalnog, kako bi imali definirane prognostičke lateralne rubne uvjete. Povremeno se događa neki poremećaj prođe kroz rubno područje modela tako brzo da ga ne otkrije procedura povezivanja rubnih uvjeta. Tada model na ograničenom području prognozira taj poremećaj lošije od globalnog modela. To je posebno opasno u situaciji kada brza i intenzivna mezociklona uđe u domenu jer tada model na ograničenom području ne prognozira olujno nevrijeme, koje je potencijalno opasno.

Ovaj rad će pokazati koliko često se to događa na području koje je bitno za operativnu prognozu modelom ALADIN na 8 i 2 km rezoluciji na DHMZ-u. Pri tome će se koristiti operativni podaci globalnih modela ARPEGE i IFS-a. U poljima ARPEGE-a će se analizirati situacije kada su brze ciklone detektirane postojećim numeričkim filterom, dok će se za polja iz ECMWF-a razviti nova metoda.

Modeli na ograničenom području se koriste kao alternativa globalnim numeričkim modelima za prognozu vremena za širok spektar istraživačkih i operativnih potreba. Koriste se za operativnu prognozu, simulacije promjena klime te za istraživanje mnogobrojnih procesa u atmosferi. Modeli za prognozu vremena su podložni različitim izvorima pogrešaka u prognozi, kao što su parametrizacije fizikalnih procesa, početni uvjeti, numerički algoritmi i djelovanje podloge. Modeli na ograničenom području imaju dodatni izvor pogreške povezan s lateralnim rubnim uvjetima. Shema kojom se lateralni rubni uvjeti uključuju u većinu modela (McDonald, 1999) je prema Davies (1976) te se koristi i u modelu ALADIN. Warner i sur. (1997) daje pregled slabosti prognoze povezanih sa lateralnim rubnim uvjetima. Termonia i sur. (2009) su pokazali da je vremenska interpolacija ulaznih podataka lateralnih rubnih uvjeta dovela do greške u polju prizemnog tlaka od 10 hPa u slučaju brzo napredujuće ciklone. Greška modela zbog greške lateralnih rubnih uvjeta napreduje kroz domenu modela tijekom prognoze (Nutter i sur. 2004) te zbog toga može prouzročiti pogrešku u bilo kojem dijelu domene, posebno za jako duge simulacije. Bitno je istaknuti da u slučaju da operativna prognoza uključuje

asimilacijski ciklus, greška modela ostaje u domeni i širi se kroz domenu tijeokm slijedećih prognoza.

Mnoge od tih ciklona nastaju ili se gibaju preko zapadnog Mediterana u blizini rubnog područja domene na kojoj se radi operativna prognoza modelom ALADIN na 8 km rezoluciji. Takve ciklone mogu ući u domenu prebrzo da bi ih procedura povezivanja na lateralnim rubovima modela ispravno interpretirala u poljima prognoze ALADIN modela.

Prognoza magle i niskih stratusa zahtjeva osjetljivu ravnotežu između parametrizacija procesa zračenja, mikrofizike, naoblake i turbulentne razmjene. Analizom brojnih opcija koje se mogu koristiti za svaku od ovih parametrizacija tražiti će se optimalna kombinacija za prognozu magle i niske naoblake u unutrašnjosti Hrvatske.

.1 Pregled dosadašnih istraživanja

Dosadašnja znanstvena istraživanja napravljena modelom ALADIN na analizi atmosferskih procesa su brojna te su doprinijela kompleksnosti modela i kvaliteti prognoze, a ovdje su nabrojana samo neka. Semi-lagranžijanska horizontalna difuzija (SLHD, Váňa i sur. 2008) je horizontalna difuzija koja se temelji na fizikalnim svojstvima polja vjetra te je time ovisna o stanju atmosfere za razliku od uobičajene numeričke horizontalne difuzije. U model je uključena jednostavna shema za mikrofiziku sa trodimenzonalnim prognostičkim poljima za vodene i ledene čestice u oblaku, kišu i snijeg (Catry i sur. 2007) koja koristi statističku sedimentaciju oborine (Geleyn i sur. 2008). Vertikalna turbulentna difuzija je modificirana u skladu sa Geleyn i sur. (2006) te uključuje prognostičku turbulentnu kinetičku energiju. U modelu je razvijena i prognostička shema za konvekciju, koja uključuje prognostička polja vertikalne brzine updrafta i downdrafta i zapremine ćelije modela updrafta i downdrafta (**?**).

Prognoza magle i niskih stratusa je bila glavni predmet istraživanja u COST Action 722 (Jacobs i sur. 2008). Niz jednodimenzionalnih modela je dizajniran specijalno za prognozu magle, npr. Duynkerke (1991) analizira situacije s maglom korištenjem podataka s tornja Cabauw. COBEL jednodimenzoinalni model ovisi o početnim uvjetima tako da je razvijena specifična asimilacija za inicijalizaciju (Bergot i sur. 2007). S time u vidu, prognoziranje pojave magle i niskih stratusa je dodatni izazov s operativnim modelom od kojeg očekujemo ispravnu prognozu intenzivnih i brzih procesa s istim postavkama.

Cilj rada je detaljnom analizom čestine brzih ciklona uz pomoću postojećih i predloženih metoda postići smanjenje pogreške u prognozi modela ALADIN zbog propagiranja pogrešaka nastalih pri uključivanju lateralnih rubnih uvjeta iz globalnog modela. Slijedeći korak je analiza vremenskih situacija sa brzo napredujućih

poremećajima u polju tlaka te postizanje boljeg razumjevanje procesa koji dovode do opasnih vremenskih prilika. Na koncu, pronalašenje optimalne konfiguracije modela bi omogućilo uspješnu prognozu intenzivnih procesa kao olujno nevrijeme i osjetljive ravnoteže kao što je magla.

Za istraživanje će se koristiti model na ograničenom području za numeričku prognozu vremena ALADIN (Aire Limitée Adaptation Dynamique Développement International, ALADIN International Team 1997, termonia2017). Model se koristi za operativnu prognozu na Državnom hidrometeorološkom zavodu od 2000 godine te u nacionalnim meteorološkim službama još 15 država (u različitim konfiguracijama ALADIN Sustava. U modelu postoje brojne opcije tako da je moguće koristiti model u velikom broju konfiguracija: hidrostatski ili nehidrostatski, numerička ili semilagranžijanska horizontalna difuzija, eulerovska ili lagranžijanska advekcija, prognostička turbulentna kinetička energija, mikrofizičke varijable te konvekcija. Prvobitna operativna konfiguracija je opisana u (**?**). Do sada je znatno izmjenjena tako da hidrostatski operativni model na 8 km rezoluciji koristi prognostička TKE i 4 mikrofizičke varijable (Tudor et al. 2013; **?**).

Termonia (2004) je razvio numerički filter koji otkriva brze poremećaje u polju tlaka reduciranog na srednju morsku razinu. Međutim filter treba biti implementiran u globalni model iz kojeg se uzimaju lateralni rubni uvjeti te korišten tijekom operativne prognoze globalnim modelom. Dobiveno filtrirano polje se treba distribuirati zajedno sa ostalim meteorološkim poljima koji se koriste pri povezivanju s lateralnim rubnim uvjetima. U globalni model ARPEGE, koji se trenutno koristi za prognostičke lateralne rubne uvjete u operativnoj prognozi, ugrađen je rekurzivni visoko propusni filter koji primjenjen na polje tlaka omogućuje detekciju brzih poremećaja tlaka (Termonia, 2004), a u operativnoj primjeni je u modelu ARPEGE od 23 siječnja 2006. Termonia i sur. (2009) su analizirali situacije nastale tijekom 2006 godine relevantne za području Belgije na koje opasni vremenski poremećaji dolaze sa Sjevernog mora.

U ovom radu bi se analizirali poremećaji koji djeluju na područje Hrvatske, što uključuje i zapadni Mediteran, za razdoblje od 2006 za model ARPEGE te za razdoblje od kraja listopada 2010 godine za model ECMWF-a.

U radu će se proučiti dobiveno filitrirano polje tlaka i provjeriti da li su velike vrijednosti filtriranog polja uvijek povezane sa napredovanjem ciklone. Analiza će se provesti za cijelo područje koje se koristi u operativnoj prognozi i provjeriti koliko često u operativnu domenu ALADIN-a na 8 km rezoluciji uđe ciklona dovoljno velikom brzinom da se ne može dobro detektirati u lateralnim rubnim uvjetima pa za posljedicu imamo grešku u prognozi. Analizirati će se broj situacija u kojoj se detektira brz prolazak ciklone kroz lateralne granice te provjeriti svaka situacija.

Na DHMZ-u kao operativne lateralne rubne uvjete možemo koristiti i prog-

nostička polja modela iz ECMWF-a. Filter (Termonia, 2004) nije primjenjen u poljima operativne prognoze ECMWF-a, kao ni u jednom drugom globalnom modelu, koliko je poznato. Stoga će se u radu razviti metoda kojom bi se operativno iz dobivenih prognostičkih polja ECMWF-a mogle detektirati brze ciklone i testirati na radzoblju za koje na DHMZ-u imamo datoteke za lateralne rubne uvjete (od 27. listopada 2010). Takva metoda se može razviti na temelju Termonia (2003) u kombinaciji sa digitalnim filterom selektivne skale Termonia (2008).

Detaljna analiza vremenske situacije sa kratkotrajnim opasnim vremenskim pojavama. Definirana je konfiguracija modela na visokoj rezoluciji koja najbolje prognozira opasne vremenske pojave, pogotovo izbor tretmana prognostičkih mikrofizičkih i konvektivnih varijabli u modelu ALADIN.

ALADIN je namjenjen za operativnu prognozu, tako da je nužno da postavke koje omogućuju dobru prognozu intenzivnih meteoroloških procesa kao što su oluje ne umanjuju kvalitetu prognoze u mirnijim vremenskim situacijama. Primjera radi, magla je također potencijalno opasna vremenska pojava, koja ugrožava sigurnost prometa te ju je zato nužno ispravno prognozirati, ali je za njeno prognoziranje potrebna osjetljiva ravnoteža brojnih procesa u modelu. Zbog toga se konfiguraciju koja omogućuje uspješno prognoziranje intenzivnih olujnih nevremena testirati i na vremenskim prilikama s maglom ili niskom slojevitom naoblakom.

.2 Metode za automatsko otkrivanje brzih promjena u polju tlaka u

Potencijalno opasni meteorološki uvjeti su, između ostalih, olujno nevrijeme, prolazak ciklone ili fronte, olujni vjetar ili gusta magla. Modeli na ograničenom području omogućuju modeliranje i prognoziranje tih procesa na većoj rezoluciji nego globalni modeli, koristeći specifične postavke modela prilagođene za to područje. Ovaj rad istražuje mogućnosti modela ALADIN za prognoziranje opasnih vremenskih pojava karakterističnih za šire područje Republike Hrvatske. Istraživanje je usmjereno na posljedice (pre)brzog ulaska ciklone u domenu modela na ograničenom području. Ciklona može ući u domenu modela na ograničenom području prebrzo da bi ju model mogao ispravno prepoznati u lateralnim rubnim uvjetima.

U ovom radu istražujemo koliko su ti događaji česti, istražuju se mehanizimi detekcije takvih događaja kako bismo mogli primjeniti metode koje takav problem rješavaju u operativnoj prognozi. Ovakvo rješenje možemo primjeniti za prognoziranje opasnih vremenskih prilika kao što su olujni vjetar i/ili intenzivna oborina. Pri tome će se voditi računa da odabrane postavke modela dobro prognoziraju olujne vremenske nepogode kao i one s maglom i slojevitom niskom naoblakom.

Ovaj rad se prvenstveno bavi problemom koji proizlazi iz vremenske interpolacije lateralnih rubnih uvjeta za model na ograničenom području. Prognostički lateralni rubni uvjeti se uzimaju iz modela na većoj skali te su obično dostupni s intervalnom od nekoliko sati. Međutim, te lateralne rubne uvjete koristimo u svakom vremenskom koraku modela na ograničenom području, koji je nekoliko minuta (ili manje). Zbog toga moramo lateralne rubne uvjete interpolirati u vremenu.

Operativni prognostički lateralni rubni uvjeti su dostupni s intervalom od 3 sata, što može biti nedovoljno često da bi model na ograničenom području pravilno razlučio oluju (idruge procese malog prostornog raspona) koja brzo napreduje kroz lateralnu granicu. Očekuje se da će se ovaj problem dodatno pogoršati s povećanjem horizontalne rezolucije modela, kako globalnog na velikoj skali iz kojeg se uzimaju prognostički lateralni rubni uvjeti tako i modela na ograničenom području koji ih koristi.

Kako bi otkrili intenzivne poremećaje u polju prizemnog tlaka koji se brzo gibaju kroz domenu modela, u operativnom globalnom modelu ARPEGE u Meteo Franceu se izračunava filtrirano polje prizemnog tlaka (MCUF). To polje se distribuira u datotekama s prognostičkim lateralnim rubnim uvjetima zajedno s konvencionalnim meteorološkim poljima i koristi u operativnoj prognozi vremena ALADIN modelom na ograničenom području.

Provedena je analiza polja filitriranog prizemnog tlaka za razdoblje od 23. siječnja 2006. do 15. studenog 2014. u radu Tudor (2015). Polje filtriranog prizemnog tlaka je dobar pokazatelj postojanja poremećaja u polju prizemnog tlaka koji brzo napreduju kroz domenu. Prostornu i vremensku distribuciju polja filtriranog prizemnog tlaka možemo povezati sa uobičajenim stazama ciklona i područjima koja su poznata kao mjesta gdje nastaju ciklone.

Postoji i alternativni set operativnih prognostičkih lateralnih rubnih uvjeta iz operativne prognoze IFS-a u ECMWF-u. Taj set je također raspoloživ sa vremenskim korakom od 3 sata, ali ne i polje filtriranog prizemnog tlaka. U ovom radu je predloženo i testirano nekoliko metoda koje omogućuju detektiranje przo propagirajućih poremećaja u polju tlaka a posteriori iz prognostičkih polja IFS-a koja su dostupna u datotekama s prognostičkim lateralnim rubnim uvjetima:

- izračunato je polje filtriranog prizemnog tlaka ALADIN modelom na rezoluciji polja prognostičkih lateralnih rubnih uvjeta,
- izračunata je funkcija pogreške korištenjem prognoze od jednog vremenskog koraka na rezoluciji polja prognostičkih lateralnih rubnih uvjeta, i to:
  - bez inicijalizacije,
  - inicijaliziranih digitalnim filterom,

  - inicijaliziranih digitalnim filterom selektivne skale,

- također je izračunata amplituda promjene tlaka svedenog na srednju morsku razinu i prizemnog tlaka iz polja u datotekama s prognostičkim lateralnim rubnim uvjetima.

Većina metoda daje signal za brzo propagirajuće poremećaje u polju prizemnog tlaka, ali inicijalizacija digitalnim filterom reducira oluje ispod razine detekcije (isuviše da bi se mogao postaviti jasan kriterij za detekciju). Funkcija greške primjenjena bez filtriranja i amplituda daju više šuma, ali je i signal za brzo propagirajuće poremećaje u polju tlaka također jači tako da je moguće definirati kriterij za detekciju (koji je veći od kriterija za druge metode).

Ove metode su primjenjene i testirane na ALADIN numeričkom modelu za prognozu vremena na ograničenom području, ali se mogu primjeniti i u drugim modelima na ograničenom području te doprinijeti poboljšanju rezultata klimatskih modela na ograničenom području.

.3 Alternativne formulacije za uključivanje lateralnih rubnih uvjeta

Modeli na ograničenom području koriste veću rezoluciju i naprednije parametrizacije fizikalnih procesa nego globalni numerički modeli za prognozu vremena, ali imaju dodatni izvor pogreške modela, a to su prognostički lateralni rubni uvjeti. U operativnom kontekstu, u kojem se model na velikoj skali izvršava u drugom prognostičkom centru i neovisno o modelu na ograničenom području, model na velikoj skali informaciju o svojim poljima prenosi modelu na ograničenom području samo u uskoj zoni uz lateralne granice domene modela na ograničenom području koje zovemo povezujuća zona i to u disktretnim vremenskim koracima koje razdvaja interval povezivanja od nekoliko sati.

Vremenska rezolucija lateralnih rubnih uvjeta može biti manja od vremena potrebnog da bi neka meteorološka pojava prošla lateralnu granicu - povezujuću zonu. Korisnik modela na ograničenom području koji ovisi o prognostičkim lateralnim rubnim uvjetima dobivenim iz nezavisne prethodne analize ili modela koji se operativno koristi u drugoj ustanovi, može uočiti da su uobičajene sheme za vremensku interpolaciju podataka na velikoj skali daju prognostičke lateralne rubne uvjete koji nisu adekvatne kvalitete.

Problem brzog poremećaja u polju tlaka koji nije prepoznat operativnom shemom povezivanja lateralnih rubnih uvjeta je istražen korištenjem jednostavnog jednodimenzionalnog modela. Implementirana je i testirana metoda za spektralno ug-

nježđivanje. Također su prikazani rezultati spektralne vremenske interpolacije u kombinaciji s tradicionalnom metodom relaksacije za povezivanje u prostoru.

.4 Važnost nehidrostatske dinamike

Od 2000. godine, operativna prognoza modelom ALADIN na DHMZ-u uključuje dinamičku adaptaciju polja vjetra na rezoluciju 2 km. Dinamička adaptacija polja vjetra na topografiju u većoj rezoluciji daje poboljšanu prognozu vjetra na 10 m nad tlom, pogotovo u situacijama sa jakom i olujnom burom. Prognoza vjetra u takvim situacijama se pokazala pouzdanom unatoč korištenju hidrostatske dinamike (na rezoluciji 2 km), smanjenom broju nivoa u vertikali (iznad graničnog sloja atnosfere) i izostavljanju fizikalnih parametrizacija, osim turbulencije.

Tijekom noći sa 1. na 2. veljače 2007. i u kasno poslijepodne 3. veljače 2007. su se dogodila dva slučaja olujne bure koji nisu prognozirani operativnom dinamičkom adaptacijom. Slučajevi su analizirani korištenjem mjerenja tlaka i vjetra na 10 m sa dvije automatske postaje koje se nalaze na lokacijama pod utjecajem tih epizoda bure (Split i Makarska). Napravljeni su i eksperimenti modelom ALADIN na visokoj rezoluciji.

Također su korištena radiosonfdažna mjerenja sa obje postaje gdje se ta mjerenja izvode, Zadar i Zagreb. Lokacije radiosondažnih mjerenja su udaljene od područja pogođenih epizodama olujne bure koje se ovdje proučavaju, ali su najbliže dostupne sondaže koje omogućuju procjenu kvalitete modelirane vertikalne strukture atmosfere i daju uvid u realne vertikalne profile na području gdje se slučaj dogodio.

Napravljene su simulacije modelom ALADIN do 72 sata unapred na rezoluciji 2 km sa nehidrostatskom dinamikom i potpunim paketom fizikalnih parametrizacija (uključujući konvekciju). Također je napravljen alternativni set simulacija sa hidrostatskom dinamikom. Prikazani su rezultati za najmanje difuzivne postavke horizontalne difuzije. Problem horizontalne difuzije na visokoj rezoluciji je izvan područja ovog rada te nije detaljnije analiziran.

Utjecaj nehidrostatike postaje važniji za uske planine. To možemo vidjeti u rezultatima modela jer su najveće razlike u simulacijama s hidrostatskom i nehidrosttskom dinamikom mogu uočiti na području Makarske u prvoj analiziranoj situaciji.

Uz pomoć nehidrostatske dinamike model jest predvidio kratku epizodu jake bure u Splitu za prvi slučaj bure, ali maksimum u brzini vjetra se dogodio prerano, poslijepodne umjesno na večer, te je prognozirana brzina vjetra dosegla najniže vrijednosti u trenutku kada su izmjerene najveće brzine vjetra.

Model nije dobro prognozirao vertikalnu strukturu atmosfere zato što je promašio temperaturunu inverziju koja se formirala blizu vrha planine. Tempera-

turna inverzija neposredno iznad vrha planine podržava nastanak planinskih valova i rotora. Duboki stabilni sloj zraka u kojem horizontalna brzina vjetra reaste s visinom iznad planine dovodi do zarobljenih planinskih valova. Brze promjene u brzini vjetra mogu biti posljedica nastanka rotora ili promjene amplitude ili valne duljine planinskih valova. Međutim, isti eksperiment je prognozirao prejaku buru na Makarskom području u prvom analiziranom slučaju kao posljedicu prejakih promjena u polju tlaka. Drugi slučaj bure u Makarskoj je bolje prognoziran.

.5 Prognoza magle i niskih stratusa u dolinama

Provedeni su eksperimenti prognoze magle i niskih stratusa korištenjem ALADIN numeričkog modela za prognozu vremena na ograničenom području. Eksperimenti su prikazani za situaciju sa dugotrajnom maglom. Model je korišten sa različitim shemama za parametrizaciju zračenja, dijagnostiku naoblake i horizontalnu difuziju. Korištene su različite reprezentacije topografije, povećana vertikalna razlučivost sa i bez varijabli koje opisuju TKE i prognostičke kondenzirane varijable (vodene i ledene čestice u oblaku, kiša i snijeg). Neke od kombinacija reproduciraju maglu i niski stratus (kao što se vidi na satelitskim slikama) i dnevni ciklus temperature i vlage na 2 m (u usporedbi s mjerenjima).

Rezultati eksperimenata pokazuju da shema dijagnostike naoblake i pretpostavka preklapanja igraju bitniju ulogu u uspješnoj prognozi magle i niske naoblake nego sofisticiranija shema za zračenje ili uvođenje prognostičke TKE, kiše, snijega, vodenih i ledenih čestica u oblaku. Realističnije polje topografije i fizikalna shema horizontalne difuzije bitno popravljaju modelirani niski stratus i temperaturu na 2 m u područjima s promjenjivom topografijom.

ALADIN model za numeričku prognozu vremena na ograničenom području je imao poteškoća s prognozom magle i niskih stratusa. Tijekom prve polovice prosinca 2004. godine, niski stratus i magla su prekrivali doline u unutrašnjosti Republike Hrvatske (i šire okolno područje). Ovi oblaci nisu prognozirani u operativnoj ALADIN prognozi. S obzirom na to da ovo nije bio izolirani slučaj greške u prognozi modela u vremenskoj situaciji s maglom, bilo je bitno naći da li postoje postavke modela koje bi prognozirale nastanak i razvoj niskih stratusa i magle. Početni i rubni uvjeti za eksperimente su uzeti iz operativne prognoze globalnim modelom ARPEGE u Meteo Franceu (koji su korišteni i za operativnu prognozu). Polja ARPEGE-a su također opeisivala atmosfersko stanje bez magle i niskih stratusa. U to vrijeme se asimilacija podataka radila u ARPEGE-u (ne i u lokalnoj operativnoj ALADIN aplikaciji). Međutim, jednom kada je prognoza dovoljno različita od stvarnog stanja atmosfere, mjerenja nisu asimilirana. Posljedično, analizirana polja ne sadrže detalje stanja atmosfere koji su nužni za formiranje i razvoj niskih

stratusa i magle. Problem se zadržava kroz uzastopne prognoze. Ovaj problem je potaknuo razvoj empiričkih shema za subinverzijsku naoblaku koja inicira pozitivnu uzajamno povratnu vezu divergencije toka zračenja, turbulencije i mikrofizike (kondenzacije, tj. nastanka oblaka). Ova shema nadilazi problem pogrešnih početnih profila temperature i vlage i omogućuje razvoj stratusa i magle.

Ovaj rad uspoređuje utjecaj različitih parametrizacijskih shema u modelu ALADIN na prognozu naoblake u slučajevima magle i niskog stratusa. Pretpostavka preklapanja oblaka igra vrlo bitnu ulogu kao i formula koja se koristi za dijagnosticiranje naoblake. Obje je potrebno pažljivo odabrati kako bi se postavio ispravan ulaz naoblake u shemu za zračenje koji podržava daljnji razvoj oblaka.

Iako nastanak i razvoj magle nije na prvi pogled osobito intenzivan i brz proces, nužno je izračunavati doprinos zračenja barem svakih sat vremena kako bismo uopće omogućili razvoj magle u modelu. U suprotnom se koriste stari koeficijenti prijenosa zračenja koji su izračunati za atmosferu bez oblaka. To sprečava uzajamno povratni proces koji vodi do razvoja niskih stratusa i magle. Drugi fenomeni kao i tranzijentni slučajevi magle trebaju češće izračunavnje koeficijenata prijenosa zračenja. Za pravilnu prognozu, potrebno je izračunavati doprinos zračenja svaki vremenski korak integracije (nekoliko minuta). Nedovoljno često izračunavanje koeficijenata prijenosa zračenja i posljedične promjene temperature može izazavati numeričku nestabilnost (**?**) te degradirati prognozu u slučajevima kada je ravnoteža zračenja između oblaka i ostatka atmosfere bitna za razvoj oblaka.

Numerička horizontalna difuzija djeluje na nivoima modela koji slijede nagib terena te zbog toga miješa (izglađuje polja modela između dna doline i grebena planine u blizini. Intenzitet numeričke horizontalne difuzije je isti u u svim vremenskim situacijama na cijeloj domeni. Nova shema za horizontalnu difuziju, semilagranižijanska horizontalna difuzija ovisi o polju deformacije tako da je intenzitet horizontalnog miješanja nizak kada je vjetar slab. Fizikalnija shema za horizontalnu difuziju dozvoljava razvoj magle u uskim dolinama (za horizontalnu razlučivost od 8 km koju koristimo u ovom radu).

Uvođenje prognostičke TKE, ledenih kristala i vodenih kapi u oblaku, te kiše i snijega ima pozitivan utjecaj na prognozu magle i niskih oblaka u dolinama i na kosinama, ali samo u kombinaciji sa semi-lagranžijanskom horizontalnom difuzijom. Kompleksan teren naglašava važnost ispravne reprezentacije nerazlučene promjenjivosti visine topografije.

Različiti prikazi topografije, sa i bez ovojnice, mogu podići visinu terena (u modelu) unutar ili iznad sloja magle (u stvarnoj atmosferi) te posljedično imaju bitan utjecaj na ispravnu prognozu temperature i relativne vlage na 2 m mad tlom. U ovom slučaju, sloj magle je bio debeo i perzistentan tako da povećana vertikalna razlučivost ima slab utjecaj na prognozu naoblake jednom kada su parametriza-

cije postavljene tako da proizvedu maglu. Međutim, povećana vertikalna rezolucija popravlja prognozu temperaturne inverzije.

Vrlo visoka horizontalna rezolucija je bila nužan, ali ne i dovoljan uvjet za ispravno modeliranje strukture graničnog sloja atmosfere u kompleksnom terenu za fenomene kao što su tok zraka u dolini ili fen. U ovom slučaju to nije bio neophodno jer su strujanja i na velikoj skali i lokalno bila vrlo slaba. Veća horizontalna rezolucija omogućuje veći nagib terena kada postaje bitan i utjecaj sjene planine na sunčevo zračenje. Stoga bi prognoziranje slučaja tranzijentne magle u uskoj dolini zahtjevao vrisoku horizontalnu razlučivost modela koja bi razlučila lokalna gibanja koja se razvijaju zbog različitog zagrijavanja strana doline.

Proučavanje drugih slučajeva magle i niskih stratusa, pogotovo u užim dolinama, zahtijeva veću horizontalnu rezoluciju i parametrizaciju zasjenjivanja doline zbog okolnih planina. Istraživanje sličajeva s tranzijentnom maglom bi dalo bolji uvid u ravnotežu dugovalnog zračenja i grijanja zbog kratkovalnog zračenja. Takvo istraživanje bi također zahtjevalo bolje početne uvjete i analizu površine tla kao i asimilaciju podataka na većoj rezoluciji. Ovo istraživanje je otkrilo koja konfiguracija modela omogućuje prognozu magle i niskih stratusa. Prije uključivanja ove konfiguracije u operativnu prognozu potvrđeno je da je predložena konfiguracija prikladna za operativnu upotrebu na većem broju slučajeva sa različitim tipovima vremena.

Ključne riječi: Model na ograničenom području, lateralni rubni uvjeti, povezivanje, oluje, vremenska interpolacija, pogre qvska interpolacije, Fourierov trensform, spektralni koeficijenti, faza, amplituda **Key words:** Limited area model; Lateral boundary conditions; Coupling; Storms; Temporal interpolation ; Interpolation error; Fourier transform; Spectral coefficients; Phase; Amplitude

Bibliography

ALADIN International team, 1997: The aladin project: Mesoscale modelling seen as a basic tool for weather forecasting and atmospheric research. *WMO Bull*, **46**, 317–324.

Alpert, P., Neeman, B.U., and Y. Shay-El, Y.; Intermonthly variability of cyclone tracks in the Mediterranean, J. Climate, 3, 1474–1478, 1990.

Baumhefner, D. and D. Perkey, 1982: Evaluation of lateral boundary errors in a limited-area domain. *Telus*, **34**, 409–428.

Boyd, J.P.: Limited-Area Fourier Spectral Models and Data Analysis Schemes: Windows, Fourier Extension, Davies Relaxation, and All That. Mon. Wea. Rev., 133, 2030–2042, 2005.

Branković, Č., Matjačić, B., Ivatek-Šahdan, S., and Buizza, R.: Dynamical downscaling of ECMWF EPS forecasts applied to cases of severe weather in Croatia, ECMWF RD Technical Memorandum, No. 507, 38 pp., 2007.

Branković, Č., Matjačić, B., Ivatek-Šahdan, S., and Buizza, R.: Downscaling of ECMWF Ensemble Forecasts for Cases of Severe Weather: Ensemble Statistics and Cluster Analysis, Mon. Wea. Rev., 136, 3323–3342, 2008.

Brožkova, R., Klarić, D., Ivatek-Šahdan, S., Geleyn, J.-F., Casse, V., Široká, M., Rádnoti, G., Janoušek, M., Stadlbacher, K., and Seidl, H.: DFI Blending, an alternative tool for preparation of the initial conditions for LAM, PWRP Report Series No. 31, WMO-TD, No. 1064, 2001.

Caian, M. and J.-F. Geleyn, 1997: Some limits to the variable-mesh solution and comparison with the nested-lam solution. *Quart. J. Roy. Meteor. Soc.*, **123**, 743–766.

Campinis, J., Genoves, A., Jansa, A., Guijarro, J.A., and Ramis, C.: A catalogue and a classification of surface cyclones for the Western Mediterranean, Int. J. Climatol., 20, 969–984, 2000.

Cassou, C., and Terray, L.: Oceanic forcing of the wintertime low-frequency atmospheric variability in the north atlantic european sector: a study with the arpege model, J. Climate, 14, 4266–4291, doi: http://dx.doi.org/10.1175/1520-0442(2001)014, 2001.

Charney, J.G., Fjortoft, R., von Neumann, J. 1950. Numerical integration of the barotropic vorticity equation. Tellus 2, 237–254.

Côté, J., Roch, M., Staniforth, A., Fillion, L. 1993. A variable-resolution semi-Lagrangian finite-element global model of the shallow water equations. Mon. Weather Rev. 121, 231–243.

Côté, J., Desmarais, J.G., Gravel, S., Méhot, A., Patoine, A., Roch, M., Staniforth, A. 1998. The operational CMCMRB Global Environmental Multiscale (GEM) model. Part II: MEsoscale results. Mon Weather REv. 126, 1373-1395.

Courtier, P., and Geleyn, J.-F.: A global numerical weather prediction model with variable resolution: application to the shallow water equations. Quart. J. Roy. Meteor. Soc., 114, 1321–1246, 1988.

Davies, H., 1976: A lateral boundary formulation for multi-level prediction models. *Quart. J. Roy. Meteor. Soc.*, **102**, 405–418.

Davies, H., 1983: Limitations of some common lateral boundary schemes used in regional nwp models. *Mon. Wea. Rev.*, **111**, 1002–1012.

Davies, T.: Lateral boundary conditions for limited area models. *Q. J. R. Meteorol. Soc.*, 140: 185–196, 2014.

Dee, D. P., Uppala, S.M., Simmons, A.J., Berrisford, P., Poli, P., Kobayashi, S., Andrae, U., Balmaseda, M.A., Balsamo, G., Bauer, P., Bechtold, P., Beljaars, A.C.M., van de Berg, L., Bidlot, J., Bormann, N., Delsol, C., Dragani, R., Fuentes, M., Geer, A.J., Haimberger, L., Healy, S.B., Hersbach, H., Hólm, E.V., Isaksen, L., Kàllberg, P., Köhler, M., Matricardi, M., McNally, A.P., Monge-Sanz, B.M., Morcrette, J.-J., Park, B.-K., Peubey, C., de Rosnay, P., Tavolato, C., Thépaut, J.-N., and Vitart, F.: The ERA-Interim reanalysis: configuration and performance of the data assimilation system. *Q. J. R. Meteorol. Soc.*, 137, 553–597. doi: 10.1002/qj.828, 2011.

Degrauwe, D., Caluwaerts, S., Voitus, F., Hamdi, R., and Termonia, P.: Application of Boyds Periodization and Relaxation Method in a Spectral Atmospheric Limited Area Model. Part II: Accuracy Analysis and Detailed Study of the Operational Impact. Mon. Wea. Rev., 140, 3149–3162, 2012.

Denis, B., Laprise, R., Caya, D. and Cŏté, J.: Downscaling ability of one-way nested regional climate models: the big-brother experiment. Climate Dynamics, 18, 627–646, 2002.

Denis, B., Laprise, R. and Caya, D.: Sensitivity of a regional climate model to the resolution of the lateral boundary conditions. Climate Dynamics, Climate Dynamics, 20, 107–126, 2003.

De Troch, R., Hamdi, R., Van de Vyver, H., Geleyn, J.-F., and Termonia, P.: Multiscale Performance of the ALARO-0 Model for Simulating Extreme Summer Precipitation Climatology in Belgium. J. Climate, 26, 8895–8915, 2013.

Doswell, C.A., Brooks, H.E., and Maddox, R.A.: Flash flood forecasting: An ingredients-based methodology. *Wea. Forecasting*, 11, 560–581, 1996.

Durran, D. R., 1999: *Numerical Methods for Wave Equations in Geophysical Fluid Dynamics*. Springer-Verlag, 465 pp.

El Ouaraini, R., Berre, L., Fischer, C., El Hassan Sayouty (2015) Sensitivity of regional ensemble data assimilation spread to perturbations of lateral boundary conditions, Tellus A: Dynamic Meteorology and Oceanography, 67:1, 28502, DOI: 10.3402/tellusa.v67.28502

Gilbert, J. C. and J. Nocedal, 1992: Global convergence properties of conjugate gradient methods for optimization. *SIAM J. Optimization*, **2**, 21–42.

Gospodinov I, Spiridonov V, Geleyn J-F. 2001. Second order accuracy of two-time-level semi-Lagrangian schemes. Quart. J. R. Met. Soc. 127 : 1017–1033. DOI:10.1002/qj.49712757317

Guidard, V. and C. Fischer, 2008: Introducing the coupling information in a limited-area variational assimilation. *Quart. J. Roy. Meteor. Soc.*, **134**, 723–735.

Gustafsson, N.: Control of lateral boundary conditions in four-dimensional variational data assimilation for a limited area model. *Tellus A*, 1-14. 2012.

Hamdi, R., Van de Vyver, H. and Termonia, P.: New cloud and microphysics parameterisation for use in high-resolution dynamical downscaling: application for summer extreme temperature over Belgium. Int. J. Climatol., 32: 2051–2065. doi: 10.1002/joc.2409, 2012.

Hamdi, R., Van de Vyver, H., De Troch, R. and Termonia, P.: Assessment of three dynamical urban climate downscaling methods: Brussels's future urban heat island under an A1B emission scenario. Int. J. Climatol., 34: 978–999. doi: 10.1002/joc.3734, 2014.

Haugen, J., and Machenhauer, B.: A spectral limited-area formulation with time-dependent boundary conditions applied to the shallow-water equations. Mon. Wea. Rev., 121, 2618–2630, 1993.

Hortal, M.: The development and testing of a new two-time-level semi-Lagrangian scheme (SETTLS) in the ECMWF forecast model. Q.J.R. Meteorol. Soc., 128: 1671–1687, 2002.

Ivatek-Šahdan, S. and Ivančan-Picek, B.: Effects of different initial and boundary conditions in ALADIN/HR simulations during MAP IOPs, Meteorol. Z., 15, 187–197, 2006.

Ivatek-Šahdan, S., and Tudor, M.: Use of high-resolution dynamical adaptation in operational suite and research impact studies, Meteorol Z, 13(2), 1–10, 2004.

Juang, H.-M. and S.-Y. Hong, 2001: Sensitivity of the ncep regional spectral model to domain size and nesting strategy. *Mon. Wea. Rev.*, **129**, 2904–2922.

Juang, H.-M. and M. Kanamitsu, 1994: The nmc nested regional spectral model. *Mon. Wea. Rev.*, **122**, 3–26.

Laprise, R.: Resolved scales and nonlinear interactions in limited-area models, J. Atmos. Sci., 60, 768–779, 2003.

Laprise, R., de Elía, R., Caya, D., Biner, S., Lucas-Picher, P., Diaconescu, E., Leduc, M., Alexandru, A., Separovic, L., Canadian Network for Regional Climate Modelling and Diagnostics: Challenging some tenets of regional climate modelling. Meteorol. Atmos. Phys., 100, 3–22, 2008.

Lionello, P., Bhend, J., Buzzi, A., Della-Marta, P. M., Krichak, S. O., Jansá, A., Maheras, P., Sanna, A., Trigo, I. F., and Trigo, R.: Cyclones in the Mediterranean region: climatology and effects on the environment, in: Mediterranean Climate Variability, edited by: Lionello, P., Malanotte-Rizzoli, P., and Boscolo, R., 325–372, Elsevier, 2006.

Lynch, P., and Huang, X-Y.: Initialization of the HIRLAM model using a digital filter. Mon. Wea. Rev, 120, 1019–1034, 1992.

Lynch, P.: The Dolph–Chebyshev Window: A Simple Optimal Filter. Mon. Wea. Rev., 125, 655–660, 1997.

Lynch, P., Giard, D., and Ivanovici, V.: Improving the Efficiency of a Digital Filtering Scheme for Diabatic Initialization. Mon. Wea. Rev., 125, 1976–1982, 1997.

McDonald, A., 1999: A review of lateral boundary conditions for limited-area forecast models. *Proc. Ind. Nat. Sci. Acad.*, **65**, 91–105.

McDonald, A., 2000: Boundary conditions for semi-lagrangian schemes: Testing some alternatives in one-dimensional models. *Mon. Wea. Rev.*, **128**, 4084–4096.

McDonald, A., 2002: A step toward transparent boundary conditions for meteorological models. *Mon. Wea. Rev.*, **130**, 140–151.

McDonald, A., 2003: Transparent boundary conditions for the shallow-water equations:testing in a nested environment. *Mon. Wea. Rev.*, **131**, 698–705.

Meinke, I., B. Geyer, F. Feser, and H. von Storch, 2006: The impact of spectral nudging on cloud simulation with a regional atmospheric model. *J. Atmos. Oceanic Technol.*, **23**, 815-824.

Mesinger, F., 1977: Forward-backward scheme, and its use in a limited area model. Contrib. Atmos. Phys., 50, 200-210.

Navon, I. M., B. Neta, and M. Y. Hussiani, 2004: A perfectly matched layer approach to the linearized shallow water equations model. *Mon. Wea. Rev.*, **132**, 1369–1378.

Nicolis, C.: Dynamics of model error: The role of the boundary conditions. J. Atmos. Sci., 64, 204–215, 2007.

Nutter, P., D. Stensrud, and M. Xue, 2004: Effects of coarsely resolved and temporally interpolated lateral boundary conditions on the dispersion of limited-area ensemble forecasts. *Mon. Wea. Rev.*, **132**, 2358–2377.

Oliger, J. and A. Sundström, 1978: Theoretical and practical aspects of some initial boundary value problems in fluid dynamics. *SIAM J. Appl. Math.*, **35**, 419–446.

Olver2010) Olver, F., D. Lozier, R. Boisvert, and C. Clark, Eds., 2010: NIST Handbook of Mathematical Functions. Cambridge University Press, 968 pp.

Rádnoti, G.: Comments on A spectral limited-area formulation with time-dependent boundary conditions applied to the shallow-water equations. Mon. Wea. Rev., 123, 3122–3123, 1995.

Radu, R., M. Deque, and S. Somot, 2008: Spectral nudging in a spectral regional climate model. *Tellus*, **60A**, 898–910.

Robert A. 1982. A semi-Lagrangian and semi-implicit numerical integration scheme for the primitive equations. J. Meteor. Soc. Japan. 60 : 319 - 325.

Robert, A. and E. Yakimiw, 1986: Identification and elimination of an inflow boundary computational solution in limited area model integrations. *Atmos.-Ocean.*, **24**, 369–385.

Simmons, A.J., and Burridge, D.M.: An Energy and Angular-Momentum Conserving Vertical Finite-Difference Scheme and Hybrid Vertical Coordinates. Mon. Wea. Rev. 109, 758–766, 1981.

Široká, M, Fischer C, Cassé, V, Brožková, R, Geleyn J-F. 2003. The definition of mesoscale selective forecast error covariances for a limited area variational analysis. Meteorol. Atmos. Phys. 82: 224244.

Stanešić, A.: Assimilation system at DHMZ: development and first verification results. Cro. Met. Jour., 44/45, 3–17, 2011.

Staniforth, A.: Regional modelling: A theoretical discussion. Meteorol. Atmos. Phys., 63, 15-29, 1997.

Termonia, P., 2003: Monitoring and improving the temporal interpolation of lateral-boundary coupling data for limited area models. *Mon. Wea. Rev.*, **131**, 2450–2463.

Termonia, P., 2004: Monitoring of the coupling update frequency of a limited-area model by means of a recursive digital filter. *Mon. Wea. Rev.*, **132**, 2130–2141.

Termonia, P., 2008: Scale-selective digital filtering initialization. *Mon. Wea. Rev.*, **136**, 5246–5255.

Termonia, P., A. Deckmyn, and R. Hamdi, 2009: Study of the lateral-boundary-condition temporal-resolution problem and a proposed solution by means of boundary-error restarts. *Mon. Wea. Rev.*, **137**, 3551–3566.

Termonia, P. and R. Hamdi, 2007: Stability and accuracy of the physics-dynamics coupling in spectral models. *Quart. J. Roy. Meteor. Soc.*, **133**, 1589–1604.

Termonia, P., Degrauwe, D., and Hamdi, R.: Improving the Temporal Resolution Problem by Localized Gridpoint Nudging in Regional Weather and Climate Models. Mon. Wea. Rev., 139, 1292–1304, 2011.

Termonia, P. and F. Voitus, 2008: Externalizing the lateral boundary conditions from the dynamic core in semi-implicit semi-lagrangian models. *Tellus*, **60A**, 632–648.

Termonia, P., Voitus, F., Degrauwe, D., Caluwaerts, S., and Hamdi, R.: Application of Boyds Periodization and Relaxation Method in a Spectral Atmospheric Limited-Area Model. Part I: Implementation and Reproducibility Tests. Mon. Wea. Rev., 140, 3137–3148, 2012. doi: http://dx.doi.org/10.1175/MWR-D-12-00033.1

Termonia, P. and Fischer, C. and Bazile, E. and Bouyssel, F. and Brožková, R. and Bénard, P. and Bochenek, B. and Degrauwe, D. and Derkova, M. and El Khatib, R. and Hamdi, R. and Mašek, J. and Pottier, P. and Pristov, N. and Seity, Y. and Smolíková, P. and Spaniel, O. and Tudor, M. and Wang, Y. and Wittmann, C. and Joly, A., 2017. The ALADIN System and its Canonical Model Configurations AROME CY41T1 and ALARO CY40T1. Geoscientific Model Development Discussions. 1–45. doi: 10.5194/gmd-2017-103

Tudor, M., and Ivatek-Šahdan, S.: The case study of bura of 1^{st} and 3^{rd} February 2007, Meteorol. Z., 19(5), 453–466, 2010.

Tudor, M., Ivatek-Šahdan, S., Stanešić, A., Horvath, K., Bajić, A.: Forecasting Weather in Croatia Using ALADIN Numerical Weather Prediction Model. In: Climate Change and Regional/Local Responses. Eds: Zhang, Y. and P. Ray, InTech, Rijeka, 59–88, 2013.

Tudor, M. and Termonia, P.: Alternative formulations for incorporating lateral boundary data into limited area models, Mon. Wea. Rev., 138, 2867–2882, 2010.

Uppala, S. M., Kållberg, P. W., Simmons, A. J., Andrae, U., Bechtold, V. D. C., Fiorino, M., Gibson, J. K., Haseler, J., Hernandez, A., Kelly, G. A., Li, X., Onogi, K., Saarinen, S., Sokka, N., Allan, R. P., Andersson, E., Arpe, K., Balmaseda, M. A., Beljaars, A.

C. M., Berg, L. V. D., Bidlot, J., Bormann, N., Caires, S., Chevallier, F., Dethof, A., Dragosavac, M., Fisher, M., Fuentes, M., Hagemann, S., Hólm, E., Hoskins, B. J., Isaksen, L., Janssen, P. A. E. M., Jenne, R., Mcnally, A. P., Mahfouf, J.-F., Morcrette, J.-J., Rayner, N. A., Saunders, R. W., Simon, P., Sterl, A., Trenberth, K. E., Untch, A., Vasiljevic, D., Viterbo, P. and Woollen, J.: The ERA-40 re-analysis. Q.J.R. Meteorol. Soc., 131: 2961–3012. doi: 10.1256/qj.04.176, 2005.

Vánnitsem, S., and Chome, F.: One-way nested regional climate simulations and domain size. J. Climate, 18, 229–233, 2005.

Voitus, F., P. Termonia, and P. Bénard, 2009: Well-posed lateral boundary conditions for spectral semi-implicit semi-lagrangian schemes: Tests in a one-dimensional model. *Mon. Wea. Rev.*, **137**, 315–330.

von Storch, H., H. Langenberg, and F. Feser, 2000: A spectral nudging technique for dynamical downscaling purposes. *Mon. Wea. Rev.*, **128**, 3664–3673.

Waldron, K. M., J. Peagle, and J. D. Horel, 1996: Sensitivity of a spectrally filtered and nudged limited area model to outer model options. *Mon. Wea. Rev.*, **124**, 529–547.

Warner, T., R. Peterson, and R. Treadon, 1997: A tutorial on lateral boundary conditions as a basic and potentially serious limitation to regional numerical weather prediction. *Bull. Amer. Meteor. Soc.*, **78**, 2599–2617.

Wernli, H., Dirren, S., Liniger, M.A., and Zillig, M.: Dynamical aspects of the life cycle of the winter storm Lothar (24–26 December 1999). Q. J. R. Meteorol. Soc., 128, 405–429, 2002.

Žagar, N., Honzak, L., Žabkar, R., Skok, G., Rakovec, J., and Ceglar, A.: Uncertainties in a regional climate model in the midlatitudes due to the nesting tecnique and the domain size, J. Geophys. Res. Atmos., 118, 6189–6199, 2013.

Curriculum Vitae

Personal information

Name: Martina

Last name: Tudor

e-mail martina.tudor@cirus.dhz.hr

Affilliation: Meteorological and Hydrological Service of Croatia

Address: Grič 3, HR10000 Zagreb, Croatia

Phone: +385 1 4565 721 +385 91 4564 111

Date and place of birth: 20 July 1976, Celje, Slovenia

Home: Slave Sajko 5, HR10310 Ivanić–Grad, Croatia

Education

1994–2000 BSc Department of Gepophysics, Faculty of Science, University of Zagreb
Diploma: Prijenos česti zraka na područje Hrvatske

2000–2007 MSc Department of Gepophysics, Faculty of Science, University of Zagreb
Diploma: Numeričke nestabilnosti fizikalnih parametrizacija u prognostičkom modelu ALADIN
(Numerical instabilities of physical parameterizations in the prognostic model ALADIN)

2010– PhD in Atmospheric sciences, Department of Gepophysics, Faculty of Science, University of Zagreb

Seminars, summer schools and trainings

15 – 26 May 2000 ALATNET Seminar of High Resolution Modelling, Radostovice (CZ).

3 – 7 Sep 2001 ECMWF Seminar on Key isues in the parameterization of subgrid physical processes, Reading (UK).

27 May – 1 June 2002 ALATNET Seminar on numerical methods, Kranjska gora (SI).

ALADIN mini coupling workshop, Ljubljana (SI), 17 – 21 Veljača 2003.

17 – 22 Aug 2003 Summer School on Mountain Meteorology, Trento (IT).

26 – 30 Jul 2004 Summer School on Mountain Meteorology, Trento (II).

6 – 10 Sep 2004 ECMWF Seminar on Recent developements in numerical methods in atmosphere and ocean modelling, Reading (UK).

Employment

2000– Meteorological and Hydrological Servide of Croatia

Proffesional research stays

2 Apr – 14 May 2000 Developement of PBL diagnostics for DIAGPACK, Prague (CZ).

8 Oct – 3 Nov 2000 PBL height diagnostics, Prague (CZ).

10 Mar – 6 Apr 2001 PBL height diagnostics, Prague (CZ).

15 Oct – 15 Dec 2001 PBL height and fibrillations, Toulouse (FR).

17 Aug – 4 Oct 2002 Stability of physics scehems and fibrillations, Prague (CZ).

1–30 Mar 2003 Robustness of physical parameterization, Toulouse (FR).

1–30 Jun 2003 Physics-dynamics interface for predictor-corrector scheme, Prague (CZ).

15 Sep – 31 Oct 2003 Phasing, Toulouse (FR).

1–29 Feb 2004 Phasing, Toulouse (FR).

15 Mar – 9 Apr 2004 Aladin-Arome equations, Prague (CZ).

27 Jun – 24 Jul 2004 Physics timestepping for predictor-corrector scheme, Prague (CZ).

1 Nov – 18 Dec 2004 MesoNH physics, Toulouse (FR).

7 – 11 Nov 2005 Alaro0 moist physics and pTKE scheme, Prague (CZ).

16 Jan – 16 Feb 2006 Alaro0 phasing, Brussels (BE).

26 Feb – 28 Mar 2006 DART06a research cruise, Adriatic.

9 Apr – 6 May 2006 Alaro0 phasing, Prague (CZ).

13 – 31 Aug 2006 DART06b research cruise.

23 Oct – 18 Nov 2006 Physics-dynamics interface, Prague (CZ).

Published papers

Papers in CC

1. Bencetić Klaić, Z. Pasarić, Z., Tudor, M. 2009. On the interplay between sea-land breezes and Etesian winds over the Adriatic. Journal of Marine Systems. 78, Suppl. 1, s101-s118.

2. Catry, B., Geleyn, J.-F., Tudor, M., Bénard, P., Trojakova A., 2007. Flux conservative thermodynamic equations in a mass-weighted framework, *Tellus, Ser. A,* 59, 71–79.

3. Ivančan-Picek, B., Tudor, M., Horvath, K., Stanešić, A., Ivatek-Šahdan, S., 2016. Overview of the first HyMeX Special Observation Period over Croatia. Nat. Hazards Earth Syst. Sci. Discuss., doi:10.5194/nhess-2016-247.

4. Ivatek-Šahdan, S., M. Tudor (2004), Use of high-resolution dynamical adaptation in operational suite and research impact studies, *Meteorol Z* 13(2), 1–10.

5. Janeković, I., Mihanović, H., Vilibić, I., Tudor, M., 2014. Extreme cooling and dense water formation estimates in open and coastal regions of the Adriatic Sea during the winter of 2012, J. Geophys. Res. Oceans, 119, 3200–3218, doi:10.1002/2014JC009865

6. Kalinić, H. Mihanović, H. Cosoli, S. Tudor, M. Vilibić, I. 2016. Predicting ocean surface currents using numerical weather prediction model and Kohonen neural network: a northern Adriatic study. Neural Computing and Applications. 11, 1-10.

7. Martin, P.J., J.W. Book, D.M. Burrage, C.D. Rowley, M. Tudor (2009), Comparison of model simulated and observed currents in the central Adriatic during DART, *Journal of Geophysical Research - Oceans* 114, C01S05. doi:10.1029/2008JC004842.

8. Mihanović, H., Vilibić, I., Carniel, S., Tudor, M., Russo, A., Bergamasco, A., Bubić, N., Ljubešić, Z., Viličić, D., Boldrin, A., Malačić, V., Celio, M., Comici, C., Raicich., F., 2013. Exceptional dense water formation on the Adriatic shelf in the winter of 2012. Ocean science. 9, 561–572.

9. Renko, T. Kozarić, T. Tudor, M. 2012. An assessment of waterspout occurrence in the Eastern Adriatic basin in 2010 : Synoptic and mesoscale environment and forecasting method. Atmospheric research. 123, 1, 71-81.

10. Rixen, M., Book, J.W., Carta, A., Grandi, V., Gualdesi, L., Stoner, R., Ranelli, P., Cavanna, A., Zanasca, P., Baldasserini, G., Trangeled, A., Lewis, C., Trees, C., Grasso, R., Giannechini, S., Fabiani, A., Merani, D., Berni, A., Leonard, M., Martin, P., Rowley, C., Hulbert, M., Quaid, A., Goode, W., Preller, R., Pinardi, N., Oddo, P., Guarnieri, A., Chiggiato, J., Carniel, S., Russo, A., Tudor, M., Lenartz, F., Vandenbulcke, L. 2009. Improved ocean prediction skill and reduced uncertainty in the coastal region from multi-model super-ensembles. // Journal of Marine Systems. 78, Suppl. 1, 282-289.

11. Termonia, P. and Fischer, C. and Bazile, E. and Bouyssel, F. and Brožková, R. and Bénard, P. and Bochenek, B. and Degrauwe, D. and Derkova, M. and El Khatib, R. and Hamdi, R. and Mašek, J. and Pottier, P. and Pristov, N. and Seity, Y. and Smolíková, P. and Spaniel, O. and Tudor, M. and Wang, Y. and Wittmann, C. and Joly, A., 2017. The ALADIN System and its Canonical Model Configurations AROME CY41T1 and ALARO CY40T1. Geoscientific Model Development Discussions. 1–45. doi: 10.5194/gmd-2017-103

12. Tudor, M., and Ivatek-Šahdan, S.: The case study of bura of 1^{st} and 3^{rd} February 2007, Meteorol. Z., 19(5), 453–466, 2010.

13. Tudor, M. and Termonia, P.: Alternative formulations for incorporating lateral boundary data into limited area models, Mon. Wea. Rev., 138, 2867–2882, 2010.

14. Tudor M., 2010. Impact of horizontal diffusion, radiation and cloudiness parameterization schemes on fog forecasting in valleys. Met. Atm. Phy. Vol.108, 57-70.

15. Tudor, M., 2013. A test of numerical instability and stiffness in the parametrizations of the ARPÉGE and ALADIN models. Geoscientific model development, 6, 901–913.

16. Vandenbulcke, L., Beckers, J.-M., Lenartz, F., Barth, A., Poulain, P.-M., Aidonidis, M., Meyrat, J., Ardhuin, F., Tonani, M., Fratianni, C., Torrisi, L., Pallela, D., Chiggiato, J., Tudor, Martina, Book, J. W., Martin, P., Peggion, G., Rixen, M. 2009. Super-ensemble techniques: Application to surface drift prediction. Progress in Oceanography. 82, 3, 149-167.

17. Vilibić, I., Book, J.W., Beg Paklar, G., Orlić, M., Dadić, V., Tudor, M., Martin, P.J., Pasarić, M., Grbec, B., Matić, F., Mihanović, H., Morović, M. 2009. West Adriatic coastal water excursions into the East Adriatic. Journal of Marine Systems. 78, S1; S132-S156.

18. Vilibić, I. Šepić, J. Mihanović, H. Kalinić, H, Cosoli, S. Janeković, I. Žagar, N. Jesenko, B. Tudor, M. Dadić, V. Ivanković, D. 2016. Self-Organizing Maps-based ocean currents forecasting system. Scientific Reports. 6, 22924/1-22924/7.

19. Vilibić, I. Kalinić, H. Mihanović, H. Cosoli, S. Tudor, M. Žagar, N. Jesenko, B. 2016. Sensitivity of HF radar-derived surface current self-organizing maps to various processing procedures and mesoscale wind forcing. Computational geosciences. 20, 115-131

Other publications

1. Book, J.W., Martin, P., Rixen, M., Dykes, J., Wang, S., Ladner, S., Tudor, M., Chiggiato J. 2007. Real-time coastal monitoring and predistion for operations and research. NRL Review. 07; 185-187.

2. D. Drvar, I. Stiperski, M. Tudor i V. Tutiš, 2005. Testing the new subgrid-scale orography representation on bora cases Cro. Meteorol. J., 40, 304-307.

3. Geleyn, J-F., Vãña, F., Cedilnik, J., Tudor, M., Catry, B., 2006. 'An intermediate solution between diagnostic exchange coefficients and prognostic TKE methods for vertical turbulent transport.' WGNE Blue Book.

4. Horvath, K., Bajić, A., Ivatek-Šahdan, S., Hrastinski, M., Odak Plenković, I., Stanešić, A., Tudor, M., Kovačić, T. 2015. Overview of meteorological research on the project Weather intelligence for wind energy - WILL4WIND. Cro. Meteorol. Jour., 50; 91-104.

5. I. Janeković i M. Tudor 2005. The Adriatic Sea wave response to severe bura wind. Cro. Meteorol. J., 40, 316-319.

6. Mazzocco Drvar, D., Plačko-Vršnak, D., Tudor, M., Trošić, T., 2012. Flash-flood in Pula in the night between 24 and 25 September 2010. Cro. Meteorol. J., 47, 35–43.

7. Tudor, M. 2011. The meteorological aspects of the DART field experiment and preliminary results. Cro. Meteorol. J., 44/45; 31-46.

8. M. Tudor, V. Tutiš, I. Stiperski i F. Vaña, 2005. Testing the new semi-lagrangian horizontal diffusion scheme, Cro. Meteorol. J., 40, 346-349.

9. M. Tudor, I. Stiperski, V. Tutiš i D. Drvar, 2005. Comparison of few radiation and cloudiness parametrisations on a persistent low stratus case Cro. Meteorol. J., 40, 342-345.

10. Tudor, M. Ivatek–Šahdan, S. 2002. MAP IOP 15 case study. Cro. Meteorol. J., 37, 1-14.

11. Tudor, M., Ivatek–Šahdan, S. 2004. Use of high-resolution dynamical adaptation for the extreme wind estimate. WGNE Blue Book. 2004, 5; 15-16

12. Tudor, M., Janeković, I. 2016. Modelling origin and transport fate of waste materials on the southeastern Adriatic coast (Croatia). Geofizika. 33, 1; 53-77.

13. Tudor, M., Stanešić, A., Ivatek-Šahdan, S., Hrastinski, M., Odak Plenković, I., Horvath, K., Bajić, A., Kovaičić., T., 2015. Changes in the ALADIN operational suite in Croatia in the period 2011-2015. Cro. Meteorol. J. 50. 71–89.

14. Tudor, M., Stanešić, A., Ivatek-Šahdan, S., Hrastinski, M., Odak Plenković, I., Horvath, K., Bajić, A., Kovaičić., T., 2015. Operational validation and verification of ALADIN forecast in meteorological and hydrological service of Croatia. Cro. Meteorol. J. 50. 47–70.

15. Vakula, Z., Kalin, L., Tudor, M., Ivatek-Šahdan, S. 2005. Verification in Croatian Meteorological and Hydrological Service. WGNE Blue Book. 4, 5; 25-26.

16. Vučetić, V., Ivatek-Šahdan, S., Tudor, M., Kraljević, L., Ivančan-Picek, B., Strelec Mahović, Nataša. 2007. Analiza vremenske situacije tijekom kornatskog požara 30. kolovoza 2007. Cro. Meteorol. J. 42; 41-65.

Book chapters

1. Tudor, M., Ivatek-Šahdan, S., Stanešić, A., Horvath, K., Bajić, A.: Forecasting Weather in Croatia Using ALADIN Numerical Weather Prediction Model. In: Climate Change and Regional/Local Responses. Eds: Zhang, Y. and P. Ray, InTech, Rijeka, 59–88, 2013.

ALADIN and ALADIN–HIRLAM Newsletter

1. K. Horvath, A. Bajić, S. Ivatek–Šahdan, M. Hrastinski, I. Odak, A. Stanešić, M. Tudor, T. Kovai, 2015. Weather Intelligence For Wind Energy EU Project WILL4WIND. ALADIN-HIRLAM Newsletter, 4, 50–57.

2. Ivatek–Šahdan, S., A. Stanešić, M. Tudor, A. Bajić, M. Hrastinski, T. Kovačić, K. Horvath, I. Odak Plenkovi, 2015. Operational ALADIN forecast in Croatia: current status and plans. ALADIN-HIRLAM Newsletter, 4, 58–65.

3. Tudor,M., J. Šepić, I. Vilibić, I. Janeković, S. Ivatek–Šahdan, A. Stanešić, 2017. High-resolution operational NWP for forecasting meteotsunamis. 9th ALADIN-HIRLAM Newsletter. Sept 2017. 37–42.

4. M. Tudor, S. Ivatek–Šahdan, A. Stanešić, 2016. Fields in the clim files for ISBA (in combination with PGD). ALADIN-HIRLAM Newsletter, 7, 65–72.

5. M. Tudor, S. Ivatek–Šahdan, A. Stanešić, A. Baji, K. Horvath, I. Odak Plenković, M. Hrastinski, 2016. NWP at Meteorological and Hydrological Service of Croatia - 2016. ALADIN-HIRLAM Newsletter, 7, 89–92.

6. M. Tudor, S. Ivatek–Šahdan, A. Stanešić, 2017. Sea surface temperature in operational forecast (example of Adriatic Sea). ALADIN-HIRLAM Newsletter, 8, 23–32.

7. M. Tudor, A. Stanešić, S. Ivatek–Šahdan, A. Bajić, M. Hrastinski, T. Kovačić, K. Horvath I. Odak Plenković, 2016. Operational forecast and research in Croatia in 2015. ALADIN-HIRLAM Newsletter, 6, 42–47.